A Satellite and Ground Based Study of Fine Structure in VLF Whistlers.

PAULO S. CALDEIRA

Submitted in partial fulfilment of the
requirements for the degree of
Master of Science
in the
Space Physics Research Institute
of the
Department of Physics,
University of Natal.

Durban
November 11, 1992

Preface

The work described in this thesis was carried out at the Space Physics Research Institute of the Department of Physics, University of Natal, Durban, South Africa, from February 1991 to March 1992, under the supervision of Dr. A.R.W. Hughes. Data used in this thesis were recorded at Sanae and Halley Bay stations in Antarctica in 1985.

The hardware described in this thesis was built at the SPRI by the author and members of the workshop. Where use has been made of the work of others it is duly acknowledged.

Acknowledgements

The author would like to thank the following persons for their direct and indirect assistance.

- My supervisor, Dr. A.R.W. Hughes, for the assistance and encouragement on this project, and endless amounts of patience shown.
- Mr. J. Lichtenberger, Dr. G. Tarcsai, Dr. D. Hamar and S. Pástzor for the assistance in using and understanding the whistler analysis software, and for making my stay in Budapest such a memorable one.
- Mr. R. J. Atkinson for being my technical support in the design and construction of the hardware, and for all the long hours he put into the project.
- Mr. W. de Beer of the mechanical workshop, and other members of the mechanical and electronic workshop for the assistance in the construction of the antennas and other hardware.
- Mr. G. Tilbury, for always having something encouraging to say.
- Members of the Space group who were always around to answer any questions, in particular Ms. T. Holloway for the computer support.
- To Isabel, for being the driving force when I needed a shoulder to lean on, and for the understanding when I was totally irritable and unreasonable.
- Finally, to my parents and family, for all the support and encouragement.

Abstract

The matched filtering technique for improving the spectral resolution of VLF whistlers, originally developed by Bhégin and Siredey (1964), has proven to be useful for extracting information about the magnetospheric plasma ducts along which a whistler has travelled. Ground based whistlers recorded at Sanae and Halley Bay, Antarctica, on day 149, 1985, show similarities in fine structure, namely a trace splitting at frequencies below 3.720 kHz. The travel time differences between the two traces below this frequency increase with decreasing frequency. It is shown that the path length of whistler energy is frequency dependant, and since electron gyrofrequency increases with decreasing altitude, the plasma density enhancement requirements for the wave to remain trapped in the duct increases with decreasing altitude. If this increasing enhancement is not present the wave will escape from the duct, the lower frequencies escaping first. It is proposed that the trace splitting observed in the fine structure analysis of these whistlers are the lower frequencies escaping from the topside and bottomside of the duct, and so travelling along two paths to the receiver having different path lengths and hence different travel times. The higher frequencies remain trapped in the duct, and therefore display only one trace.

A satellite receiving system to receive the VLF data received by the Signal Analyser and Sampler (SAS) equipment aboard the ACTIVE satellite has been constructed at Durban. The design and construction is described in chapter 3. Due to the high noise environment no data has been collected to date in Durban. It is hoped that the receiving system can be moved further inland to a noise-free site for testing.

This thesis is read with the "Whistler Analysis Software using Matched Filtering and Curve Fitting techniques - Users Reference Manual" written by the author to facilitate use of the matched filtering software.

Contents

List of Figures

Chapter 1

Introduction

1.1 Historical Background

Since the early 1950's much work has been done in an attempt to fully understand the region of space permeated by the earth's magnetic field known as the magnetosphere, and the effects of this field on solar wind plasma in this region. Many methods have been developed to study this interaction, and the space age has opened up the use of probes that can study plasma characteristics in situ. The disadvantages of space probes of course are the costs involved, and scientists have become resourceful in developing cheaper methods.

One of the most significant developments in the study of the magnetosphere was by Storey (1953) who, based on work done by Fuchs, Barkhausen and Eckersley, among others, described whistlers as electromagnetic radiation propagating along geomagnetic field lines, and later *[Storey, 1957]* that electron density distributions along the path of propagation could be inferred from the shape of whistler frequency-time spectra. During the International Geophysical Year [1957] a concentrated effort was put into researching whistlers and other very low frequency (VLF) phenomena, such as hiss and chorus.

In 1972 C.G. Park proposed various models to accurately determine path lattitude and electron density along the path of propagation, given the whistler whose nose frequency was present, and provided the time of arrival of the whistler relative to the initiating spheric could be measured. In a paper the following year, L.C. Bernard described a method to calculate the nose frequency and time of arrival of the whistler from any two points on the whistler trace, so facilitating the use of Park's models for non-nose whistlers. These methods are still used today for accurate determination of whistler parameters.

1.2 Scope and Objectives

Duct formation and its effects on whistler propagation have been researched by many authors, one of the most prominent being H.J. Strangeways. Strangeways (1980, 1982a, 1982b) has used the technique of ray tracing to determine the path of a ray in a duct of enhanced or depressed plasma density, and has inferred many features of ducts from these calculations. Chapter 2 describes some of his work, as well as a general theoretical description of trapping of whistler waves in ducts. The theory of whistler propagation is discussed, as well as some uses of this theory for magnetospheric modelling.

Satellite VLF receiving systems have become very useful for this type of research because of the low noise environment in which the data is recorded. Chapter 3 describes the design and construction of a satellite receiving system for the SAS experiment aboard the ACTIVE satellite. Data is being received at Budapest, Hungary, and at Wallops Island, Virginia, and it was hoped that the SAS transmissions could be received in Durban. Due to the high noise environment, however, this was not possible, and some data were obtained from Budapest for analysis.

Whistler fine structure has been analysed by Lichtenberger et. al. (1991), Hamar et. al. (1982) and Hamar et. al. (1990) using a technique for enhancing the spectral resolution of whistler traces called matched filtering. The matched filtering procedure is described in chapter 4, as well as Bernard's method of extrapolating the nose frequency and time of arrival of a non-nose whistler. The use of these parameters in Park's models of the magnetosphere is detailed.

A software package written by Tarcsai, Lichtenberger and Hamar at the Eötvos University Department of Geophysics, Budapest is available in Durban for fine structure analysis. The package allows the user to produce a fast fourier transform of digitised VLF data, select points along the whistler trace, and then fit a theoretical whistler curve to the data using Bernard and Park's formulas. The matched filtering procedure is then run on a window of points around the whistler trace, the width of which is set by the user, and the result is better time resolution than has been possible with conventional whistler analysis. This allows the user to look at small time differences in the travel time of various frequency ranges of the whistler, and provides insight into duct structure and its effect on whistler propagation. Whistlers arriving simultaneously at Sanae and Halley Bay research stations in Antarctica have been analysed, and remarkable similarities in fine structure have been found. Propagation mechanisms are proposed to explain the observed fine structure. Fine structure analysis is shown to be a useful tool in the analysis of whistler propagation and duct structure.

Chapter 2

Whistlers and the Magnetosphere

Storey [1953] is widely regarded as the pioneer of whistler research, after his discovery that the audio frequency tones received by any long wire or loop antenna connected to a suitable receiver, were caused by electromagnetic radiation from lightning strikes, propagating along the earth's geomagnetic field lines between hemispheres. This electromagnetic radiation released by a bolt of lightning is radiated over a large portion of the electromagnetic spectrum, including the audio frequency range, and can travel between hemispheres along two paths : the signal can travel in the earth - ionosphere waveguide, with an estimated velocity of 0.95 times the velocity of light *[Rycroft, 1987]*, with very small travel-time delays (of the order of milliseconds) over the audio frequency range. This sounds like a loud 'click' when heard by a receiver, and is called an 'atmospheric' or simply 'spheric'.

Alternatively, if the earth's magnetic field lines are orientated in a suitable way relative to the signal source, this energy can be trapped in a 'duct' of enhanced plasma density aligned along geomagnetic field lines, and propagate in this 'duct' through the magnetosphere to the conjugate point of that field line in the opposite hemisphere of the earth. A signal travelling in this manner will experience time delays which are frequency dependent. This is known as the whistler mode of propagation. A signal of this form sounds like a pure gliding tone of decreasing frequency with time, known as a 'whistler'. There is an optimum frequency that experiences a minimum time delay, and this is called the nose frequency, and a whistler exhibiting this nose frequency is called a nose whistler. Figure 2.1 shows the paths of propagation of energy caused by a lightning strike, and a frequency - time spectrogram of a nose whistler. The nose frequency f_n experiences the minimum travel time delay, t_n, relative to the initiating spheric.

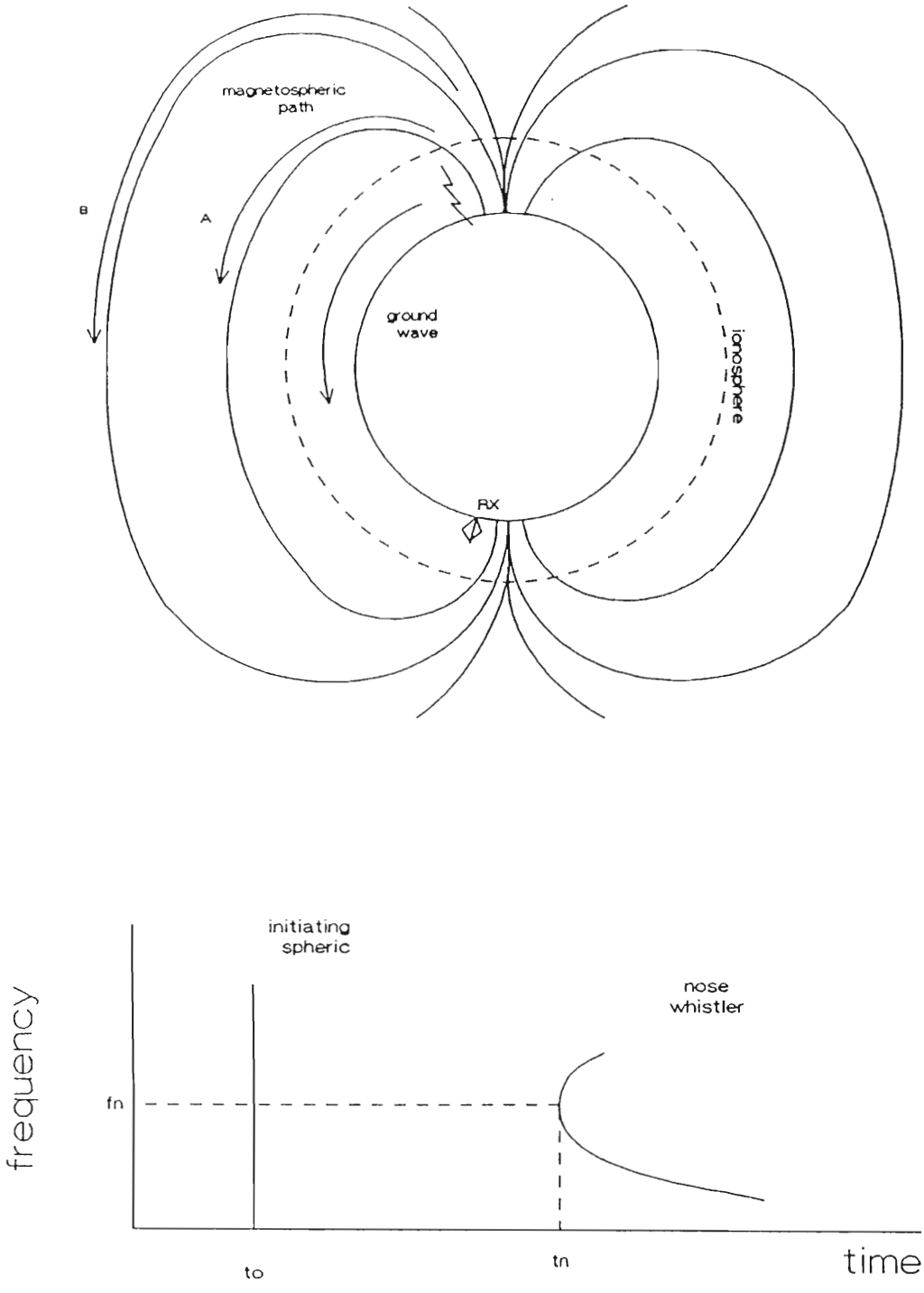

Figure 2.1: (Above) The different paths of whistler propagation, showing earth-ionosphere path and magnetospheric paths via ducts of enhanced ionisation. The signal is received by receiving stations (RX) in the vicinity of the field line along which the whistler has propagated. (Below) The spectrogram of an initiating spheric at time t_o and of a whistler at a later time t_n. Time delay $(t_n - t_o)$ is typically of the order of 100 to 200 milliseconds.

2.1 Whistler Types

The spectrogram shown in Figure 2.1 is of an ideal whistler that has travelled in a single duct, and that exhibits a nose frequency. The majority of whistlers do not exhibit this nose frequency, and are called non-nose whistlers. The energy radiated from a lightning flash may propagate along different ducts near each other, and since the path lengths for these field lines may not be equal, and the plasma densities along these paths will vary, the whistlers will arrive at the receiver in the conjugate hemisphere with slightly different delay times. Whistlers exhibiting these characteristics are called 'multipath' whistlers. Similarly, multiple lightning flashes in the same vicinity and occuring almost simultaneously can illuminate the same duct, and the resulting whistler train is called a 'multiflash' whistler.

Satellite receivers of VLF data are now very common. Whistlers observed aboard satellites very often have only travelled a fraction of the way along the field line, and as a result experience very small time delays, the noticeable time delays occuring at the lower frequencies. These are known as 'fractional hop' whistlers. If propagation conditions allow, the energy can be only partially released from the duct at the end of the field line, and the remaining energy reflected back along the path. Multiple reflections can occur, and the travel time is increased accordingly, causing 'multi - hop' whistlers.

The frequency - time characteristics of these different types of whistlers are shown in Figure 2.2

2.2 Whistler Propagation Mechanisms

Models of whistler propagation assume that electromagnetic waves propagate in a homogenous gaseous medium, consisting of equal numbers of positive and negative charges, and permeated by a static electric field. This is known as the magneto-ionic theory *[Ratcliffe, 1959]*. The polarisation of the medium is assumed to be proportional to the amplitude of the wave, and the effects of thermal motion of the charged particles is negligible. In the magnetosphere, the parameters of the medium vary slowly enough for this model to be accurate.

The Appleton-Hartree equations (2.1 and 2.2) describe the wave refractive index and wave polarization in an anisotropic homogenous medium with wave normal in the positive z-direction :

$$n^2 = 1 - \frac{X}{1 - iZ - \frac{\frac{1}{2}Y_T^2}{1-X-iZ} \pm \frac{1}{1-X-iZ}[\frac{1}{4}Y_T^4 + Y_L^2(1-X-iZ)^2]^{\frac{1}{2}}} \quad (2.1)$$

and polarisation is given by

$$R = -\frac{H_y}{H_x} = \frac{E_x}{E_y} = \frac{-i}{Y_L(1-X-iZ)}\left(\frac{1}{2}Y_T^2 \pm [\frac{1}{4}Y_T^4 + Y_L^2(1-X-iZ)^2]^{\frac{1}{2}}\right) \quad (2.2)$$

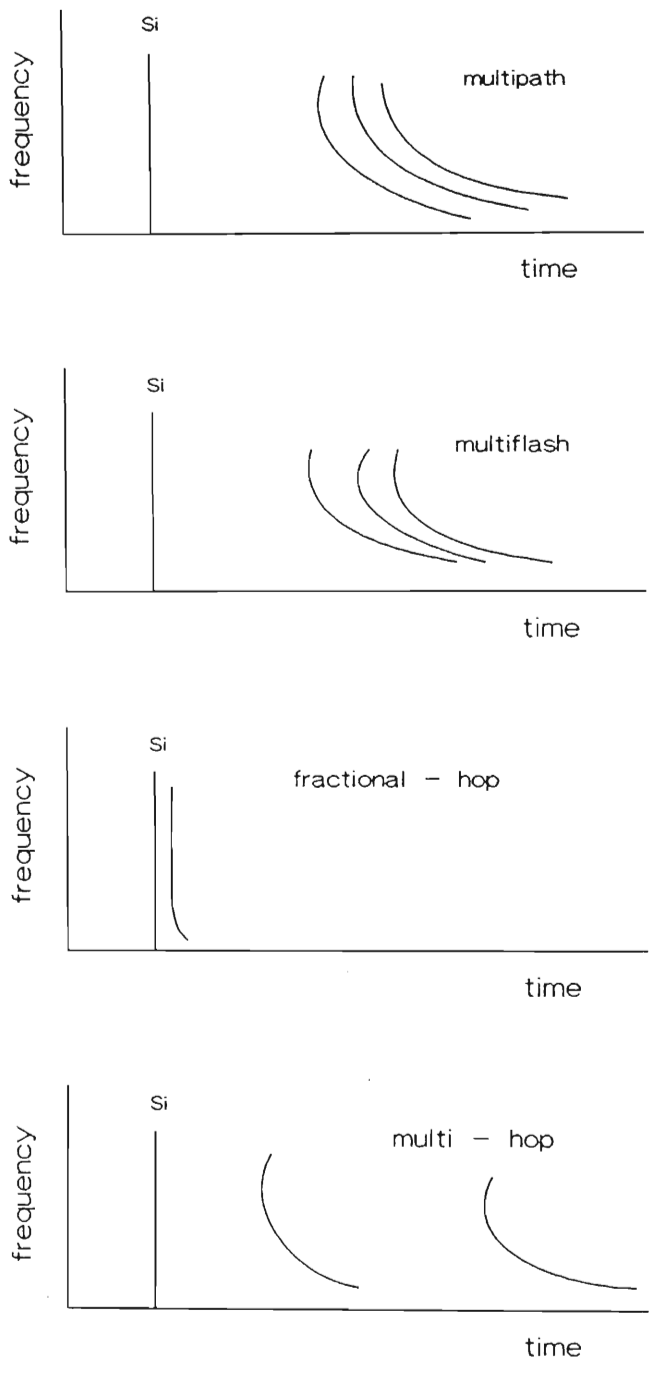

Figure 2.2: Spectrograms of different types of whistlers. 'Si' in each case is the initiating spheric.

where

$$
\begin{aligned}
n &= \textit{complex refractive index.} \\
i &= \sqrt{-1} \\
X &= \frac{f_0^2}{f^2} \\
f_0 &= \textit{plasma frequency.} \\
f &= \textit{wave frequency.} \\
Y &= \frac{f_H}{f} = \sqrt{Y_L^2 + Y_T^2} \\
f_H &= \textit{electron gyrofrequency.} \\
Z &= \frac{\nu}{\omega} \\
\nu &= \textit{collision frequency of electrons with heavy particles.} \\
\omega &= 2\pi f \\
H_x, H_y &= \textit{magnetic field components of wave.} \\
E_x, E_y &= \textit{electric field components of wave.}
\end{aligned}
$$

According to the Appleton-Hartree equations, ordinary (+ sign in equation 2.1) and extraordinary mode (− sign in equation 2.1) wave propagation is possible. The whistler mode is a subset of the ordinary mode, and whistler propagation is possible only when the refractive index is real, ie. $n^2 > 0$.

An approximation of equation 2.1 is made when the direction of propagation of the wave is sufficiently close to the direction of the earth's magnetic field, known as the 'Quasi-Longitudinal' (QL) approximation *[Ratcliffe, 1959]*.
The QL approximation holds when

$$\frac{Y_T^4}{4Y_L^2} \ll | \, (1 - X - iZ)^2 \, | \, . \tag{2.3}$$

Substituting 2.3 into 2.1 yields a simplified formula for the refractive index :

$$n^2 = 1 - \frac{X}{1 - iZ \pm | \, Y_L \, |} \tag{2.4}$$

and

$$R = \mp i \, \frac{| \, Y_L \, |}{Y_L} \tag{2.5}$$

At magnetospheric altitudes, Z, the collision frequency between particles, is very small due to low particle density, hence n^2 is real for

$$n^2 = 1 - \frac{X}{1 - | \, Y_L \, |} \tag{2.6}$$

and

$$R = +i, \tag{2.7}$$

the whistler mode QL approximation.
Equation 2.7 means that the wave is circularly polarized in a clockwise direction when looking in the direction of the magnetic field line.

2.2.1 Whistler Dispersion

The group delay of a whistler at frequencies below the nose frequency is described by a quantity called the dispersion,

$$D = t\sqrt{f} \tag{2.8}$$

for frequencies less than the electron gyrofrequency.

From equation 2.4, taking the extraordinary mode (+ sign) and assuming as before that $Z = 0$,

$$n^2 = 1 + \frac{X}{|\, Y_L \,| - 1}$$

Replacing quantities X and Y by $X = f_0^2/f^2$ and $Y = f_H/f$, we get

$$n^2 = 1 + \frac{f_0^2}{f(f_h \cos\theta - f)} = 1 + \frac{B^2}{\Lambda(\cos\theta - \Lambda)} \tag{2.9}$$

where

$$\begin{aligned} \Lambda &= \frac{f}{f_H} \\ B &= \frac{f_0}{f_H} \end{aligned}$$

If $cos(\theta) < \Lambda$, where θ is the angle between the field line and wave normal direction, then $n^2 < 0$ and the wave is evanescent. The second term of equation 2.9 is normally $\gg 1$, so that

$$n^2 \approx \frac{B^2}{\Lambda(\cos\theta - \Lambda)}$$

The group refractive index is

$$\begin{aligned} n_g &= \frac{c}{v_g} = \frac{\mathrm{d}(nf)}{\mathrm{df}} \\ &= n\frac{\mathrm{d}n}{\mathrm{df}} + n \end{aligned} \tag{2.10}$$

where v_g = group velocity.

$$\begin{aligned} v_g &= 2c\frac{\Lambda^{\frac{1}{2}}(\cos\theta - \Lambda)^{\frac{3}{2}}}{B\cos\theta} \\ &= 2c\frac{f^{\frac{1}{2}}(f_H\cos\theta - f)^{\frac{3}{2}}}{f_0 f_H \cos\theta} \end{aligned} \tag{2.11}$$

The group delay of a whistler signal is then

$$T = \int_{path} \frac{1}{v_g} ds \tag{2.12}$$

Substituting 2.11 into 2.12, for purely longitudinal propagation ($\theta = 0$) over a path of length c/B we get the 'High Density approximation' for the group delay,

$$T = \frac{1}{2\Lambda^{\frac{1}{2}}(1-\Lambda)^{\frac{3}{2}}} \; sec \tag{2.13}$$

For low frequencies ($f \ll f_H$), $\Lambda \approx 0$ and we get the 'Low Frequency' or 'Eckersley-Storey' approximation for the group delay,

$$T = \frac{1}{2\Lambda^{\frac{1}{2}}} \tag{2.14}$$

The high density approximation has a minimum at

$$\Lambda = f/f_H = 0.25,$$

the theoretical nose frequency of a whistler for strictly longitudinal propagation.

2.3 Duct Trapping of Whistler Waves

The excitation of and leakage from ducts of enhanced or depressed ionisation aligned with the earth's magnetic field is not very well understood. A common assumption is that energy gets in at the one end of a duct and leaks out of the other end. Walker *[1972]*, Alexander *[1971]* and more recently Strangeways and Rycroft *[1980]* have proposed mechanisms whereby ducts are excited from the side, which explains whistler propagation over a wider range of latitudes.

2.3.1 End Trapping Mechanisms

In the 'end trapping' mechanism, a 'trapping cone' exists by which waves falling inside this cone excite the duct and propagate along it. Consider two electron density profiles around a magnetic field line. The first (Figure 2.3a) is an enhancement of ionisation, peaking in the centre of the duct, and the second (Figure 2.3b) a depletion of ions, or trough. These enhancements are a function of distance (y) from the field line.

The path of a ray trapped in the duct is also shown, the limit of the duct being the point at which ray R_2 is parallel to the field line. The electron density at this point is $N(P)$, and at the centre of the duct the electron density is $N(0)$. There exists a critical angle that the wave normal can make with the field line direction for trapping to occur, which is frequency dependent. The relation between initial

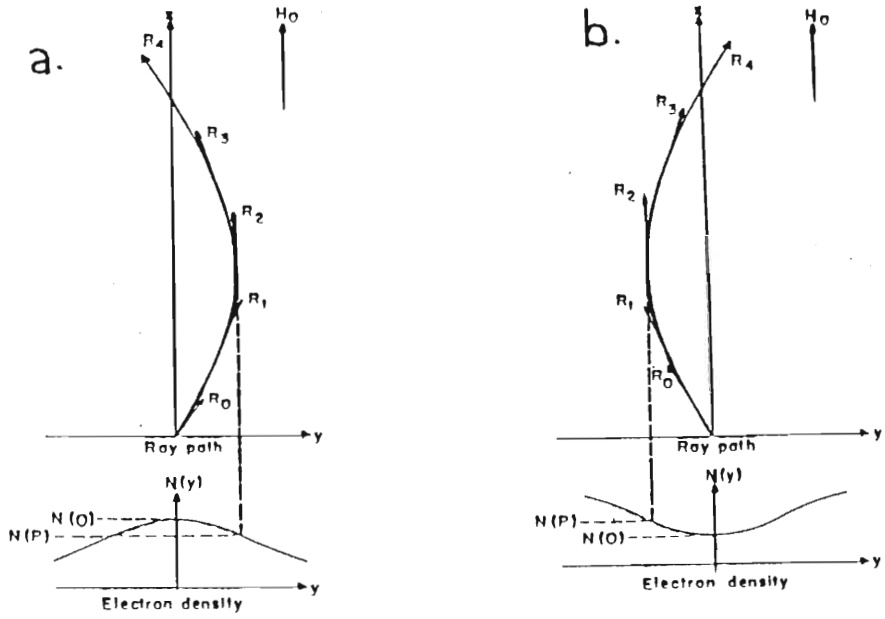

Figure 2.3: Electron enhancement and depletion functions around magnetic field lines. Path of rays trapped in the duct are also shown. *[Helliwell, 1965]*

wave normal angle θ_0 and electron density ratio $N(P)/N(0)$ for trapping is given by *[Helliwell, 1965]*

$$\frac{N(P)}{N(0)} = \frac{1-\Lambda}{\cos\theta_0 - \Lambda}\cos^2\theta_0 \tag{2.15}$$

where $\Lambda = f/f_H$.

There are two regions of interest in the frequency domain. If

$$0 < \Lambda < 0.5$$

ie. for

$$0 < f < 0.5 f_H$$

then whistler mode trapping occurs, and the wave is guided by a field aligned *enhancement* of ionisation. The critical (maximum) wave normal angle for trapping to occur in this mode is

$$\cos\theta_c = 2\Lambda.$$

For higher frequencies

$$0.5 f_H \leq f < f_H$$

trapping is only possible in troughs of ionisation *[Helliwell, 1965, pp.45]*. Typical values of electron density and magnetic field strength in the plasmasphere are not suited to ducting of whistlers in depletions (troughs) of ionisation. The reason

for this is that at some point in the path the gyrofrequency will rise to such a value that wave frequency is below the half-gyrofrequency cutoff *[Walker, 1976]*.

A 3-dimensional surface plot of the ratio $N(0)/N(P)$ given by the reciprocal of equation 2.15 is shown in Figure 2.4. Only the whistler mode of propagation ($f/f_H < 0.5$) is shown here. It is seen from this plot that at low wave normal angles (< 60 degrees) only a small density enhancement is neccesary for trapping, typically a few percent.

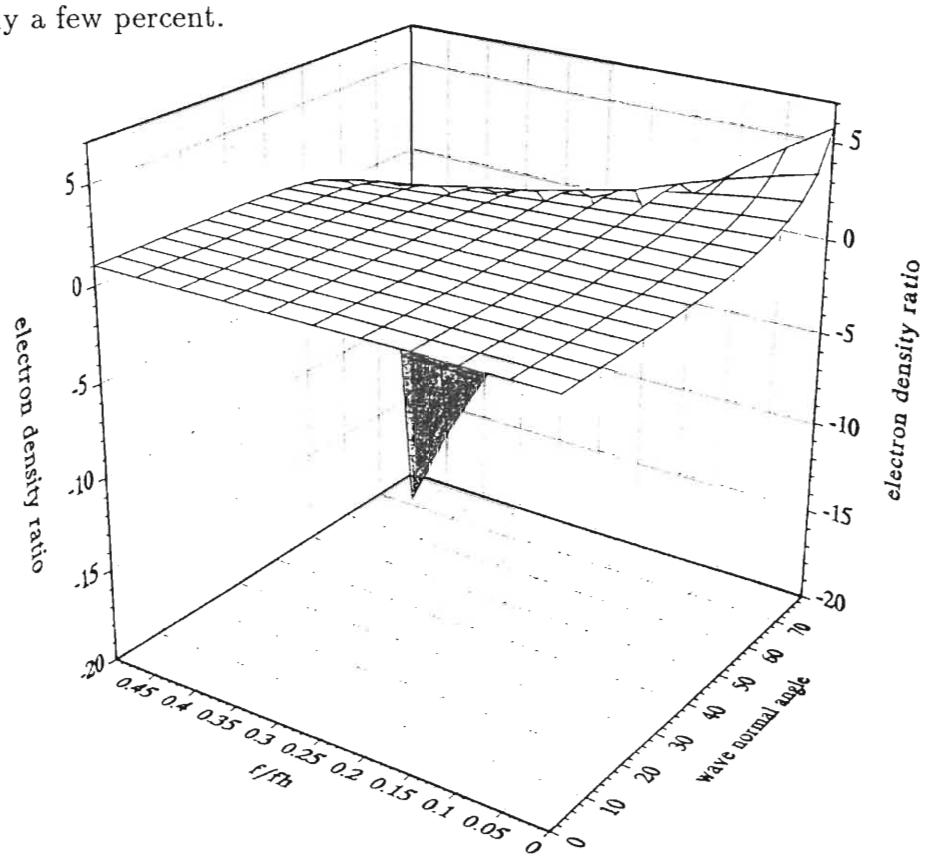

Figure 2.4: Surface plot of ion density ratio $N(0)/N(P)$ required for duct trapping showing frequency and wave normal angle (relative to the magnetic field line direction) dependencies. At high wave normal angles, large ion density enhancements are neccesary for trapping.

The half-gyrorequency cutoff is an approximation which holds true if $f_p \gg f_H$, where f_p is the plasma frequency. This condition may fail for whistlers propagating in, or just outside, the plasmapause *[Walker, 1976]*, in which case the cutoff frequency is given by the root of the cubic equation

$$2f^3 - 2f_H f^2 - 2f_n^2 f + f_H f_n = 0$$

which is less than $0.5 f_H$.

Equation 2.15 assumes that the properties of the duct remain constant along the length of the duct. Angerami (1970) pointed out the effect of a variation in electron gyrofrequency across the duct, which is to reduce the effective duct enhancement, and for frequencies approaching the half-gyrofrequency cutoff this means that a greater enhancement is neccesary for trapping. Rays that just

become trapped at the base of the duct can escape from the duct at high altitudes, as was observed for whistlers recorded aboard the OGO3 satellite *[Angerami, 1970]*.

2.3.2 Whistler Wave Trapping through the Side of Ducts.

Strangeways and Rycroft (1980) proposed mechanisms whereby whistler mode waves traversing ducts of enhanced plasma density can become field aligned at and above the refractive index minimum, and become trapped in this duct. Figures 2.5 and 2.6 show variations of phase refractive index with altitude for different L-values, and variations with frequency for a particular L-value.

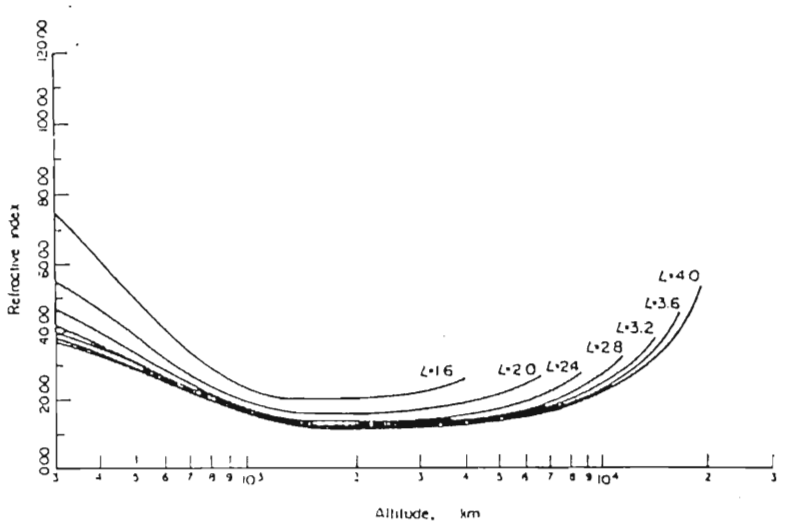

Figure 2.5: The phase refractive index along geomagnetic field lines at 4kHz for the Summer Day model. *[Strangeways et. al., 1980]*

Bernhardt and Park (1977) have found that during winter and equinoxes, VLF ducts may extend down to as low as 300 km altitude at night. Strangeways and Rycroft (1980) have proposed this is too low for duct trapping to occur through the base of ducts, but rather, side trapping is the dominant mechanism. Ray tracing calculations *[Strangeways et. al., 1980]* have shown that the wave normal angle to the geomagnetic field of a ray, entering from the side of a duct, can become field aligned under favourable conditions of plasma density and initial wave normal angle, as shown in Figure 2.7. Note the assymetry of the wave normal excursions about the centre of the duct, due to the gradient of electron density resulting from decreasing geomagnetic field strength with altitude.

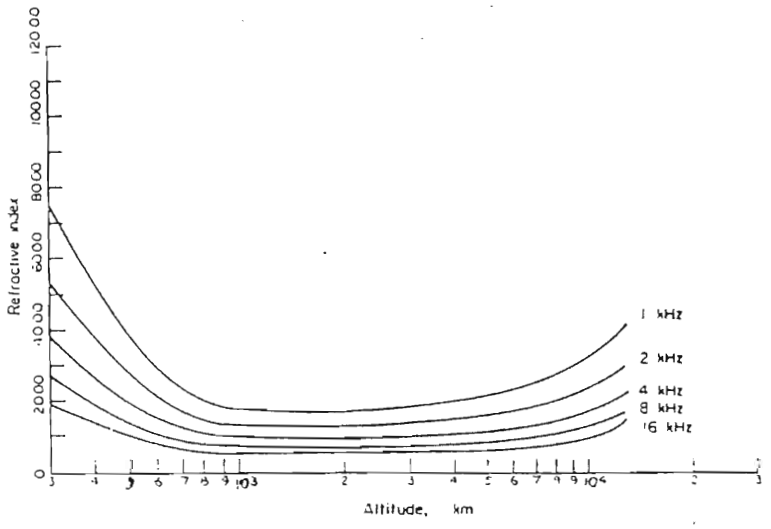

Figure 2.6: The phase refractive index along the L=3 field line for the Winter Night model. *[Strangeways et. al., 1980]*

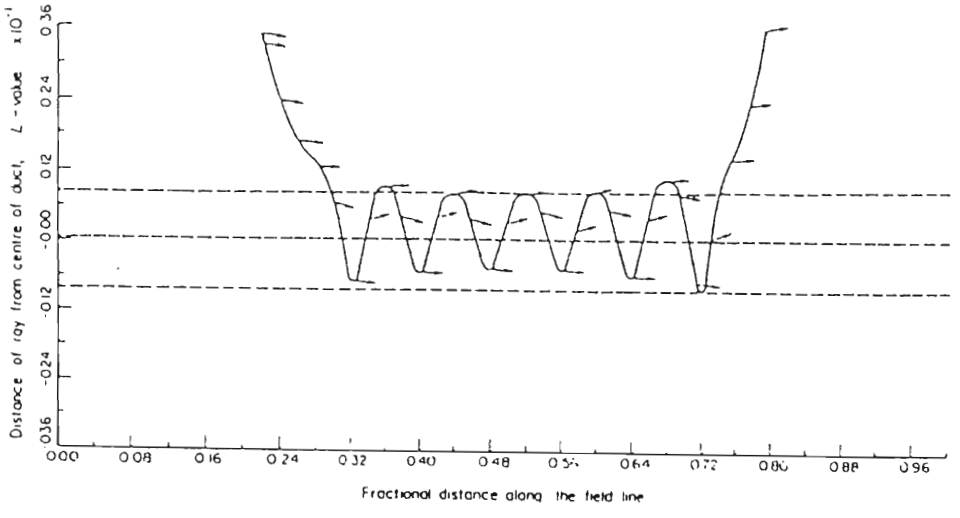

Figure 2.7: Ray trapping through the side of a duct. Wave normal direction is indicated by arrows, and geomagnetic field lines appear as horizontal lines. *[Strangeways et. al., 1980]*

Strangeways (1986) explained the variation in upper cut-off frequency of whistlers with latitude as different whistler frequencies escaping from the duct at different altitudes. He suggested that whistler leakage from a duct occurs when the wavelength of the wave equals the duct width. Since duct width increases with altitude due to diverging geomagnetic field lines, for a downcoming whistler wave it is seen that lower frequencies will escape from the duct at higher altitudes, as shown in Figure 2.8.

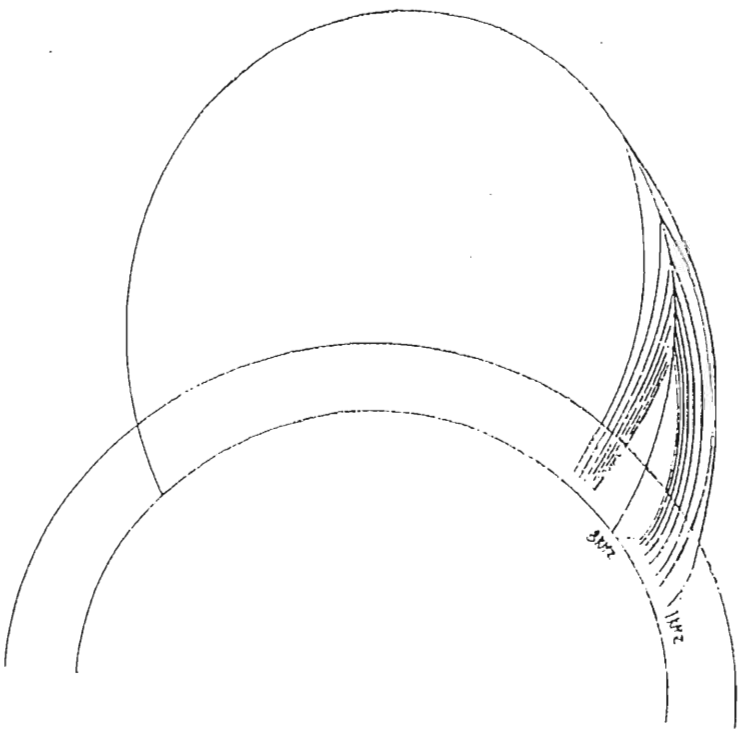

Figure 2.8: Unducted paths for downcoming 1-8kHz rays, after frequency dependant leakage from a duct. Lower frequencies will escape from the duct at higher altitudes. *[Strangeways, 1986]*

Since the lowest frequency waves spend the least time in the duct, their travel time delay will not be the same as for higher frequencies, and as a result the whistler will exhibit a lower dispersion. This in turn leads to a lower estimation of the L-value along which the whistler has propagated. For smaller L-values this error would be greatest, since the unducted part of the path would represent a larger fraction of the total path.

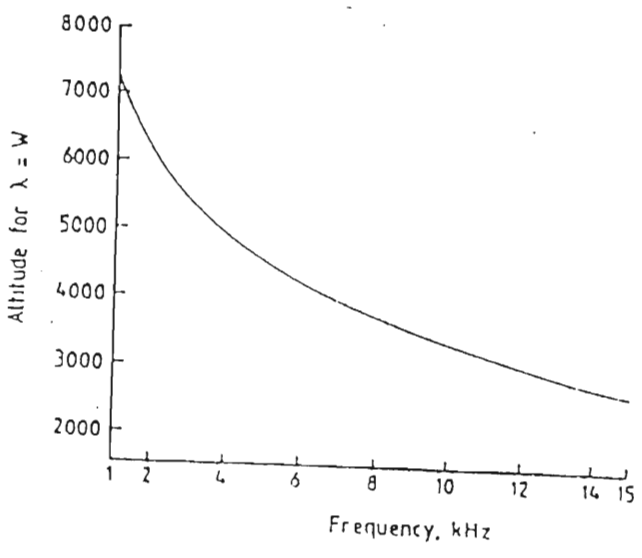

Figure 2.9: The variation of altitude of duct leakage according to the criterion $\Lambda = W$ for the L=2.4 field line and Winter Night model, and for a duct with width 1.5km at 300 km altitude. *[Strangeways, 1986]*

2.4 Fine Structure of Whistler Ducts

Strangeways (1982) examined the effect of multiple ducts, or local maxima of plasma density within a broader enhancement, as shown in Figure 2.10.

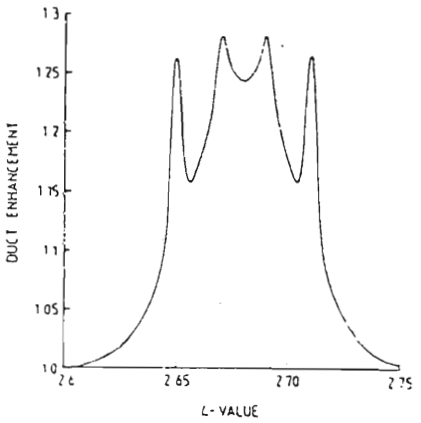

Figure 2.10: Electron Density Enhancement as a Function of L-value for the Fine Structure Duct. *[Strangeways, 1982].*

A ray propagating through a duct in which the ray does not become trapped has little effect on the direction of the ray, and rays can traverse several ducts before becoming trapped in one that has a suitable enhancement and is suitably positioned. A mechanism which Strangeways called "double duct trapping" can also occur, where two two ducts close together ($\Delta L < 0.07$) reinforce trapping by guiding the high frequency components, greater than the half electron gyrofrequency cutoff for enhancements of plasma density, in the depletion of plasma density between these ducts, as shown in Figure 2.11.

Bernhardt (1979) has also shown that ducts with high enhancement and/or narrow width can also guide waves with frequency above half the electron gyrofrequency at the equatorial plane down to low altitudes.

In ducts with fine structure in plasma density enhancements, such as is shown in Figure 2.10, "second degree trapping" can occur, that is to say, the ray may be trapped through the side of the duct with a gaussian plasma density distribution, and then trapped further in one of the fine structure enhancements at high altitude. A computer simulated illustration is shown in Figure 2.12. Several modes are possible, with some rays propagating in the main duct and others propagating in the localised fine structure enhancements.

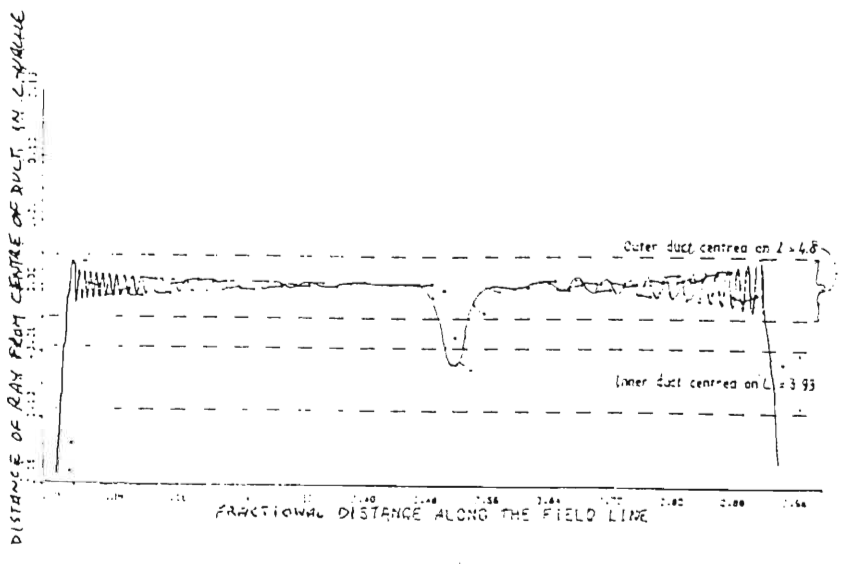

Figure 2.11: Computer simulation of the ray path showing two-duct trapping of a 7.5 kHz ray. The two ducts are centered at L=3.93 (enhancement 60%) and L=4.0 (enhancement 15%). The wave normal direction at various points are shown by arrows, a horizontal arrow denoting a field aligned wave normal. *[Strangeways, 1982]*

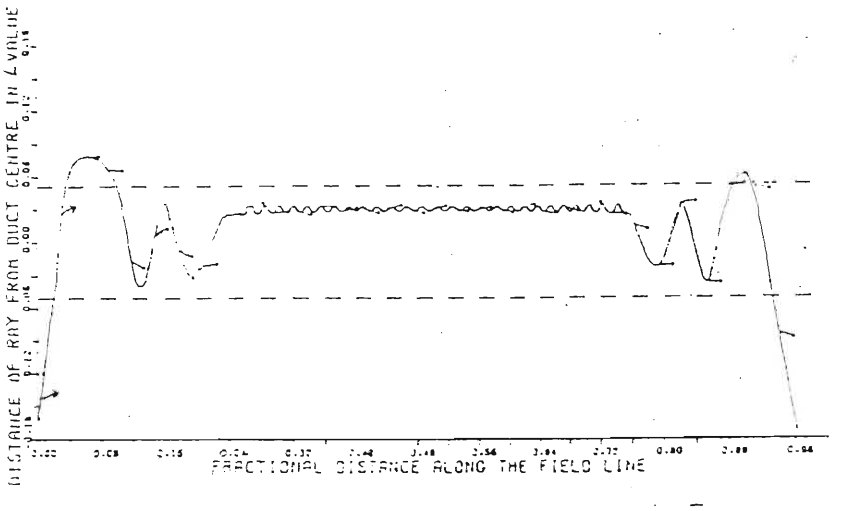

Figure 2.12: Ray path showing second degree trapping of a 4kHz ray in a fine structure duct. The ray is first trapped through the side of the main duct (enhancement 25%), and then trapped further in the narrower duct (enhancement 15%) at high altitudes. After escape from the fine structure peak, the duct will again propagate in the main duct before escaping through the side. *[Strangeways, 1982]*

2.5 Whistlers as a Plasmaspheric Diagnostic Tool

Whistlers provide a cheap and easy way of probing the plasmasphere and outer magnetosphere. The nose frequency of a whistler observed on a spectrogram is a function of the duct along which the energy has propagated, and the time delay at the nose is a function of the electron density along this path *[Helliwell, 1965], [Park, 1972].* From observations of whistlers over a broad lattitude range, an electron density profile with altitude can be derived. This method was functional in the discovery of the plasmapause *[Carpenter, 1963]*, a sharp boundary of decreased electron density, demarcating the transition from the plasmasphere to the plasmatrough. A typical electron density profile measured by the OGO 5 satellite is shown in Figure 2.13, clearly showing the "knee" in electron density discovered by Carpenter.

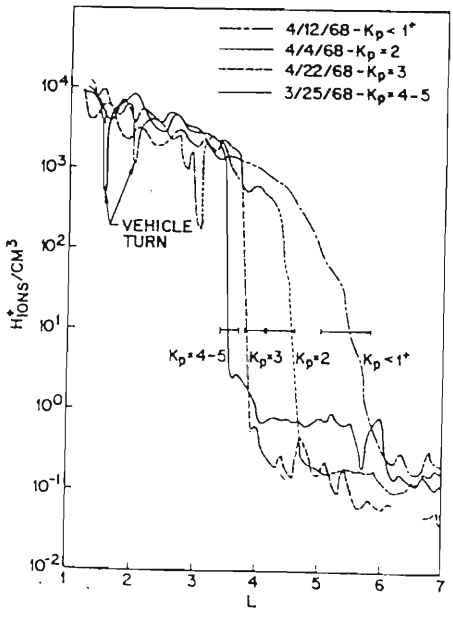

Figure 2.13: Ion density profiles showing plasmapause position changes with increased magnetic activity as measured by the OGO 5 satellite. The L-value of the 'knee' is very dependent on the magnetic activity index K_p. *from [Chappel, 1972]*

Whistler direction finding equipment, such as the goniometer *[Bullough and Sagredo, 1973]*, has been used to study duct size and motion. Duct dimension studies have been made by Hansen et. al. *[1983]* who predicted duct lifetimes to vary greatly, from 30 minutes up to several days. Lalmani *[1984]* found duct lifetimes of between 50 minutes and 1 hour at low lattitudes. Tracking of duct

motion has been used to determine the E-W component of the electric field in the equatorial plane *[Block and Carpenter, 1974]*, and Hughes and Smith *[1986]* have used the direction of arrival of whistlers at Sanae and Halley Bay stations, Antarctica, to determine the direction of plasma convection, and hence the source of the driving field. Plasma temperatures at high altitudes, over a wide range of L-values, have been measured by McChesney and Hughes *[1983]* using data recorded simultaneously by the ISIS-1 satellite and on the ground. They assumed an isothermal plasma distribution, but observations have shown that the temperature may change considerably along a magnetic field line. Sazhin et. al. (1990) have shown that it may be possible to determine temperature from changes in whistler dispersion.

Chapter 3

The ACTIVE Satellite Receiving System

3.1 Introduction

The ACTIVE (Intercosmos-24) satellite was launched from the Soviet Union on September 28, 1989. Initial apogee and perigee altitudes were 2500km and 500km respectively, with orbital inclination and period of 82.6° and 115.7 minutes.
The Signal Analyzer and Sampler (SAS) experiment placed on board the satellite is a collaborative effort between IZMIRAN, Moscow, the Department of Microwave Telecommunications, Technical University of Budapest, and the Department of Geophysics, Eötvos University, Budapest. Magnetic field components and VLF electric field data were sampled digitally, and transmitted in real time on the SAS telemetry system on a carrier frequency of 460.4 MHz. To date data have been received at Budapest, Hungary, and Wallops Island, USA. It was hoped that data would also be received at Durban, but due to unforseen technical difficulties, which are explained later in the chapter, this was not possible. However, this description of the receiving system hardware provides a base to build on for future satellite receiving stations.

3.2 The SAS Experiment

The Signal Analyser and Sampler (SAS) experiment *[J.Lichtenberger et. al., 1991]* was placed aboard the ACTIVE satellite to study ducted VLF whistler propagation, VLF duct structure, and to look more closely at the hyperfine structure of whistlers, that is to say, to achieve higher frequency - time resolution than is possible with conventional whistler analysis techniques. Originally the experiment was designed to measure the three orthogonal magnetic field and two orthogonal electric field components but, due to a technical malfunction at launch, only two magnetic and two electric field components were available initially, and

later only electric field data were available, and this is the status at present. This has been a major setback, as 5 field components are needed to determine the wave normal direction and the direction of propagation of a whistler.

The SAS instrument consists of two subsystems, namely the Data Processor and the Telemetry Transmitter. The data processor has two modes of operation: a narrowband mode, in which the bandwidth of the VLF signal is limited to 900 Hz, with centre frequency selectable between 500Hz and 21 kHz, in 500 Hz steps. The sampling frequency in this mode is 2 kHz, and the data are stored as 512 byte data frames, including timing and other essential information. The other mode is the wideband mode, in which only a single electric field component in the 20 Hz to 22 kHz is sampled, at a sampling frequency of 10 kHz. Due to this low sampling frequency, spectral overlapping causes high noise levels above about 5 kHz but the data below 5 kHz is relatively noise free and the whistler traces can be easily identified. The VLF data are transmitted in real time with an effective isotropic radiated power (EIRP) of 2.5 watts into an impedance of 50 ohms. The signal is phase shift keying (PSK) modulated, at a data bit-rate of 80 kbits.s^{-1}.

In addition to processing data, the Data Processor block also receives control data from the ground. An onboard memory of 64 kbytes allows recording of approximately 6 seconds (at 10 kHz sampling rate) of data to be recorded at any time along the pass, in a store and forward mode of operation.

3.3 Receiving System Requirements

A block diagram of the receiving system is shown in Figure 3.1.
The antenna used is an array of four 8-turn right hand circularly polarized (RHCP) helically wound antennas, designed for the downlink frequency of 460.4 MHz. The antenna is mounted on a steel tower, at an altitude of four metres, on the roof of the Physics building, and its azimuth and elevation is controlled by a tracker especially bought for the purpose. The signals from the four discrete antennas are fed into a power combiner, and then into a front end low noise amplifier (LNA) attached directly to the power combiner to eliminate cable losses. The amplified signal is then fed down a 20 metre length of low loss co-axial cable into the laboratory below, and amplified again.

The spectrum analyzer is used at this point to check the signal-to-noise ratio, and to look for interfering signals that could affect reception. The receiver used is the YAESU FRG-9600, which does not have a PSK mode, so only the front end of the receiver is used, that is, the input amplification and mixer stages. The signal is mixed down from 460 MHz several times, and is taken off at the intermediate frequency (IF) of 10.7 MHz, amplified and level shifted to be compatible with the input requirements of 0 to 5 V of the PSK demodulator. The demodulator coverts this PSK coded 10.7 MHz signal to baseband, retrieving a square wave bit stream of frequency 40 kHz or 80 kHz, depending on whether the data is binary

0 or 1. Because of this high bandwidth, normal audio tape cannot be used for recording, and the data are recorded on the video channel of a VHS recorder. An oscilloscope connected between the demodulator and the VCR is used to detect the square wave, and confirm proper operation of the circuit.

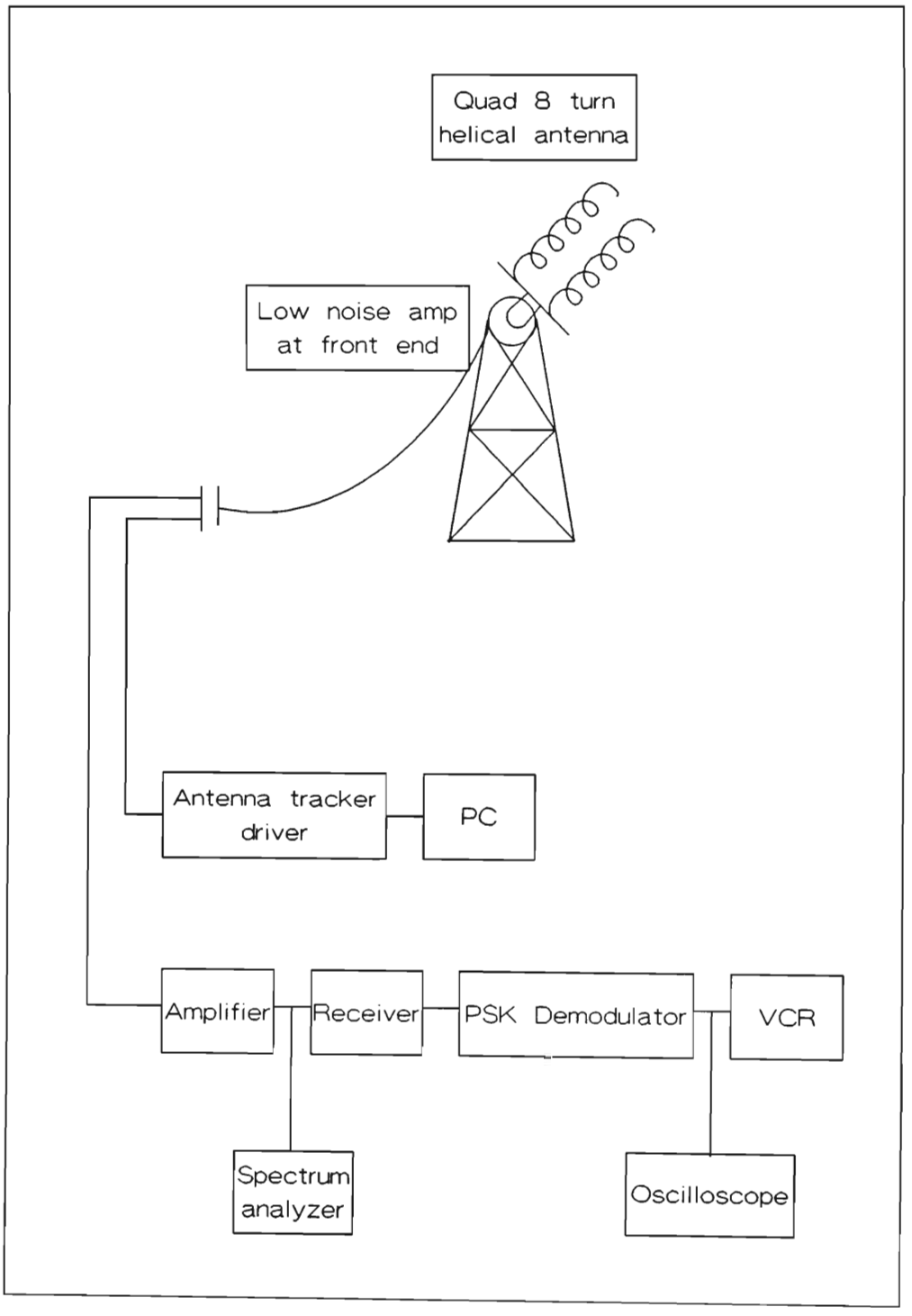

Figure 3.1: Satellite Receiving System block diagram

3.3.1 Initial design

In order to obtain design parameters for the receiving antenna and front end preamplifier, it is necessary to calculate specifications to which this equipment must be designed, using the information known about the satellite.

The power output of the ACTIVE telemetry system is 2.5 watts EIRP into 50 ohms. The satellite has perigee and apogee altitudes of 500 km and 2500 km respectively but the usual range of the satellite when its receiving footprint extends over Durban is between 1800 km and 3000 km.

A wave travelling through a medium experiences an attenuation, called Free Space Path Loss, given by the formula

$$FSPL = 10 \log \left(\frac{\lambda}{4\pi D} \right)^2 \tag{3.1}$$

where λ is the free space wavelength, in our case 0.652 metres.
D is the satellite range from the receiver.

The table below gives some indication of the FSPL for different receiver to satellite ranges.

Range (D)	FSPL
1000 km	145.7 dB
2000 km	151.7 dB
3000 km	155.24 dB

The effective isotropic radiated power radiated by the satellite

$$\begin{aligned} EIRP &= 10 \log \frac{P_{out}}{1\text{mW}} \text{ dbm} \\ &= 10 \log \frac{2.5\text{W}}{1\text{mW}} \text{ dbm} \\ &= 33.98 \text{ dbm} \end{aligned} \tag{3.2}$$

Hence the signal level at received at the antenna is

$$\begin{aligned} P_r &= EIRP - FSPL \\ &= 33.98 - 151.7 \text{ dbm } at\ 2000km \\ &= -117.7 \text{ dbm} \end{aligned} \tag{3.3}$$

A limiting factor when attempting to receive a weak signal such as that transmitted by satellite is the system noise figure and sensitivity, which are related by the expression

$$Sensitivity = 10\log(kT_sB) \text{ dBm} \tag{3.4}$$

where T_s = system noise temperature in kelvins
k = 1.38×10^{-20} mW/HzK
B = Receiver bandwidth in hertz.

In an electrical component, thermal agitation of electrons causes electrical noise, known as Johnson noise. The noise temperature is proportional to the thermal noise power generated by any system or device, and is related to the noise figure (NF) of that device or system by the expression

$$NF = 10\log\left(1 + \frac{T}{T_o}\right) \text{ dB} \tag{3.5}$$

where T_o = standard reference noise temperature of 290 K
T = system or component noise temperature.

The FRG-9600 receiver used for the ACTIVE system has a noise figure of approximately 10 dB, giving a receiver noise temperature of

$$\begin{aligned} T_r &= 290\left(10^{\frac{NF}{10}} - 1\right) \\ &= 290\left(10^1 - 1\right) \\ &= 2610 \text{ K} \end{aligned}$$

An approximate antenna noise temperature is given by

$$T_a = \frac{FG\lambda^2}{3.468} \tag{3.6}$$

where F = solar flux ($\times 10^{-22} W.m^{-2}.Hz^{-1}$)
G = antenna gain as a ratio = $10^{\frac{G(dB)}{10}}$
λ = wavelength in meters.

At a frequency of 460 MHz, the solar flux F is approximately $1 \times 10^{-20} Wm^{-2}Hz^{-1}$, and the gain of the antenna used is 17 dB, as will be shown later in the chapter, so that

$$\begin{aligned} T_a &= \frac{100 \times 50.11 \times 0.652^2}{3.468} \\ &= 614.24 \text{ K} \end{aligned}$$

The total system noise temperature is then

$$T_s = T_a + 290(L_r - 1) + L_r T_r \tag{3.7}$$

where T_a = antenna noise temperature
T_r = receiver noise temperature
L_r = feed line loss as a ratio

For a 20 metre lenght of RG-214 low loss feed line, assume a worst case loss of 2 dB, then $L_r = 1.6$, and

$$\begin{aligned} T_s &= 614.24 + 290\,(1.6 - 1) + 1.6 \times 2610 \text{ K} \\ &= 4964.24 \text{ K} \end{aligned}$$

From eqn. 3.4 the receiver sensitivity is then

$$\begin{aligned} sensitivity &= 10 \log\,(kT_sB) \text{ dBm} \\ &= 10 \log\left(1.38 \times 10^{-20} \times 4964.24 \times 2 \times 10^5\right) \\ &= -108.63 \text{ dBm} \end{aligned}$$

This means that a signal 108.63 dB below 1mW (0dBm = 1mW) will be equal to the noise in the system, that is to say, will give a signal-to-noise ratio of 0dB. Including the antenna gain of 17 dB, this increases the sensitivity of the receiving system to

$$sensitivity = -108.63 - 17 = -125.63 \text{ dBm}$$

The received power calculated from eqn. 3.3 at a range of 2000 km is -117.7 dbm, hence before amplification at the front end of the antenna the S/N ratio is

$$S/N = -117.7 - (-125.63) = 7.93 \text{ dB}$$

A front end amplifier gain of approximately 10 to 20 dB will improve the S/N ratio at the receiver to between 17.93 and 27.93 dB, which is sufficient for the Yaesu receiver.

The Yaesu receiver specification requires a signal of 1μV for a S/N ratio of 12 dB. The power received at the antenna calculated by eq. 3.3 is -117.7 dBm. With an antenna gain of 17 dB, this is equivalent to receiving

$$P_r = -117.7 + 17 = -100.7 \text{ dBm}$$

on a dipole antenna. This corresponds to a voltage of

$$V = \sqrt{P \times R}$$

where R = 50 ohms
P = power received
= -100.7 dBm
= 1 $\times 10^{-13}$ watts

Hence

$$V = 2.24\ \mu\text{V}$$

Amplification by the front end low noise amplifier should will improve this already adequate S/N ratio.

3.4 Antenna Design

The polarization of the signal transmitted by the satellite is circularly polarized in the right-hand sense, which means that the radio wave 'threads' its way through space in a clockwise direction when looking in the direction of propagation. Various types of antennas are available for receiving RHCP signals, the most efficient being the helix antenna in terms of achieving high gain with small space requirements. The helix also has a high bandwidth, so construction parameters are not critical, and its fairly high beamwidth allows for easy tracking of orbiting satellites, such as ACTIVE.
Figure 3.2 shows the basic construction of the helical antenna, as well as the radiation pattern of the antenna when used in the axial mode. Other radiation patterns are possible, depending on the pitch P used.

From section 3.3.1 the wavelength λ at 460.4 MHz is 0.652 m. The circumference of the helix for optimum gain at wavelength λ is given by

$$Circumference \approx (1.066 + 0.003\,(N - 5))\ \lambda \tag{3.8}$$

where N = number of turns.
For an 8-turn helical antenna

$$Circumference = \pi D \approx 1.075\lambda$$

where D = diameter of the helix.
Therefore

$$D \approx 0.223\ \text{m}$$

This type of antenna has a very wide bandwidth, of the order of 100 MHz [2], and so the exact diameter is not critical. The half power (-3dB) beamwidth is given by

$$Beamwidth \approx \sqrt{\frac{12300}{N}}\ degrees \tag{3.9}$$

For the 8 turn antenna used this yields a beamwidth of approximately 33.9 degrees.

The antenna gain is directly proportional to the number of turns used, and is approximated by

$$Gain(dB) \approx 10 \log (15N \tan \alpha) \tag{3.10}$$

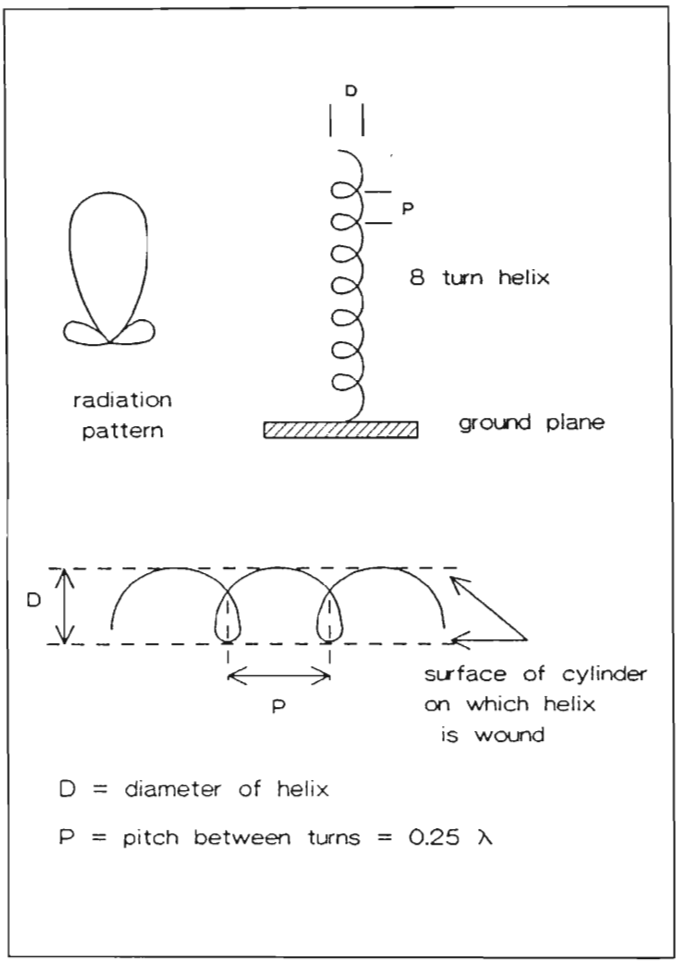

Figure 3.2: Helical antenna construction and radiation pattern

where α is the pitch angle,

$$\begin{aligned} \tan\alpha &= \frac{c}{p} \\ &= \frac{\lambda}{\lambda/4} \\ &= 0.25 \\ \alpha &= 14.036\ degrees \end{aligned}$$

For an 8 turn antenna G $\approx$ 14.77 dB.

It is very important to match the feed impedance, normally 50 ohms, to the nominal impedance of the antenna, given by

$$Z = 140 \times \frac{circumference}{\lambda}\ \Omega$$

Since C = 1.075 λ, this yields

$$Z = 150\ \Omega$$

This is done by a quarter wave matching section of impedance

$$Z = \sqrt{Z_1 \times Z_2}\ \Omega \tag{3.11}$$

where Z1 and Z2 are the impedances to be matched, namely 50 Ω and 150 Ω. Therefore

$$\begin{aligned} Z &= \sqrt{50\Omega \times 150\Omega} \\ &= 86.6\ \Omega \end{aligned}$$

The cable that resembles this impedance most closely is RG 062 with an impedance of 93 Ω. A quarter wavelength of 16.3 cm is used.

The reflector used at the base of the helix can be a square or circular solid plate or mesh, approximately 0.6 λ to 1 λ in diameter.

3.4.1 The ACTIVE Helical Antenna Array

The ACTIVE downlink has a bandwidth of 100 kHz, which is extremely high for the 2.5 watts of power being used to transmit this signal. The NOAA and METEOR weather satellites, which transmit visible images of cloud cover over the earth, also use 2.5 watts, but this power is spread over a much lower bandwidth of 2 kHz, hence facilitating signal reception. The altitude of the weather satellites is 800 km, whereas ACTIVE's usual altitude is between 1500 and 2500 km, causing far higher free space path losses. As a result, a high gain is required from the antenna used for reception of ACTIVE, therefore an array of four helical antennas is used, which gives a gain improvement of at least 3 dB when compared to a single helix. The antenna was constructed using steel strapping material, which is a stainless steel ribbon about 12 mm wide and 1 mm thick, and wrapping this around a length of PVC drain pipe. One has to compensate for the higher dielectric permittivity of PVC by decreasing the diameter of the helix by about 10 %, 200 mm pipe being the closest diameter. 8 turn helicals having a gain of about 14 dB are used, yielding a design gain of the array of 17 dB. Quarter wave matching sections of RG062 are used to match each of the individual antennas to 50 Ω, and then the four antennas are matched through a power combiner, described in section 3.4.2.

A photograph of the array mounted in situ on the tracker is shown in Figure 3.3.

The antennas are mounted on the tracker, as far away from each other as possible for higher beamwidth. The measured 3dB beamwidth of this array is approximately 30 degrees.

A plot of the near field gain (transmitter to antenna range of 100 metres) in the passband is shown in Figure 3.4.

Figure 3.3: Helical Antenna Array on the roof of the Physics building

3.4.2 Power Combiner

A commercially designed air-line coaxial power combiner [*Radio ZS, September 1989*] is used to combine the signals received by the four antennas and match the impedances to 50 Ω. The air-line combiner consists of two metal tubes, one inside the other, the characteristic impedance of which is a function of the ratio of the inner to outer conductor. The tubes can be round or square, the easiest in terms of construction being a round inner in a square outer, as shown in Figure 3.5.

The impedance of this configuration is given by

$$Z_o = 138 \log \left(1.178 \frac{D}{d}\right) \tag{3.12}$$

where D = inner dimension of outer tube
d = outer diameter of inner tube

For a 50 Ω impedance, the ratio of the inner to outer conductors is 2.17. A solid

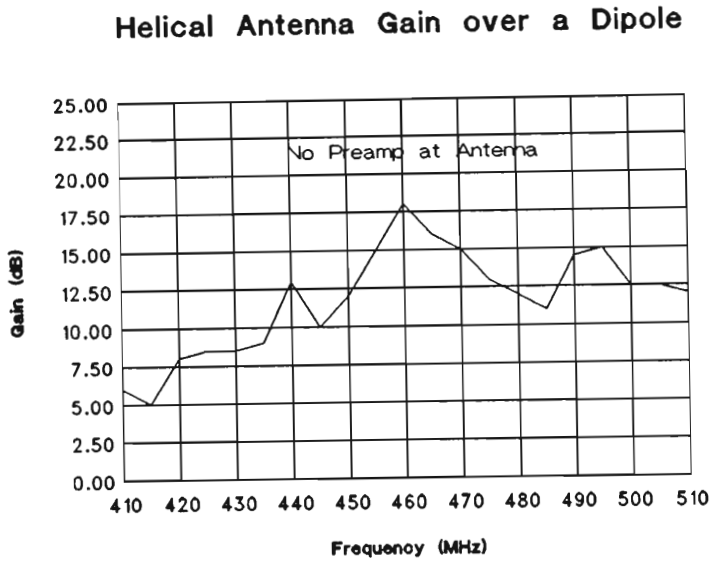

Figure 3.4: Helical antenna array near field gain

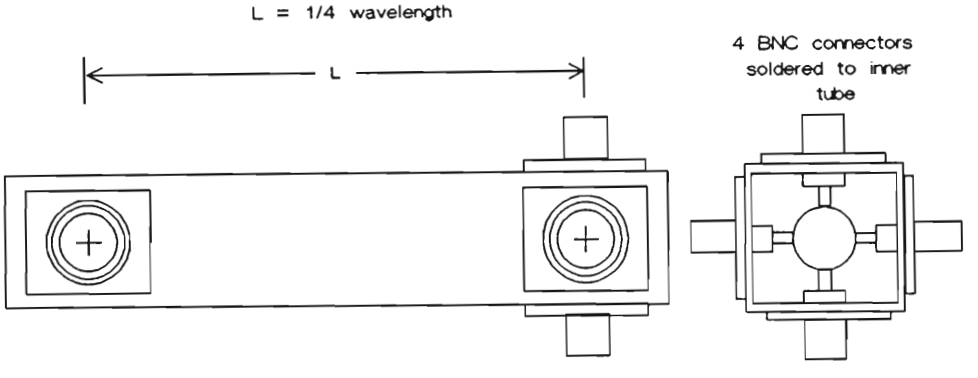

Figure 3.5: Air - Line Coaxial Power Combiner

steel bar of diameter 10 mm is used for the inner, and a square length of tubing of 22 mm inside diameter for the outer. A tube length of 16.3 cm, corresponding to a quarter wavelength, is used.

Four BNC connectors are mounted on the outer square tube and soldered onto the round inner steel bar. The four helical antennas are connected to this side. A single BNC connector is mounted a quarter wavelength away, and also soldered onto the round inner. The four 50 Ω feeds are hereby transformed to a single 50 Ω feed, with very low insertion loss, typically 1 dB. The ends of the square outer are blocked off with plastic plugs to prevent water getting in, and the combiner is mounted onto the tracker so as to keep cable lengths from antenna to combiner as short as possible, and thus reduce cable losses.

3.5 Masthead Preamplifier

For maximum receiving sensitivity and clarity of signal, the signal level needs to be as high as possible when compared to the noise being received by the antenna. To achieve this high signal to noise ratio, a low noise preamplifier at the antenna front end is used. The noise figure of the system is a measure of degradation of the signal to noise ratio as a result of noise added by the system. If a system can be divided into stages, each having a gain G and a noise figure N, then the system noise figure is

$$NF_{system} = N1 + \frac{N_2 - 1}{G_1} + \frac{N_3 - 1}{G_1.G_2} + ... + \frac{N_n - 1}{G_1.G_2...G_n} \tag{3.13}$$

where N_n = noise figure of Nth stage
G_n = gain of Nth stage

As can be seen from eqn. 3.13 the noise figure of the first stage contributes most significantly to the overall system performance. To achieve low noise figure at the front end, a GaAsFET transistor, which exhibits extremely low noise characteristics, is used for first stage amplification. A two stage design preamplifier *[John Fielding, 1990]* is used with an overall noise figure of less than 1 dB and gain of 12 to 15 dB. The circuit diagram is given in APPENDIX A.

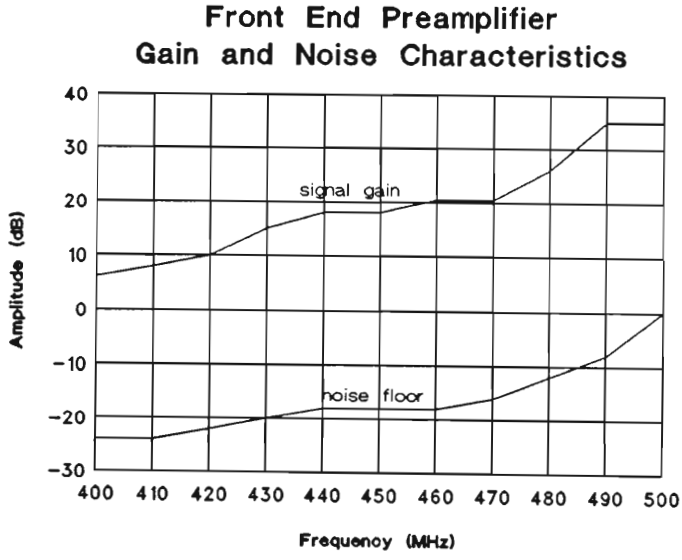

Figure 3.6: Combined Front End Preamplifier Gain and Noise Characteristics

For even higher gain, a second two stage amplifier, similar to the masthead preamp, is used at the receiver, as shown in Figure 3.1. The gain and noise characteristics of the two cascaded front end amplifiers are given in Figure 3.6. As can be seen from this figure, the gain in the passband is approximately 20.5 dB, and the noise floor is still low. At higher frequencies the gain is improved, but

the noise floor is a lot higher, resulting in an inferior signal to noise ratio. A photograph of the masthead preamp mounted on the output of the power combiner is shown in Figure 3.7.

Figure 3.7: Photograph of Masthead Preamplifier mounted on Power Combiner

The power supply to the masthead preamp is fed up the coaxial cable from the second amplifier, decoupled through a coil.

3.6 Receiver

The receiver used is the Yaesu FRG-9600 commercially available all-band receiver, which can scan from 60 to 905 MHz in 5 different modes, namely FM-narrow, FM-wide, AM-narrow, AM-wide and SSB. Since the signal transmitted by ACTIVE is PSK (phase shift keying) modulated, only the front end amplification and down-conversion stages are used. The signal is then taken off at the intermediate frequency (IF) of 10.7 MHz from the main printed circuit board of the receiver , and connected to an IF amplifier and comparator. The receiver has been modified to house this printed circuit board, which fits inside the receiver case, and the output is connected to a BNC connector on the back of the receiver case.

The IF amplifier and comparator amplifies a 2 μV input from the IF stage of the receiver to 10 mV, and levels shifts this signal through the comparator to a $4V_{peak}$, compatible with the PSK demodulator input requirements. The receiver

is used in the FM-wide mode of operation because of the high bandwidth (200 kHZ) requirements of the ACTIVE signal. In this mode receiver sensitivity is 1.0 μV for a 12 dB S/N ratio, and the received signal at the antenna is 2.24 μV even before amplification by the front end amplifiers.
The circuit diagram of the IF strip is given in APPENDIX A.

3.7 The PSK Demodulator

The downlink signal from the ACTIVE satellite is Phase Shift Keyed (PSK) modulated, which means that the phase of a carrier signal is shifted to transmit information. The ACTIVE satellite phase is shifted +1 radian to indicate binary 1 and -1 radian to indicate binary 0. The receiver output is connected to the PSK demodulator, which detects the input phase, and thereby the input binary bit stream. The PSK demodulator output is a Frequency Shift Keyed (FSK) 40 kHz or 80 kHz square wave, corresponding to binary 0 or 1. Since the frequency of this output signal is too high to record on audio cassette, the data are recorded on the video channel of a VHS video cassette recorder, and then decoded in Budapest.
The circuit diagram and circuit description are in APPENDIX A.

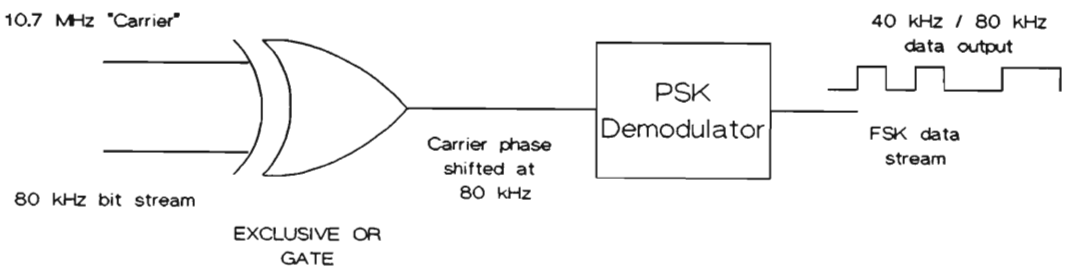

Figure 3.8: Test circuit simulating phase shifted satellite signal

A circuit used to test the PSK demodulator is shown in Figure 3.8. Two signal generators are used to simulate the IF (10.7 MHz) and bit stream (80 kHz) signals, and the phase of the IF is phase shifted at a rate of 80 kHz by feeding both signals into an EXCLUSIVE-OR gate. This is a good representation of how the carrier is phase shifted on board the satellite. This phase shifted 10.7 MHz "carrier" is connected to the PSK demodulator, which decodes the phase and outputs a 40 or 80 kHz square wave, depending on whether the phase leads or lags a reference phase generated by an oscillator in the demodulator.

3.8 Satellite Tracking

The helical antenna array is mounted on an azimuth - elevation rotator, the "EMOTATOR model EV700D5X elevation/azimuth dual type rotator", made by EMOTO Antenna company, Ltd. The rotator/tracker consists of two motors, one rotating azimuthally and the other in the vertical (elevation) plane. The accuracy of this type of tracker is approximately 3 degrees, which is good enough for our purposes considering the high beamwidth of the antennas. Control cables run from the motors to a controller in the lab below, and this controller is driven by software on a personal computer through an electronic circuit interfacing the PC to the controller. A counterweight is neccesary to balance the weight of the antenna array, so as not to overstress the elevation motor.

3.8.1 Tracking Software : Instantrack

The software package that controls the tracker is called "Instantrack" *[Franklin Antonio, 1989]* and uses Keplers laws of orbital motion to track up to 200 satellites at a time. The user needs to enter the keplerian elements of the satellite, and from these and the receiving station's geographical position the program calculates the satellites position relative to the observer. "Instantrack" also has the facility of interfacing to a tracker to automatically position the antenna to receive the signal. The interfacing hardware,designed and built by Mr. R.J. Atkinson and the author, interfaces the computer to the tracker controller. The circuit diagram and circuit description are given in APPENDIX A. A memory resident program called "ROTOR" also had to be written to enable and disable the tracker from inside "Instantrack" via hardware interrupts. "ROTOR" is run before "Instantrack" and is enabled by pressing "R" when in the real time tracking mode of "Instantrack". The source code of the turbo pascal program "ROTOR.PAS" is in APPENDIX A.

3.9 System Non-Performance

At this stage no ACTIVE data has been received at Durban. After construction and testing of all the components that make up the receiving system was completed, it was found that interference from cellular mobile radio and two way radio , as well as other beacon transmitters, saturates the front end to the extent that the satellite signal is swamped by these signals when looking at the spectrum on a spectrum analyzer. A photograph of the spectrum analyzer spectrum in the 450 to 470 MHz band is shown in Figure 3.10.

Several attempts have been made to rectify this problem. Several types of notch and bandpass filters have been tried, such as the quarter wave stub. This consists of a quarter wavelength of open circuited coaxial cable, connected in parallel to

Figure 3.9: Photograph of the VGA map display of the Instantrack program.

the antenna feed line, which behaves as a notch filter at the resonant frequency of the stub. By trimming the coaxial cable to the correct length, a notch filter is realised at the undesired frequency.

However, the Q-factor of this type of filter is not high enough, and by centering the notch at 459.5 MHz, the attenuation at 460.4 MHz, the satellite frequency, is still about 26 dB. Short-circuiting the quarter wave stub has the effect of creating a bandpass filter, but again the bandwidth of the pass band was far too high to be of any use. A second type of notch filter, a cavity resonator, was attempted. This filter again failed to have high enough Q.

3.10 Conclusion

Although the receiving station is unsuccessful in receiving the ACTIVE satellite, a lot has been learned in the way of design and construction of future satellite receivers. The principles outlined in this chapter are used for any other satellite receiving station, although the antennas used and signal modulating techniques may be different. It is doubtful whether the 460 MHz band will be used for VLF satellite telemetry again. Because of the growing number of users of cellular radio, inteference in this band has made it virtually impossible to have a successful downlink from the low power tranmitters used on board satellites. This is partic-

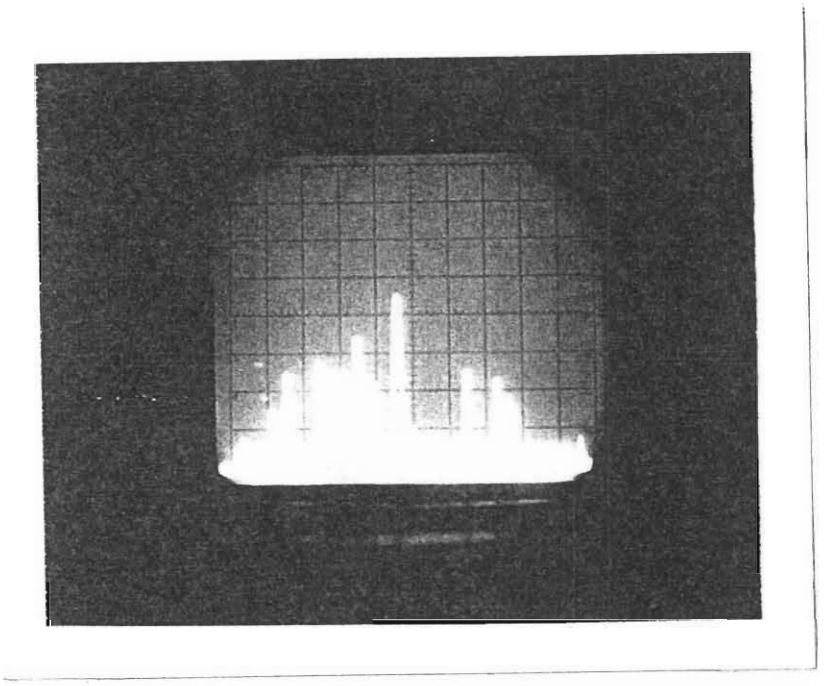

Figure 3.10: Photograph of Spectrum from 450 to 470 MHz. Centre Frequency is 460 MHz, and Freq./Division is 2 MHz. Signal at 459.5 is the main interference, a beacon transmitter.

ularly the case in Budapest, where cellular radio was almost unheard of in 1989 when ACTIVE was launched, and is now growing in the number of users due to the lifting of the Iron Curtain. Future locations of satellite receiving stations should preferably be away from the city, where interference is very high, or the interference at the desired receiving frequency should be measured in the initial stages of the project to determine whether reception is viable. Some ACTIVE satellite data has been received from Budapest, and is available in the Physics Department for analysis.

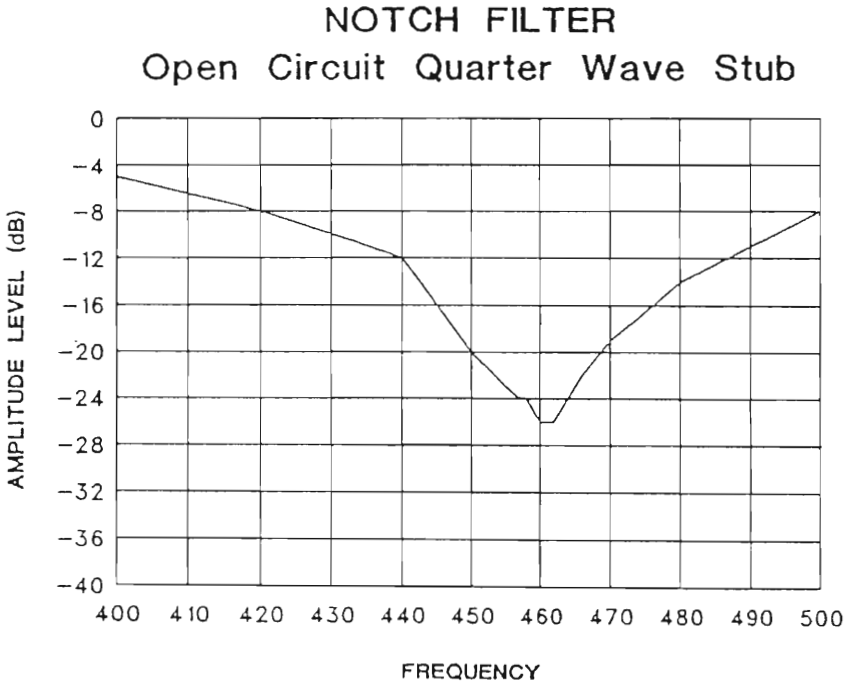

Figure 3.11: Amplitude - Frequency characteristics of the quarter wave stub notch filter.

Chapter 4

Whistler Analysis including Matched Filtering Theory.

4.1 Introduction

A software package written specifically to analyse VLF whistlers is available in the Physics Department. The software was given to us courtesy of the Department of Geophysics, Eötvos University, in Budapest, Hungary. The software uses the matched filtering technique, developed by Bhégin and Siredey [1964], to look at the hyperfine structure of whistlers, and Bernard's [1973] formula to find the whistler nose frequency f_n and travel time at the nose t_n, and these values are used in Park's [1972] models of the magnetosphere to find the path of propogation, and plasma densities along this path. Although more time consuming than conventional whistler analysis using the AVDAS *[Smith et. al., 1987]*, the results are more accurate, and the matched filter method of analysis yields new insight into the structure of ducts along which the whistler has travelled.

The software package is ideally suited to analyse data recorded aboard the ACTIVE satellite on the SAS receiving equipment, described in chapter 3. SAS data storage is problematic due to the high sampling rates required for VLF data. 2.8 Megabytes of data, representing 280 seconds of a satellite pass received in Budapest on 17 December, 1990, is available for analysis in the Physics Department. Results of the analysis of this data are shown in chapter 5. Other analog VLF data, such as that recorded aboard the ISIS satellite, or that recorded at SANAE, Antarctica, can be sampled using an Analog to Digital card for the PC, and analysed using the software. The author has also written a users reference manual to facilitate use of the package.

In this chapter the computational methods used by the main programs are discussed. A detailed description of the usage of each of the programs in the package is given in the Users Reference Manual *[Caldeira, 1992]*.

4.2 Whistler Curve Fitting

The programs used for curve fitting, FIT0 and FIT1, use Bernard's [1973] formula to find the nose frequency, and time of arrival of the nose frequency relative to the initiating spheric, and Park's [1972] models of the magnetosphere to calculate the plasma parameters. Park's model can be used directly if the nose frequency and initiating spheric are evident on the whistler spectrogram, but where the nose is not present, as is the case with the majority of whistlers, these parameters are calculated by Bernard's formula given two frequency - time points on the spectrogram.

4.2.1 Bernard's formula

Smith and Carpenter [1961], Brice [1965] and Dowden and Allcock [1971] developed methods to find the nose frequency and travel time at the nose of non-nose whistlers. However, these methods have proved either to be time consuming, or have required a large number of scaled points for any sort of accuracy. L.C. Bernard [1973] developed a relatively easy method to calculate the whistler nose parameters. Bernard's method, described in his famous paper *[Bernard, 1973]*, and outlined below, uses simple algebraic techniques and only two (f,t) pairs selected along the whistler trace for implementation.

The dispersion of of a whistler travelling in space is given by

$$D = t\sqrt{f} \tag{4.1}$$

and the whistler travel time is given by Helliwell [1965]

$$t = \frac{1}{c}\int \mu_g ds = \frac{1}{2c}\int \frac{f_0 f_H}{f^{\frac{1}{2}}(f_H - f)^{\frac{3}{2}}}\, ds \tag{4.2}$$

where μ_g = group refractive index
c = speed of light in free space
f = wave frequency
f_0 = plasma frequency
f_H = electron gyrofrequency
ds = element of path length along geomagnetic field line

Hence the dispersion is

$$D = \frac{1}{2c}\int \frac{f_0 f_H}{(f_H - f)^{\frac{3}{2}}}\, ds \tag{4.3}$$

The propagation path can be divided into two regions, a magnetospheric path above 1000 km altitude, and two ionospheric paths below 1000 km at conjugate points on the globe. The contribution of the ionospheric path to the total dispersion is very small, and is very often ignored.

To facilitate computation when finding an approximate formula for the dispersion in the magnetospheric portion of the propagation path, we substitute normalized frequencies $\Lambda = f/f_{he}$, $b = f_H/f_{he}$ and $\phi = f_0/f_{pe}$ into equation 4.3 to obtain

$$D = \frac{f_{pe}}{2cf_{he}^{\frac{1}{2}}} \int \frac{\phi b}{(b-\Lambda)^{\frac{3}{2}}}\, ds \tag{4.4}$$

where f_{pe} = plasma frequency in the equatorial plane
f_{he} = electron gyrofrequency in the equatorial plane

Since $\Lambda \ll b$, we are able to make a Taylor expansion

$$b(b-\Lambda)^{\frac{-3}{2}} = b^{\frac{-1}{2}} \left(1 + \frac{3}{2}\frac{\Lambda}{b} + \frac{15}{8}\frac{\Lambda^2}{b^2} + \ldots\right) \tag{4.5}$$

The dispersion integral of equation 4.4 is then written as

$$I = d_0 + d_1\Lambda + d_2\Lambda^2 + \ldots + d_i\Lambda^i + \ldots \tag{4.6}$$

where

$$d_0 = \int \frac{\phi}{b^{\frac{1}{2}}}\, ds, \qquad d_1 = \frac{3}{2}\int \frac{\phi}{b^{\frac{3}{2}}}\, ds, \qquad d_2 = \frac{15}{8}\int \frac{\phi}{b^{\frac{5}{2}}}\, ds, \text{ etc.}$$

The relative magnitudes of the elements of the integral in equation 4.6 can be estimated by inspection. Since $b = f_H/f_{he}$, $b \geq 1$ along the path, and approaches 1 in the equatorial plane, d_i decreases with increasing "i". Also, since b is smallest in the equatorial plane, the major contribution to the dispersion occurs here. Since this equation converges rather slowly, an empirical approximation is used by truncating the Taylor expansion at some term and replacing all the remaining d_i with an average value d :

$$I \approx d_0 + d\Lambda(1 + \Lambda + \Lambda^2 + \ldots) = d_0 + d\left(\frac{\Lambda}{1-\Lambda}\right) \tag{4.7}$$

Using this approximation the dispersion equation 4.3 becomes

$$D = D_0 \frac{f_{he} - Af}{f_{he} - f} \tag{4.8}$$

where

$$D_0 = \frac{f_{pe}d_0}{2cf_{he}^{\frac{1}{2}}} \quad = \text{ zero frequency or Eckersley dispersion.}$$

$$A = \frac{d_0 - d}{d_0}$$

A depends on the whistler path, and on the variation of f_H and f_0 along this path. To evaluate A, we differentiate equation 4.1

$$\frac{\mathrm{d}D}{\mathrm{d}f} = \frac{\mathrm{d}t}{\mathrm{d}f}\sqrt{f} + \frac{D}{2f} \tag{4.9}$$

At the nose frequency, $\mathrm{d}t/\mathrm{d}f = 0$, therefore

$$\left(\frac{\mathrm{d}D}{\mathrm{d}f}\right)_{fn} = \frac{D_n}{2f_n} \tag{4.10}$$

Differentiating equation 4.8 as above yields

$$A = \frac{3\Lambda_n - 1}{\Lambda_n(1 + \Lambda_n)} \tag{4.11}$$

Substituting equation 4.11 into 4.8 yields a useful relationship at the nose frequency

$$\frac{D_n}{D_0} = \frac{2}{1 + \Lambda_n} \tag{4.12}$$

The error in using the approximation in equation 4.8 for the dispersion is less than 1 % *[Bernard, 1973]*.

Equations 4.8 to 4.12 yield another useful expression

$$\frac{t}{t_n} = \frac{1}{2\sqrt{f/f_n}} \frac{(1 + \Lambda_n) - (3\Lambda_n - 1)(f/f_n)}{1 - \Lambda_n(f/f_n)} \tag{4.13}$$

Park's [1972] calculation of normalized nose frequency $\Lambda_n = f_n/f_{he}$ shows little variation of Λ_n for a range of L-values. Figure 4.1 shows variations in Λ_n for Park's diffusive equilibrium (DE) and collisionless (CL) models of field line plasma distribution.

Having developed an equation for the dispersion, we now calculate nose frequency f_n and travel time t_n from two frequency - time points selected along the whistler trace. We call these points (f_u, t_u) and (f_L, t_L), denoting upper and lower frequency points, respectively.

Let R be the ratio of the dispersion at these two points,

$$R = \frac{D_u}{D_L} = \frac{t_u\sqrt{f_u}}{t_L\sqrt{f_L}} \tag{4.14}$$

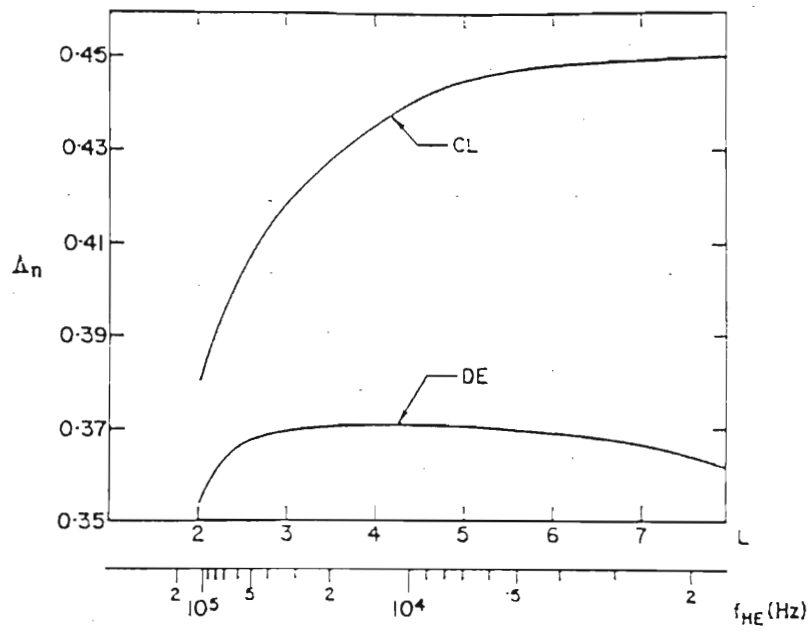

Figure 4.1: A plot of normalized nose frequency Λ_n vs. L value for a diffusive equilibrium and collisionless model of plasma distribution. Equatorial electron gyrofrequency is shown at the bottom. *[Bernard, 1973]*

From equation 4.8

$$R = \frac{\left(\frac{f_{he}-Af_u}{f_{he}-f_u}\right)}{\left(\frac{f_{he}-Af_L}{f_{he}-f_L}\right)} \tag{4.15}$$

Re-arranging terms, we obtain a quadratic in f_{he}:

$$f_{he}^2 - f_0 f_{he} + A f_u f_L = 0 \tag{4.16}$$

where

$$f_0 = \frac{(R-A)f_u + (AR-1)f_L}{R-1}$$

Since Λ_n, and therefore A, is fairly constant, as shown in Figure 4.1,

$$f_{he} = \frac{f_0 + \sqrt{f_0^2 - 4Af_u f_L}}{2} \tag{4.17}$$

and since $f_n = \Lambda_n f_{he}$,

$$f_n = \Lambda_n \frac{f_0 + \sqrt{f_0^2 - 4Af_u f_L}}{2} \tag{4.18}$$

Simplifying, $Af_u f_L \ll f_{he}^2$, and equation 4.18 becomes

$$f_n \approx \Lambda_n \left(f_0 - \frac{Af_u f_L}{f_0}\right) \tag{4.19}$$

To find the time of arrival of the whistler, we use the equation

$$t_n = \frac{D_n}{\sqrt{f_n}}$$

From equations 4.8 and 4.12 we get

$$D_n = D\frac{2}{(1+\Lambda_n)}\frac{(f_{he}-f)}{(f_{he}-Af)} \tag{4.20}$$

and finally

$$t_n = \frac{2}{\sqrt{f_n}}\frac{D}{(1+\Lambda_n)}\frac{(f_n-\Lambda_n f)}{(f_n-A\Lambda_n f)} \tag{4.21}$$

For D and f, either upper or lower frequency values may be used.

The approximations used by this method give rise to small errors in the nose frequency and travel times calculated.

Depending on how much of the whistler trace is visible, some problems may be encountered in the computation of the nose frequency, and hence travel time. From equation 4.16

$$f_0 \propto \frac{1}{R-1}$$

If the upper frequency point f_u is lower than the nose frequency, ie. only the 'tail end' of the whistler is visible, the parameter R is very small, approaching 1 in the limit, and small variations in R due to the approximations used may result in large errors in the calculation of f_n.

Bernard [1973] has shown that for $R > 1.1$ the error in the nose frequency calculation is typically less than 3 % , and for $R < 1.1$ the error may rise to 10 % . Therefore, to reduce computation errors, R is maximised by choosing f_u as high as possible, in the instance when $f_u < f_n$.

Once the nose frequency and delay time at the nose have been found by Bernard's method, they are used in Park's equations for modelling of the magnetosphere to derive the electron concentrations in the region of space through which the whistler wave has travelled.

Since Λ_n depends on the L-value along which the whistler has travelled, which can only be approximated initially, the software uses an iterative process which calculates the nose frequency and L-value using this starting value of Λ_n (described in the next subsection), and then uses these values of L and f_n to calculate a new value of Λ_n. This procedure is repeated until the value of the parameters converge to a solution. Occasionally the iterative process diverges, in which case new starting values are required.

4.2.2 Park's Models of the Magnetosphere

Park's [1972] report describes four different models of the magnetosphere, namely the Diffusive Equilibrium (DE) model, the Collisionless (CL) model, the R-4

model and the Hybrid (HY) model, which is a combination of the DE and CL models.

Propagation of the whistler wave inside the plasmapause ($L \leq 4$), where the electron density is between 100 - 1000 cm^{-3}, is best described by the DE1 model. This model assumes the electrons to move totally randomly, with frequent collisions between them, and are able to diffuse to other parts of the plasma, a 'diffusive equilibrium'. Outside the plasmapause, electron density is a lot lower, of the order of 1 - 10 cm^{-3}, and the CL and R-4 models apply. These two models yield very similar results. Due to the low electron density, the mean free path of an electron is very long, and its motion is considered to be 'collisionless' in this region.

Depending on the propagation path, a model is selected by which all the plasma parameters are calculated from the nose frequency f_n and nose frequency travel time delay t_n, found by Bernard's formula.

The equatorial electron gyrofrequency f_{heq} is a function of the magnetic field strength,

$$f_{heq} = \mid \frac{qB}{m} \mid$$

where q = charge on an electron
B = magnetic induction
m = mass of an electron

Since the field strength varies as a function of $1/r^3$, where r is the distance from the earth's centre, it can be easily calculated, and f_{heq} is similarly known.

The nose frequency of a whistler is also a function of the field line along which the whistler has travelled, so that

$$f_{heq} = K f_n \tag{4.22}$$

where K is a constant.

A plot of nose frequency and equatorial electron gyrofrequency, for both the DE1 and R-4 (collisionless) models, given by Angerami [1966], is shown in Figure 4.2.

The L - value along which the whistler has travelled is a function of the equatorial electron gyrofrequency,

$$L = \left(\frac{f_{hoeq}}{f_{heq}}\right)^{\frac{1}{3}} = \left(\frac{8.736 \times 10^5}{fheq}\right)^{\frac{1}{3}} \tag{4.23}$$

where f_{hoeq} is the reference electron gyrofrequency at the equator, corresponding to a magnetic field strength of 0.312 Gauss.

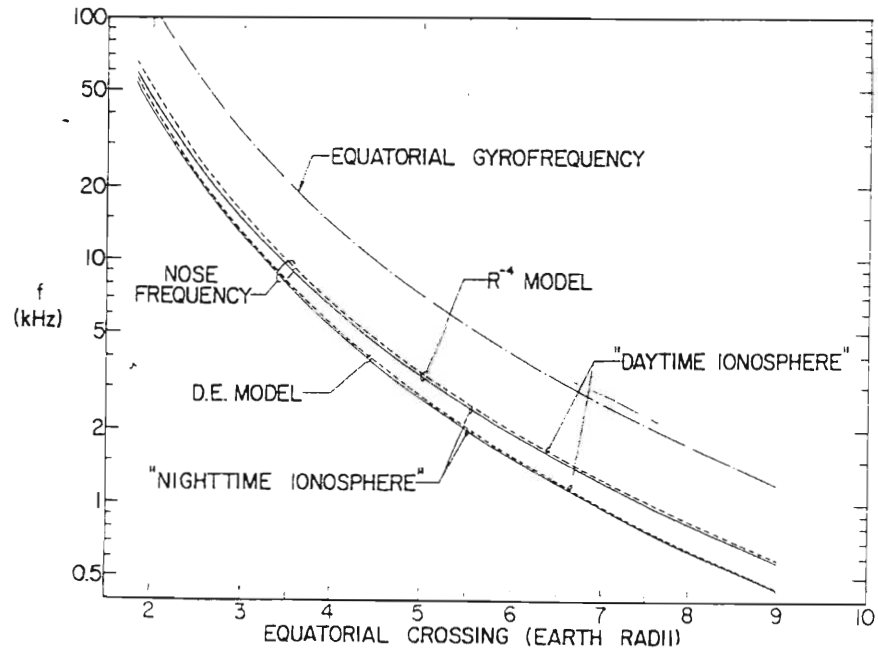

Figure 4.2: Nose frequency and equatorial electron gyrofrequency variations with L - value, for the DE1 and R-4 models

The travel time delay of the wave from the ionospheric reference altitude of 1000 km to the equator is given by

$$t(f) = \frac{1}{c}\int_{1000km}^{equator} \frac{f_0}{f^{\frac{1}{2}} f_H^{\frac{1}{2}} \left(1 - \frac{f}{f_H}\right)^{\frac{3}{2}}}\, ds \tag{4.24}$$

In the equatorial plane, equation 4.24 can be approximated as

$$t(f) = \frac{f_{peq} S_1}{c f^{\frac{1}{2}} f_{heq}^{\frac{1}{2}} \left(1 - \frac{f}{f_{heq}}\right)^{\frac{3}{2}}} \tag{4.25}$$

since f_{peq} and f_h vary slowly with path length in the equatorial plane, where f_{peq} is the plasma frequency at the equator. The path length S_1 is roughly proportional to L, $f_{heq} \propto L^{-3}$, and at the nose frequency the quantity inside parentheses

$$1 - \frac{f_n}{f_{heq}}$$

is nearly constant, so that

$$t_n(f_n) \propto \left(\frac{n_{eq} L^5}{f_n}\right)^{\frac{1}{2}}$$

where n_{eq} is the electron concentration at the equator. Therefore,

$$n_{eq} = K_{eq}\frac{f_n t_n^2}{L^5} \tag{4.26}$$

where K_{eq} is a constant. The equatorial electron density n_{eq} is proportional to the electron density at 1000km altitude n_1,

$$n_1 = K_1\frac{f_n t_n^2}{L^5} \tag{4.27}$$

where K_1 is a constant. If we consider a cylindrical volume, or tube, of area 1 cm^2, along the length of the field line, we can calculate the tube electron content N_t for that field line.

$$N_t \propto n_{eq} Aeq S$$

Cross sectional area

$$A_{eq} \propto \frac{1}{f_{heq}} \propto L^3$$

and path length

$$S \propto L$$

then

$$N_t = K_t\frac{f_n t_n^2}{L^5} \tag{4.28}$$

where K_t is constant.

From equations 4.22 to 4.28 it can be seen that, provided K, K_{eq}, K_1 and K_t are known for the model being used, and f_n and t_n have been derived from the whistler spectrogram using Bernard's formula, all the plasma parameters can be calculated. Park [1972] calculated all of these constants for different models of the magnetosphere, and gives a graphical representation of each constant as a function of nose frequency in his report *[Park, 1972]*. Alternatively, the constants can be evaluated numerically by the general equation of the form

$$K_i = a_0 + a_1 F + a_2 F^2 + a_3 F^3 + \ldots + a_i F^i$$

where

$$F = 10 log_{10} f_n$$

and the coefficients a_0 , a_1, a_2, ..., a_i have been evaluated by Park [1972], and are given below for convenience. This numerical method of evaluating the constants is used by the FIT routines.

The table below lists the coefficients used for evaluating the constants for the DE1 model.

constant	a_0	a_1	a_2
K	3.5475	-0.47351	.065879
K_eq	65.517	-22.064	2.8976
K_t	1.5778×10^{10}	-3.5512×10^9	4.3313×10^8
K_1	388.73	93.285	-29.088

The table below lists the coefficients used for evaluating the constants for the R-4 model.

constant	a_0	a_1	a_2
K	3.0156	-.65114	.12217
K_eq	36.337	-19.974	3.3715
K_t	1.0186×10^{10}	-2.7711×10^{9}	4.3506×10^{8}
K_1	1.3347×10^{5}	-6.5024×10^{4}	7.9264×10^{3}

4.3 The Matched Filtering Technique of Enhancing Spectral Resolution of Whistlers.

The matched filtering technique, originally used for VLF whistler analysis by Bhégin and Siredey [1964], is the optimum method of improving the spectral resolution of a signal of known form in the presence of white noise. Hamar et. al. [1982] showed that the temporal resolution is improved by one order of magnitude when analysing whistlers, compared to normal scaling from spectrograms. To derive the generalised frequency response of a matched filter, we consider an input signal amplitude of the form

$$u_i(t) = s_i(t) + n_i(t)$$

where $s_i(t)$ is the input waveform and $n_i(t)$ is the input noise. The output is of the form

$$u_o(t) = s_o(t) + n_o(t)$$

and the output signal to noise ratio is

$$SNR(t) = \frac{s_o^2(t)}{n_o^2(t)}$$

The objective is to define a filter response to maximise the output SNR. If we assume the input noise is white and Gaussian with a two sided power spectral density of $G_{nn}(t) = N_o/2$ $watts/Hz$, then the optimum matched filter response is of the form

$$h_{opt}(t) = \frac{2k}{N_o} s_i(t_m - t), \quad 0 \leq t \leq T \tag{4.29}$$

where k is a constant. *[Di Franco et. al., 1968].*
Equation 4.29 shows that for a known signal $s_i(t)$ of finite duration T, the impulse response of the optimum linear filter is proportional to the input signal with reversed time axis, and is centered at time t_m. This filter is called a matched filter.

The basic proof that the matched filtering technique improves the signal to noise ratio of the signal has been described by Hamar et. al. [1982], Lichtenberger et. al. [1987] and Hamar et. al. [1990]. Here the applications of these principles, as used by the BURK program [Tarcsai et. al. - Whistler Analysis Software Package] are discussed.

A signal whose frequency varies with time can be described by the equation

$$s(t) = \cos[2\pi g(t)] \tag{4.30}$$

g(t) is a phase function varying with time, and the frequency at any time t is defined by

$$f(t) = \frac{dg(t)}{dt}$$

If $s(t)$ is a whistler, we use Bernard's formula and Park's models of the magnetosphere to calculate f_n, f_{heq}, and D_0 as before. Using equation 4.8

$$t(f) = \frac{D_0(f_{heq} - Af)}{\sqrt{f}(f_{heq} - f)} \tag{4.31}$$

the function $f(t)$ can be calculated at any time t very accurately. At a time t_0 let the frequency calculated by equation 4.31 be f_0. Then the generalised whistler waveform function is given by

$$w(t_0) = A(t_0)\cos(2\pi f_0 t_0 + \alpha) \tag{4.32}$$

where α is a phase constant and $A(t)$ is the amplitude function of the wave with time.

The phase function $g(t)$ can be obtained by integrating equation 4.3,

$$g(t_i) = \int_0^{t_i} f(t)dt$$

At a time $t + \Delta t$,

$$w(t_0 + \Delta t) = A(t_0 + \Delta t)\cos(2\pi[f_0 t_0 + \int_0^{t_0+\Delta t} f(t)\ dt] + \alpha) \tag{4.33}$$

$w(t)$ only exists for $t \geq t_n$, the time of arrival of the whistler nose frequency, so that $f(t)$ has two values at $t_n + \Delta t$, one below and one above the nose frequency.

To implement the matched filter on the whistler waveform, we select a starting frequency f_0 and a filter bandwidth Δf. The epoch of frequency f_0 is calculated by equation 4.31, and then by inverting equation 4.31 we find frequency f_1 at time $t_1 = t_0 + \Delta t$, where Δt is the sampling interval of the data. Assuming the frequency variation between f_0 and f_1 to be linear, we approximate the integral in equation 4.33 by

$$\int_{t_0}^{t_0+\Delta t} f(t)\ dt = \frac{f_0 + f_1}{2}\Delta t.$$

Then substituting this equation into equation 4.33 we get

$$w(t_0 + \Delta t) \approx A(t_0 + \Delta t)\cos\left(2\pi[f_0 t_0 + \frac{f_0 + f_1}{2}\Delta t] + \alpha\right) \tag{4.34}$$

The above procedure is repeated for $f_0 + 2\Delta t$, $f_0 + 3\Delta t$, etc. The values of the whistler waveform are similarly found for $t_0 - i\Delta t$, provided $(t_0 - i\Delta t) \geq t_n$, the nose frequency arrival time. This procedure is repeated for Δt until the entire bandwidth Δf has been covered.

The filter output is of the form

$$s_0(t) = const.\ sinc[\Delta f(t - t_0)]\cos[2\pi f_0(t - t_0)] \tag{4.35}$$

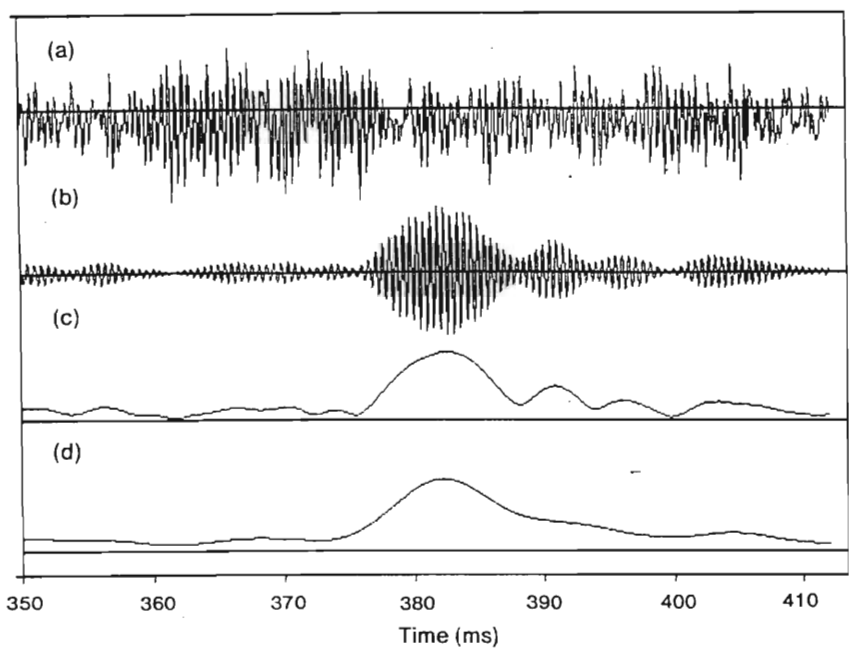

Figure 4.3: The procedure of matched filtering in determining the arrival times of the whistler components for a particular frequency. (a) Digitized waveform. (b) Matched filter output. (c) Output envelope. (d) Smoothed output envelope (Hilbert transform).

where $sinc(x) = \sin(\pi x)/(\pi x)$.
The output of this filter is smoothed by a Hilbert transform to remove the high frequency cosine component, and the maxima of the output envelope is taken as the arrival time of the whistler for that particular frequency. A graphical representation of this process is given in Figure 4.3.

To obtain the fine structure of the entire whistler trace, an iterative process is carried out on the filter centre frequency, increasing it by an amount specified in a data file used by the matched filtering program BURK. Other matched filter control parameters that can be specified in this data file are the filter start center frequency, the filter bandwidth, and the number of frequencies that are to be filtered (so setting the stop frequency).

It is found by Hamar et. al. [1990] that a filter bandwidth of 200 Hz is optimum for good separation of closely spaced whistler components and sensitivity to dispersion differences. The spectral resolution at this filter bandwidth is about $1.4/\Delta f$, where Δf is the filter bandwidth. This means that whistler components greater than 7 ms apart can be identified.

The photograph in Figure 4.4 shows the VGA screen output after matched filtering. The X - axis has been transformed so that the theoretical travel time t_0

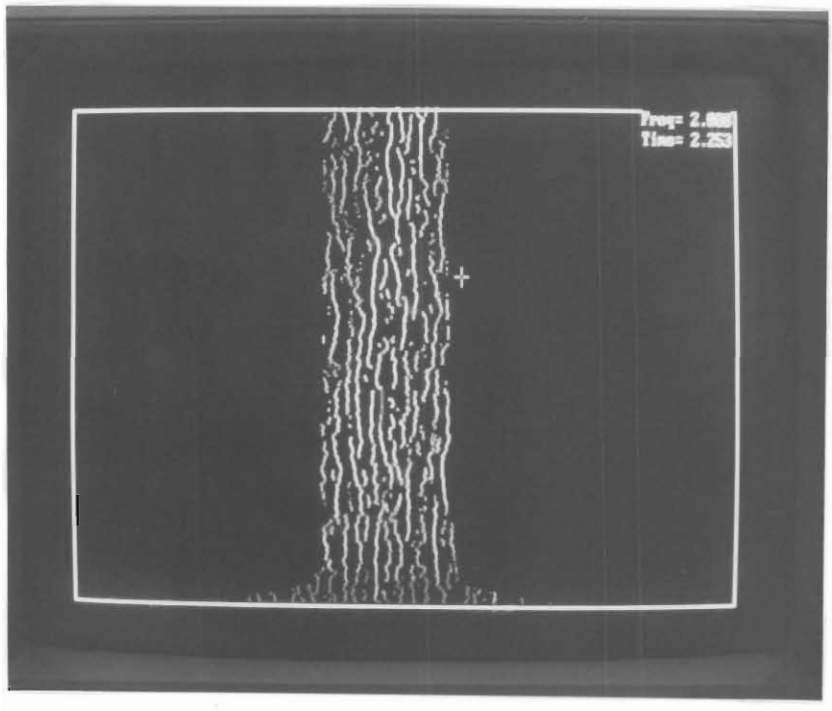

Figure 4.4: Photograph of the VGA screen output of the CELWPIX program, used to display the spectral output of the BURK program, showing the fine structure of a whistler.

computed from equation 4.31 has been subtracted from the time delay at each frequency. A perfect theoretical whistler using this method of representation would appear as a straight line parallel to the Y - axis. From the photograph it can be seen that this method is very effective when analysing the fine structure of whistlers.

Chapter 5

Similarities in Fine Structure of Whistlers Observed Simultaneously at Sanae and Halley Bay Stations, Antarctica.

5.1 Whistlers Arriving at Sanae and Halley Bay

Friedel (1987) has observed nose whistlers arriving simultaneously at Sanae and Halley Bay stations in Antarctica. These whistlers have similar nose frequencies and have propagated along similar L-values, which strongly indicates that they would have experienced very similar propagation conditions along the path. Similarities in fine structure of these whistlers are thus to be expected, especially since the path difference between the two stations is only of the order of 1000 km, or even less if the duct exit position is between the stations.

Avdas spectrograms *[Smith et. al., 1987]* of these whistler are shown in Figures 5.1 to 5.6, and nose frequencies and L-values of propagation are shown in Table 5.1.

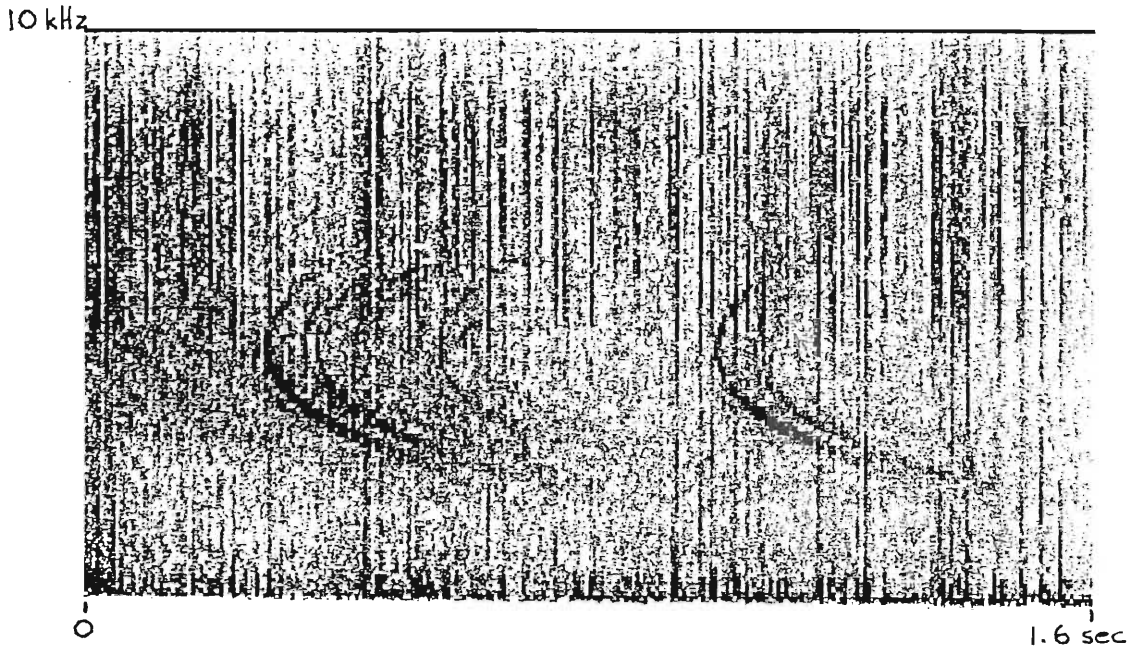

Figure 5.1: Spectrogram of whistler observed at Sanae on Day 149 05:20:36 1985

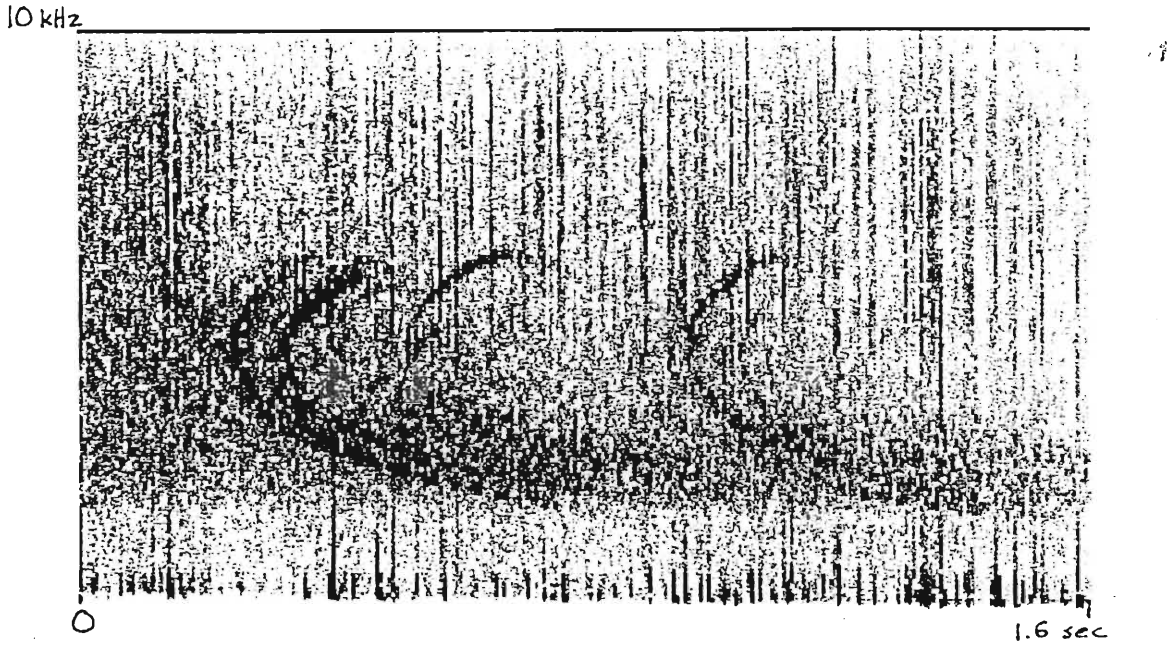

Figure 5.2: Spectrogram of whistler observed at Halley Bay on Day 149 05:20:36 1985

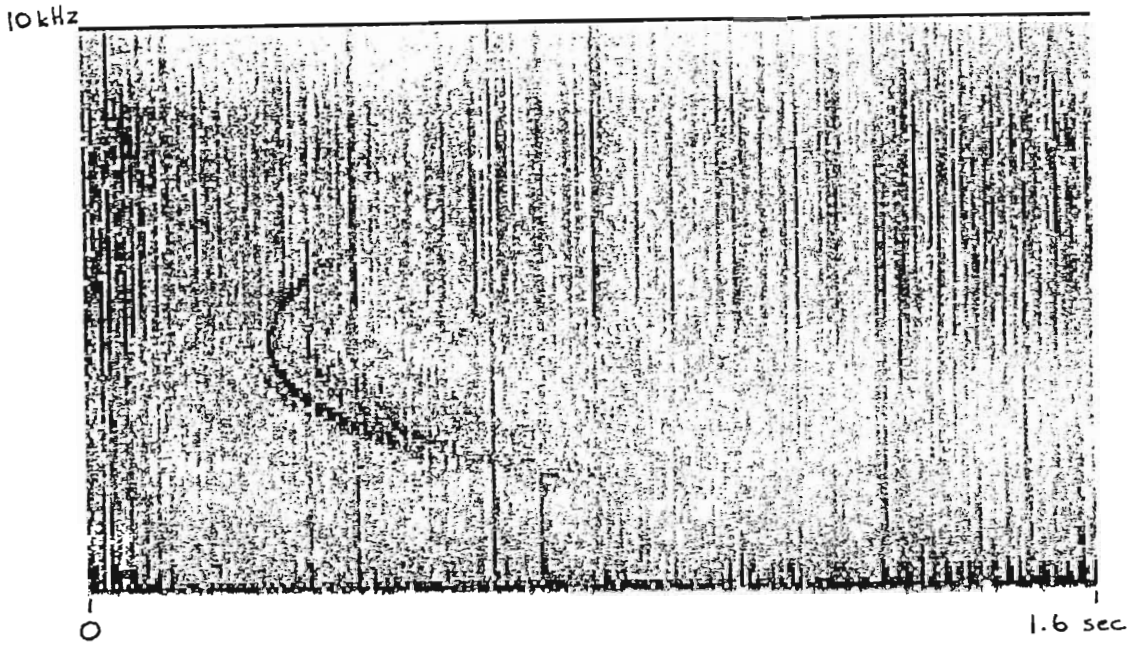

Figure 5.3: Spectrogram of whistler observed at Sanae on Day 149 05:20:44 1985

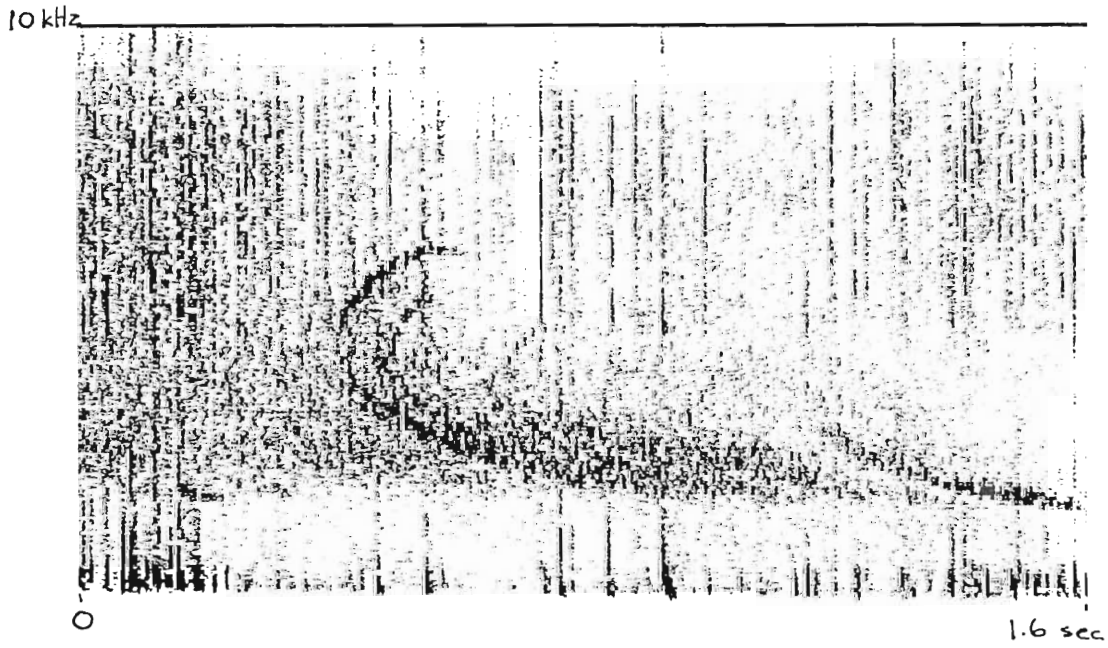

Figure 5.4: Spectrogram of whistler observed at Halley Bay on Day 149 05:20:44 1985

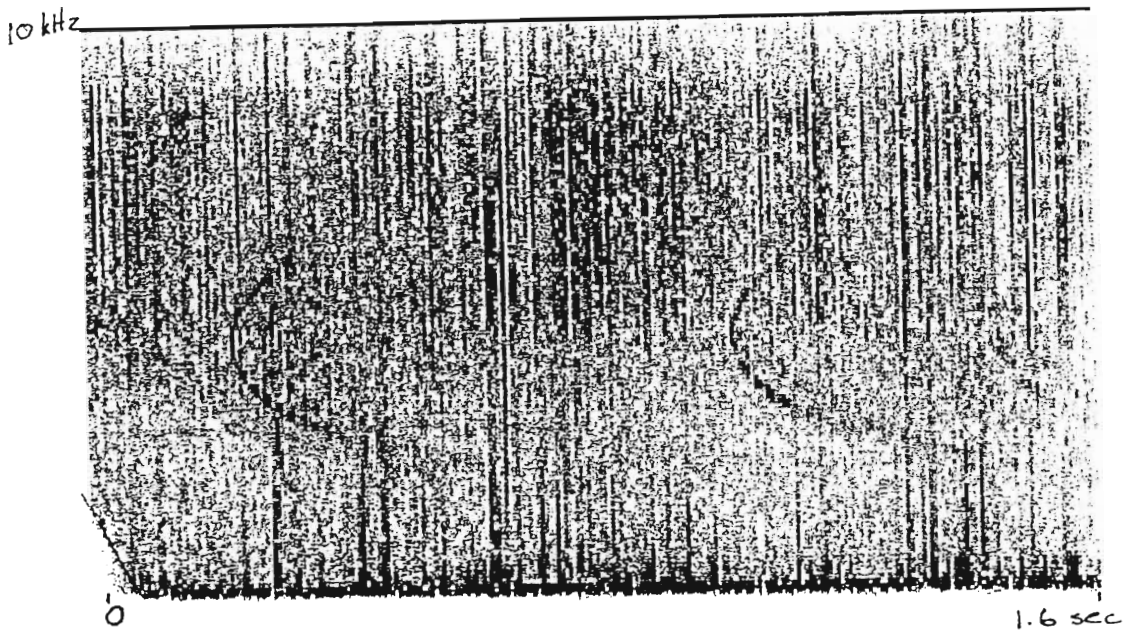

Figure 5.5: Spectrogram of whistler observed at Sanae on Day 149 05:20:49 1985

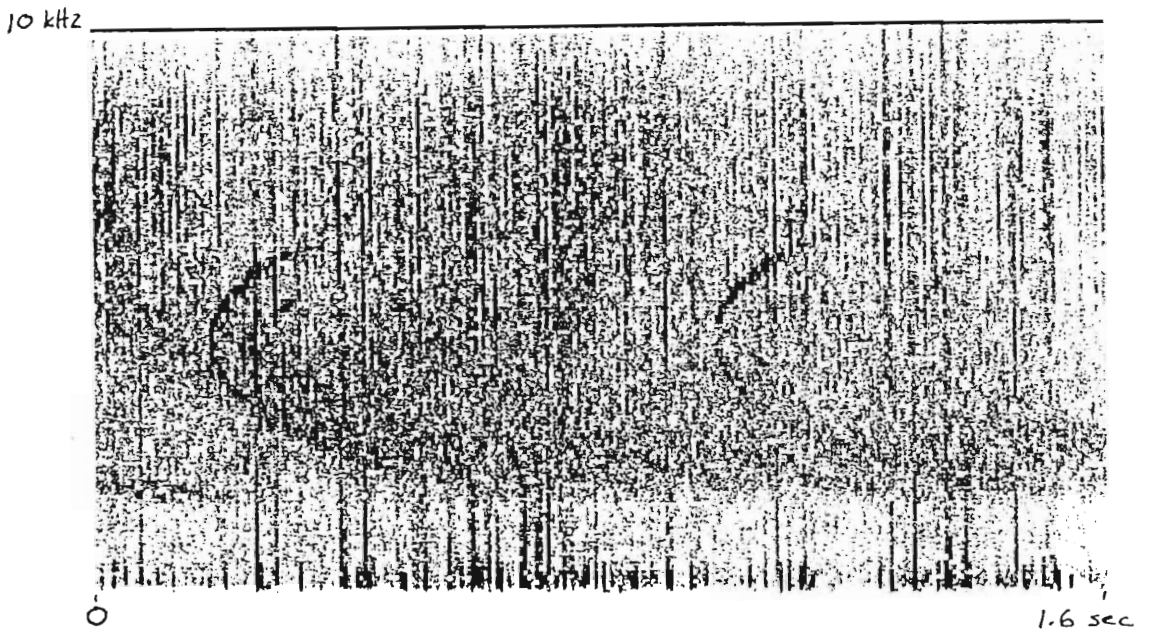

Figure 5.6: Spectrogram of whistler observed at Halley Bay on Day 149 05:20:49 1985

Station	time	f_{nose} (Hz)	L-value	dispersion ($s^{\frac{1}{2}}$)
Halley Bay	05:20:36	4247	4.25	103.8
Sanae	05:20:36	4203	4.24	122.0
Halley Bay	05:20:44	4202	4.27	108.8
Sanae	05:20:44	4321	4.23	119.2
Halley Bay	05:20:49	4330	4.22	107.0
Sanae	05:20:49	4326	4.22	124.1

Table 5.1 Nose frequencies, L-values and dispersion of whistlers arriving at Sanae and Halley Bay.

5.2 Fine Structure Analysis of Whistlers

The matched filtering technique *[Hamar et. al., 1982]* has been used to look at the fine structure of the whistlers shown in Figures 5.1 to 5.6. The data, which is recorded on Revox audio tape, is very noisy, and as a result several attempts at matched filtering were necessary using different filter bandwidths and incremental frequency steps for the whistler structure to be evident despite the noise. It has generally been found that a large filter bandwidth of 400 Hz and a small incremental frequency step of 2 Hz yielded best results, although the time taken to process each whistler is of the order of 60 to 90 minutes on a 80486 PC, and the output file generated is very large (700 kbyte to 1 Mbyte).

Photographs of the VGA screen showing the fine structure of the Sanae/Halley Bay whistlers are shown in Figures 5.7 to 5.12. An overlay on the photographs highlights the main whistler traces, which are not easily distinguishable from the noise in some places.

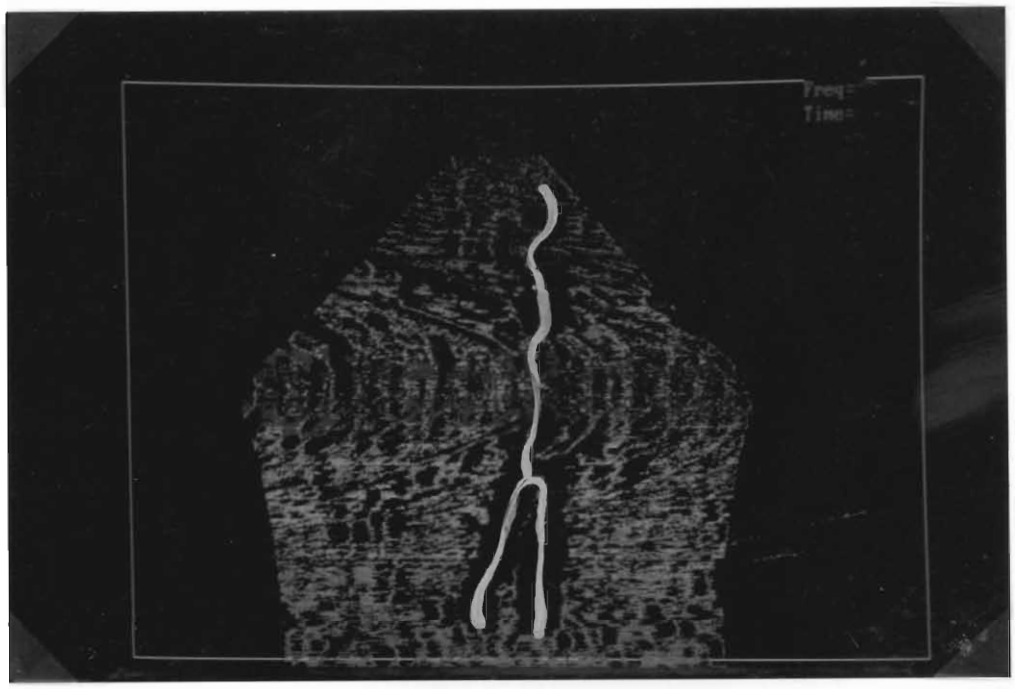

Figure 5.7: Photograph of the fine structure of a whistler arriving at Sanae at 05:20:36. Filter bandwidth of 300 Hz, frequency step of 2 Hz and width of filter window of 100 points was used.

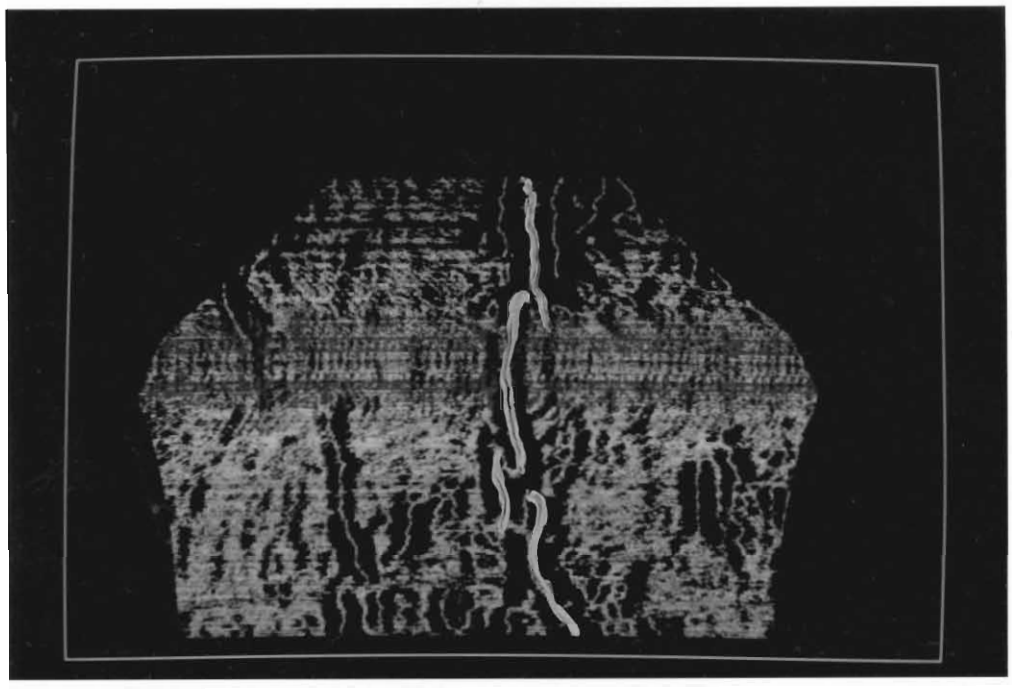

Figure 5.8: Photograph of the fine structure of a whistler arriving at Halley Bay at 05:20:36. Filter bandwidth of 400 Hz, frequency step of 1 Hz and width of filter window of 200 points was used.

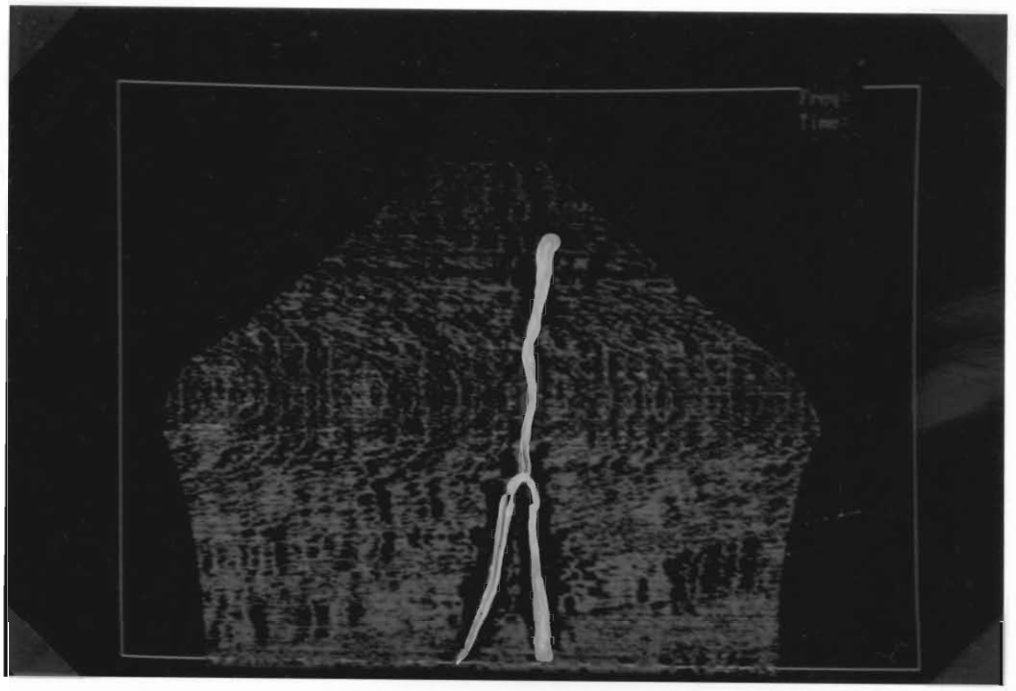

Figure 5.9: Photograph of the fine structure of a whistler arriving at Sanae at 05:20:44. Filter bandwidth of 400 Hz, frequency step of 2 Hz and width of filter window of 100 points was used.

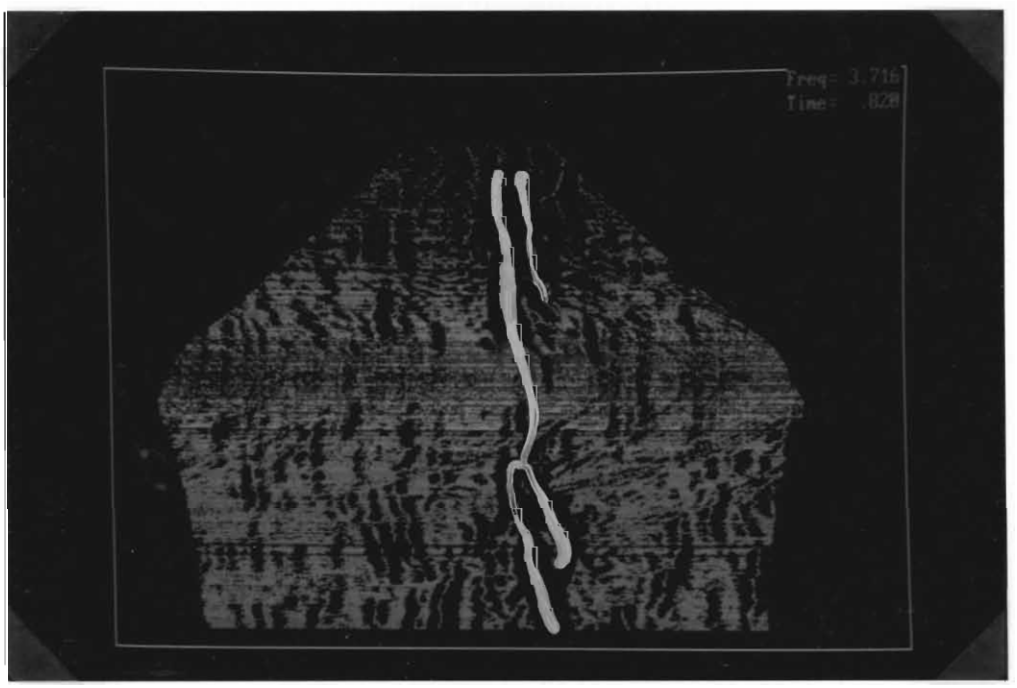

Figure 5.10: Photograph of the fine structure of a whistler arriving at Halley Bay at 05:20:44. Filter bandwidth of 400 Hz, frequency step of 2 Hz and width of filter window of 200 points was used.

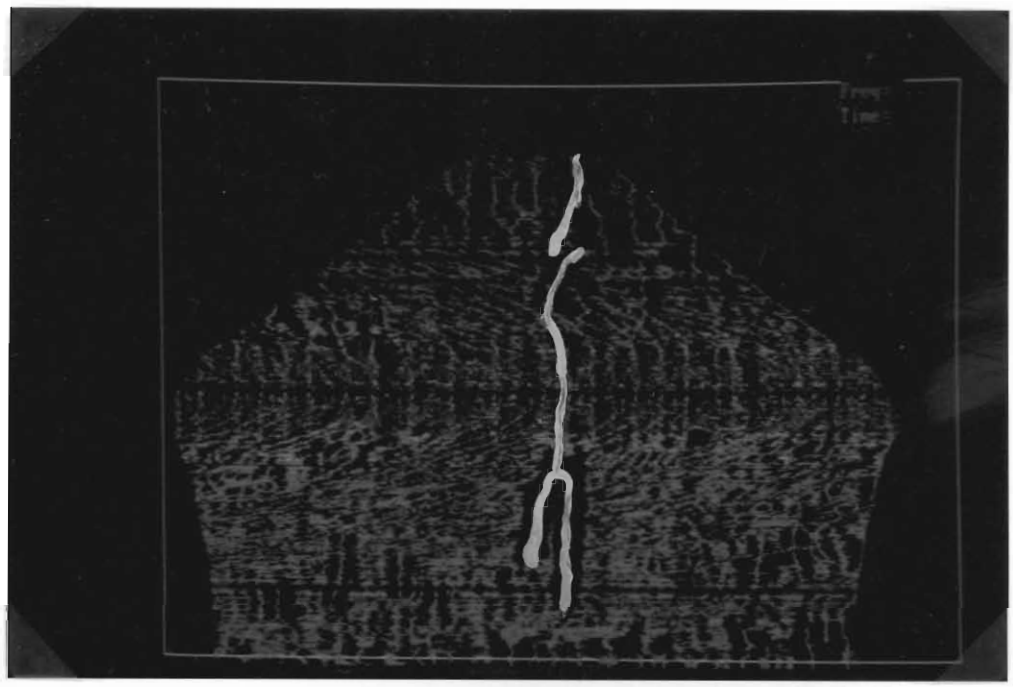

Figure 5.11: Photograph of the fine structure of a whistler arriving at Sanae at 05:20:49. Filter bandwidth of 400 Hz, frequency step of 2 Hz and width of filter window of 200 points was used.

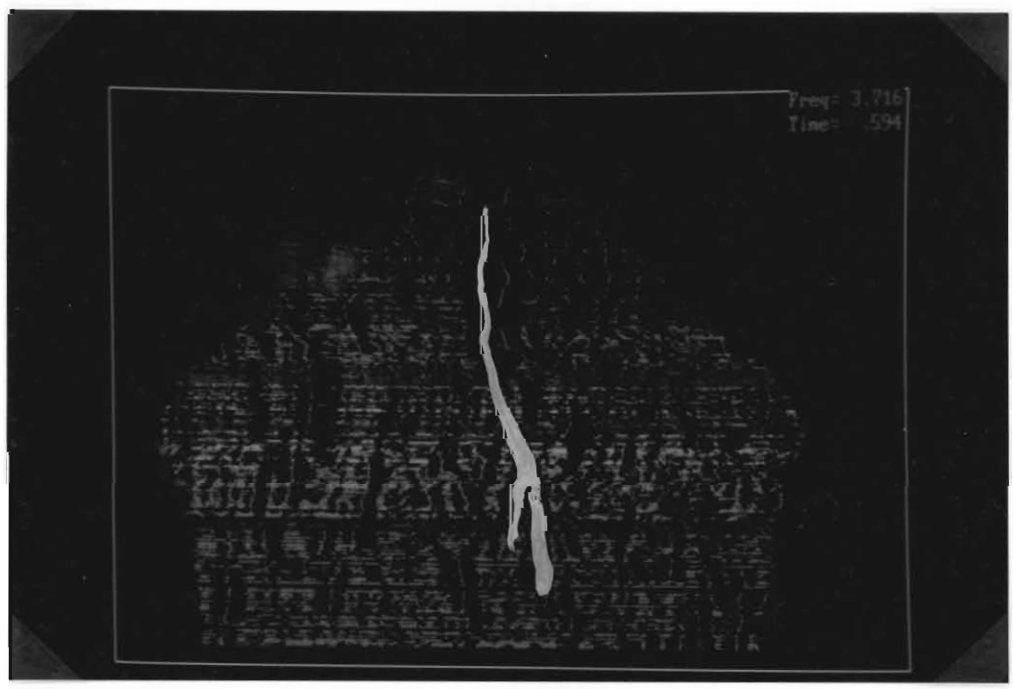

Figure 5.12: Photograph of the fine structure of a whistler arriving at Halley Bay at 05:20:49.Filter bandwidth of 400 Hz, frequency step of 5-Hz and width of filter window of 200 points was used.

From Table 5.1, it is seen that all of the whistlers analysed travelled along the L = 4.22 to L = 4.27 field line. Another whistler arriving at Halley Bay on the same day, but a few seconds later, at 05:20:58, and having propagated at a slightly lower L-value of L = 4.01, was analysed for fine structure. The spectrogram of the whistler is shown in Figure 5.13 and its fine structure in the photograph Figure 5.14.

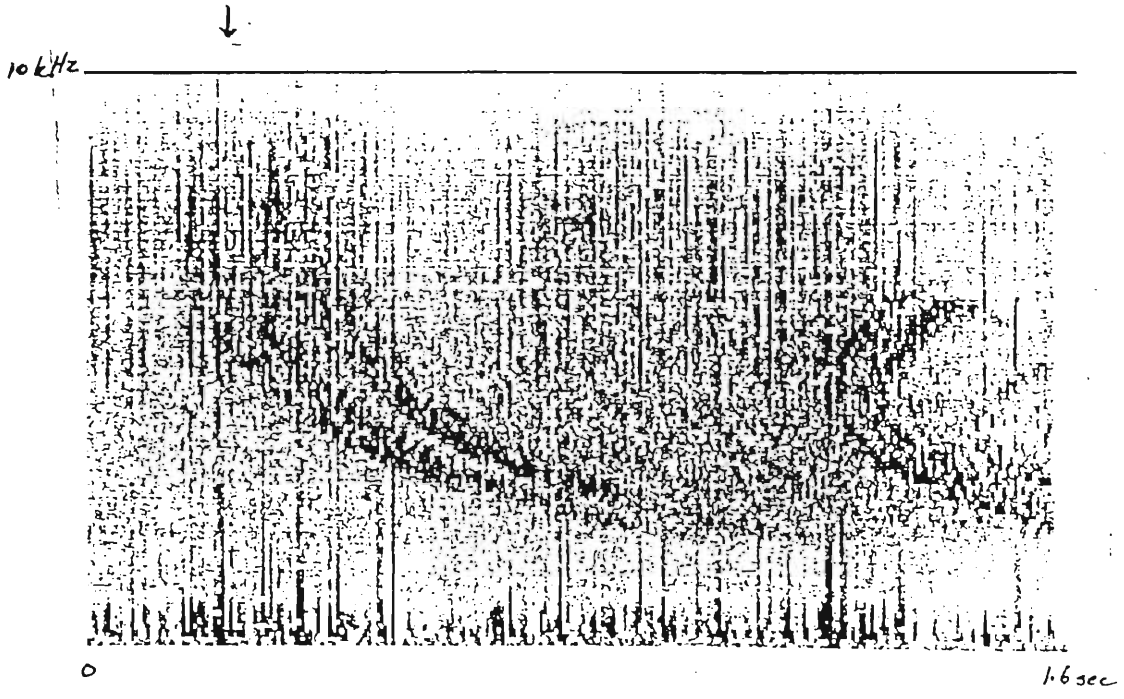

Figure 5.13: Spectrogram of whistler arriving at Halley Bay on day 149 at 05:20:58 1985. L-value of propagation is L=4.01.

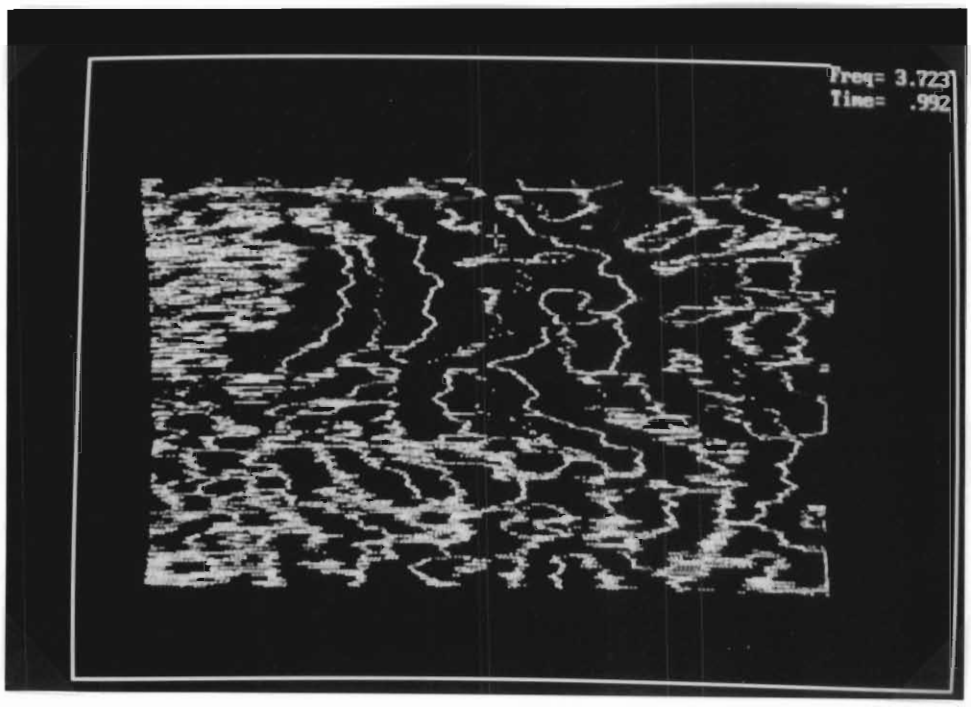

Figure 5.14: Photograph of the VGA screen showing the fine structure of the whistler arriving at Halley Bay on day 149 05:20:58 1985. Filter bandwidth of 200 Hz, frequency step of 2 Hz and a filter window width of 300 points was used.

5.3 Discussion of Results - Possible Mechanisms for Observed Trace Splitting.

From the photographs of the fine structure in Figures 5.7 to 5.12 similarities in the fine structure of 5 of the 6 whistlers can be seen. Not only do simultaneous whistlers at the two stations show the same structure, but there appears to be no short term temporal variation in the propagation conditions, since similarities exist in all three whistlers arriving at Sanae in the 13 second time interval, and in two of the three whistlers arriving at Halley Bay. The whistler arriving at Halley Bay at 05:20:36 showed different fine structure.

A definite splitting of the whistler trace occurs at frequency 3.720 kHz in the 5 similar whistlers. Two traces are visible below this frequency, diverging with decreasing frequency, and corresponding to increased travel time differences between the two traces. This is most noticeable in the Sanae whistlers. Figures 5.15 and 5.16 quantify the travel time differences with frequency, which converge to zero at frequency 3.720 kHz. The Sanae whistlers exhibit an almost linear relationship between the time delay and frequency, given by the equation

$$\Delta t = -12f + 44.4$$

where t is measured in milliseconds and f in kHz.

It is seen that the whistler of Figure 5.13 that propagated along the L=4.01 field line does not display the same fine structure. The trace splitting seen in the 5 whistlers seems to be a function of the L=4.22 to L=4.27 ducts, which does not extend to lower L-values.

Several mechanisms for trace splitting and propagation time differences have been considered.

5.3.1 Lower Hybrid Resonance Reflection.

Lower hybrid resonance (LHR) reflection is a mechanism by which a wave propagating in a plasma is reflected when the frequency of the wave is equal to the LHR frequency of the plasma at that altitude. The possibility of this mechanism being responsible for the observed dual traces of the whistlers below 3.720 kHz is investigated, the proposed explanation being that the whistler travels along a duct parallel with the field line, and when it reaches the boundary of the earth - ionosphere waveguide a portion of the energy is reflected in the normal manner for whistler mode waves. This energy then propagates upwards, and is re-reflected back down by a LHR reflection, different frequencies being reflected from different altitudes where the wave frequency equals the LHR frequency. There appears to be a maximum frequency that can be re-reflected, this being 3.720 kHz, above which no more LHR reflection occurs.

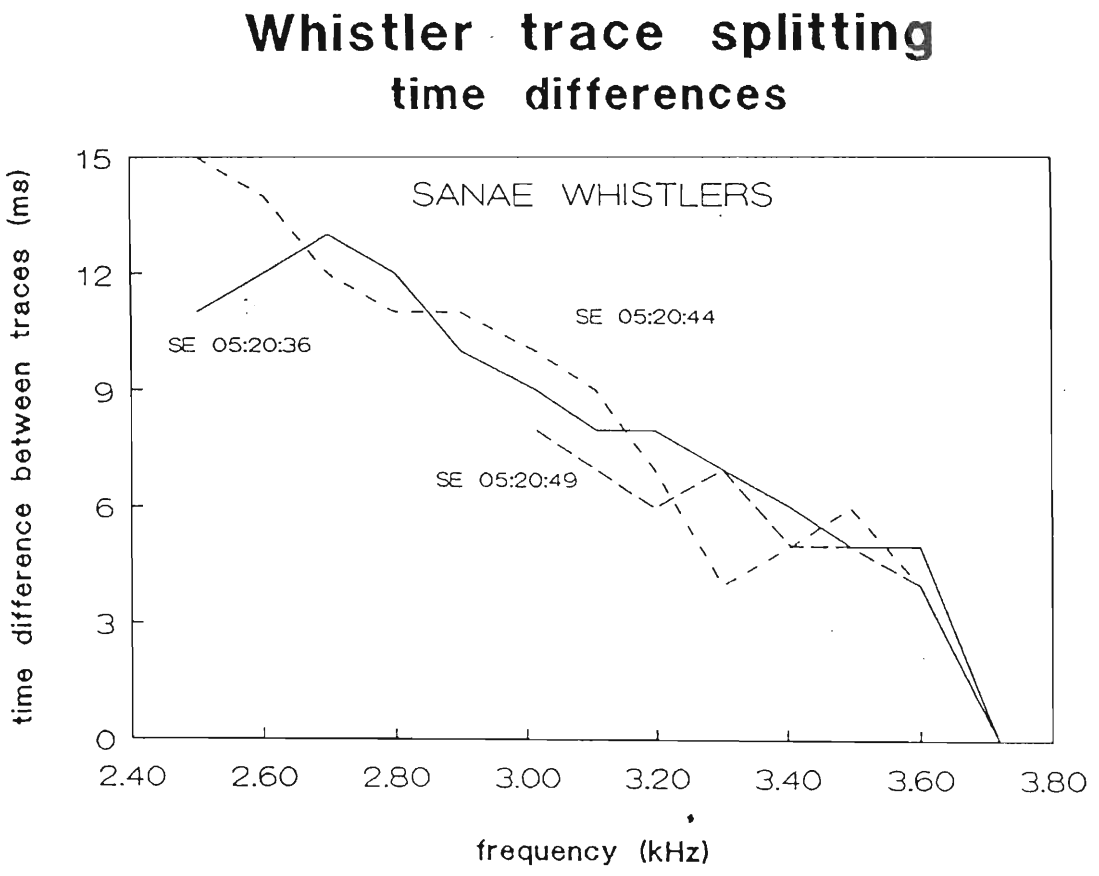

Figure 5.15: Travel time differences of the dual whistler trace below frequency 3.720 kHz of the three Sanae whistlers.

LHR noise bands were first observed on the Alouette satellites *[Barrington et. al., 1963]*, and Brice and Smith (1965) correlated these noise bands with the LHR frequency of the plasma in which the signal was propagating. Storey and Cerisier (1967) and Cerisier (1968) proposed the mechanisms by which these downward travelling waves could be reflected when the wave frequency equals the LHR frequency at that altitude. Reflection depends on the refractive index surface of a particular frequency, shown for three frequency regimes in Figure 5.17. For frequencies near the LHR frequency, the surface closes at infinity for wave normal angles of 90 degrees, and propagation with wave normal angles greater than 90 degrees can occur, ie. reflection of the wave.

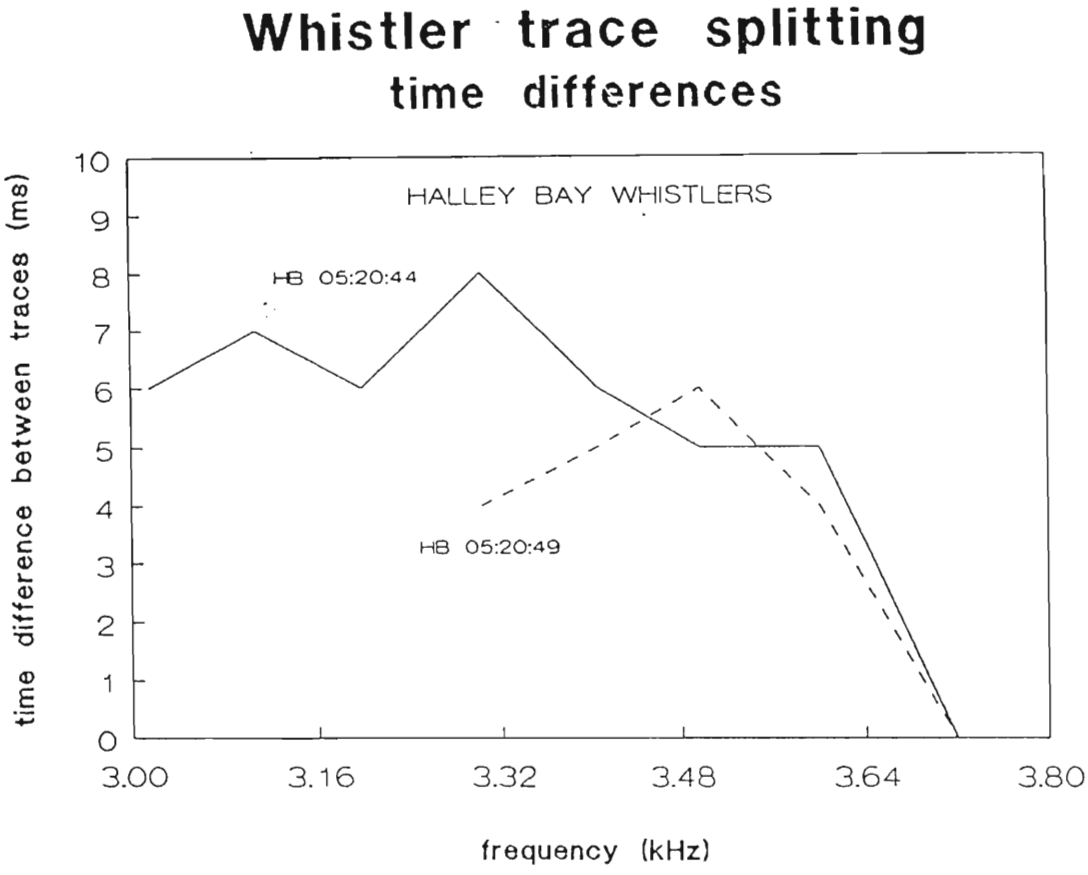

Figure 5.16: Travel time differences of the dual whistler trace below frequency 3.720 kHz of the two Halley Bay whistlers which show trace splitting.

The LHR frequency is given by

$$\frac{1}{f_{LHR}^2} = \left(\frac{1}{f_0^2} + \frac{1}{f_H^2}\right)\frac{m_p}{m_e}M \tag{5.1}$$

$$1/M = \Sigma\alpha_i/m_i$$

where f_0 = plasma frequency
f_H = electron gyrofrequency
m_p = proton mass
m_e = electron mass
M = effective mass

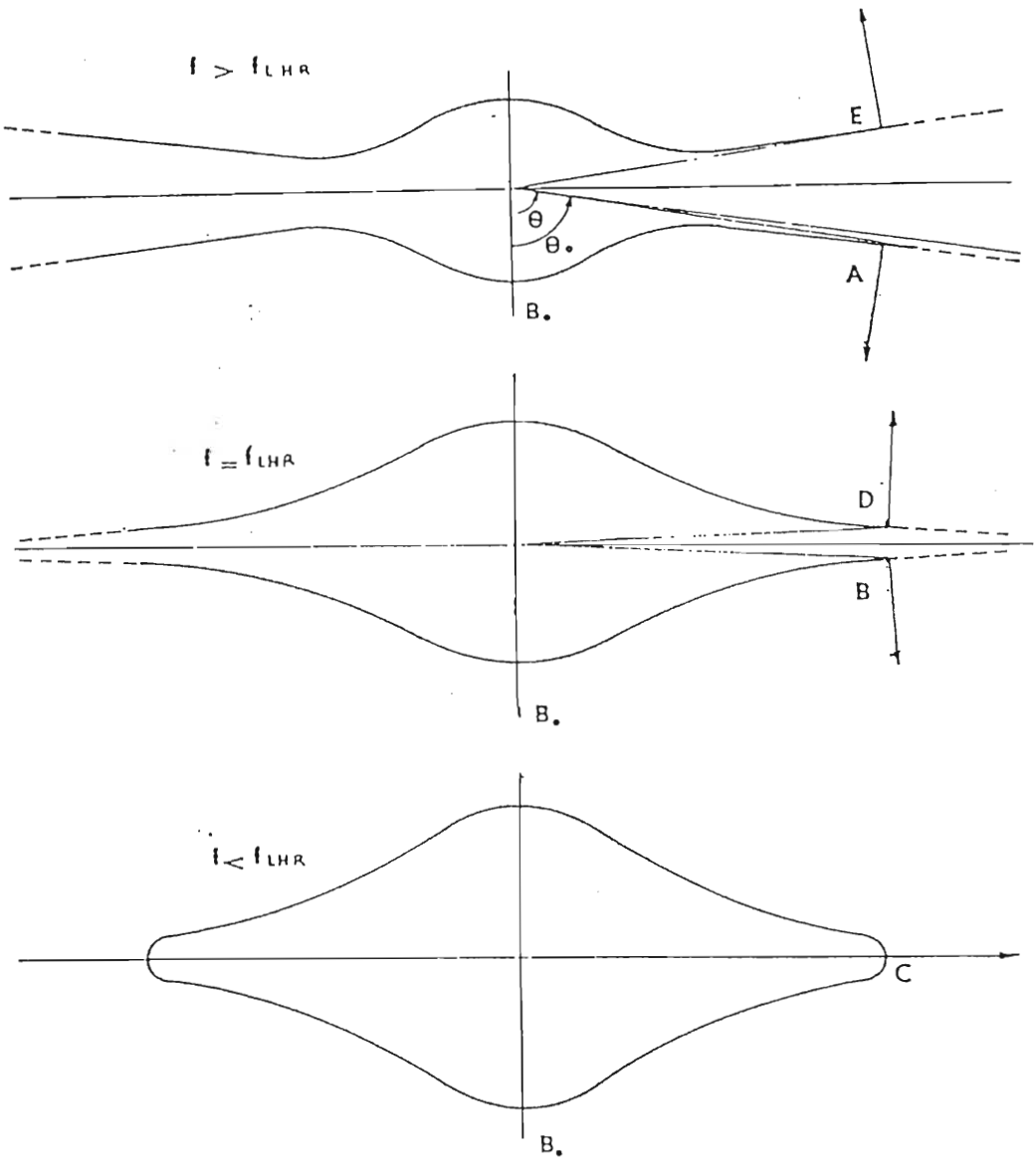

Figure 5.17: Refractive index surfaces for frequencies below, equal to and above the lower hybrid resonance frequency. The surface 'closes' at infinity for frequency $f = f_{LHR}$, and reflection is possible.

α_i = fractional composition of i'th ionic species
m_i = relative mass of i'th ionic species.

Cerisier (1968) has quoted LHR frequencies of 7.8 kHz at 500 km altitude, while McChesney and Hughes (1983) have found slightly lower LHR frequencies of between 4 - 5 kHz at 1400 km altitude while studying noise bands on data from the ISIS1 and ISIS2 satellites. Analysis of the photographs of Figures 5.7 to 5.12 shows trace splitting at 3.720 kHz, seemingly too low to be caused by a LHR reflection. Values of the LHR frequency were derived using various ionospheric models proposed by the URSI/Cospar task group on the International Reference Ionosphere (1990). These altitude profiles are shown in Figures 5.18 and 5.19 and the calculations to derive these graphs are shown in Appendix B.

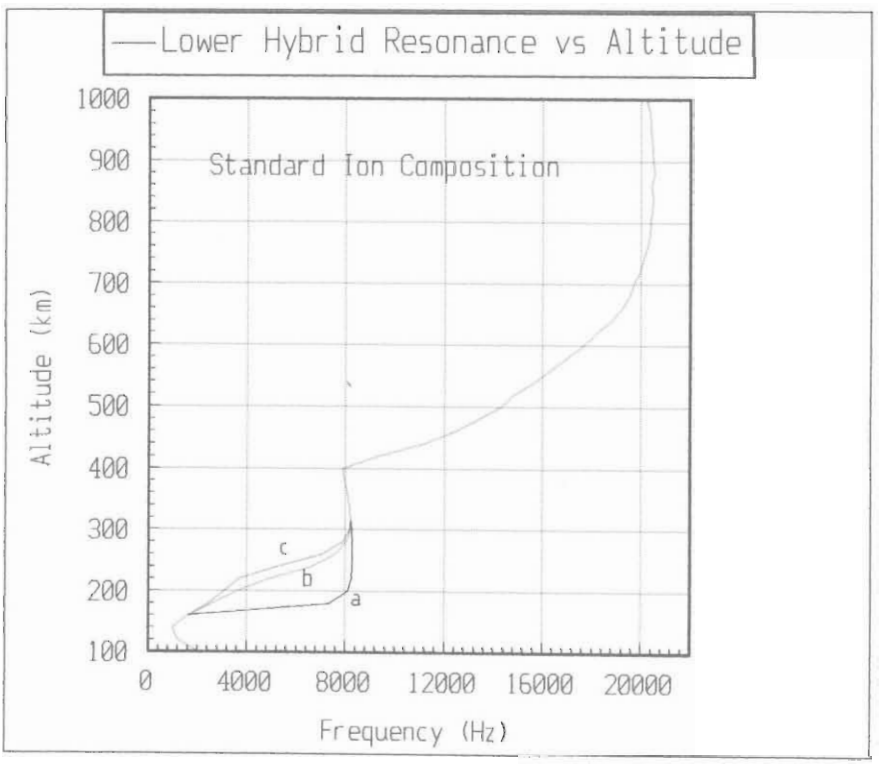

Figure 5.18: Lower Hybrid Resonance versus Altitude for a standard ion composition model and (a) Lay function electron density (b) Standard electron density (c) Gulyaeva electron density models.

As can be seen from Figures 5.18 and 5.19 LHR frequencies of as low as about 1 kHz are possible at altitudes of about 140 km, going up to about 20 kHz at 1000 km altitude. It is seen from Figures 5.15 and 5.16 that the travel time differences are 0 to 15 milliseconds, which for a wave travelling at the speed of light corresponds to a path length of 0 to 4500 km. Since the wave is travelling in a medium with a finite refractive index, its velocity is lower, and path lengths of

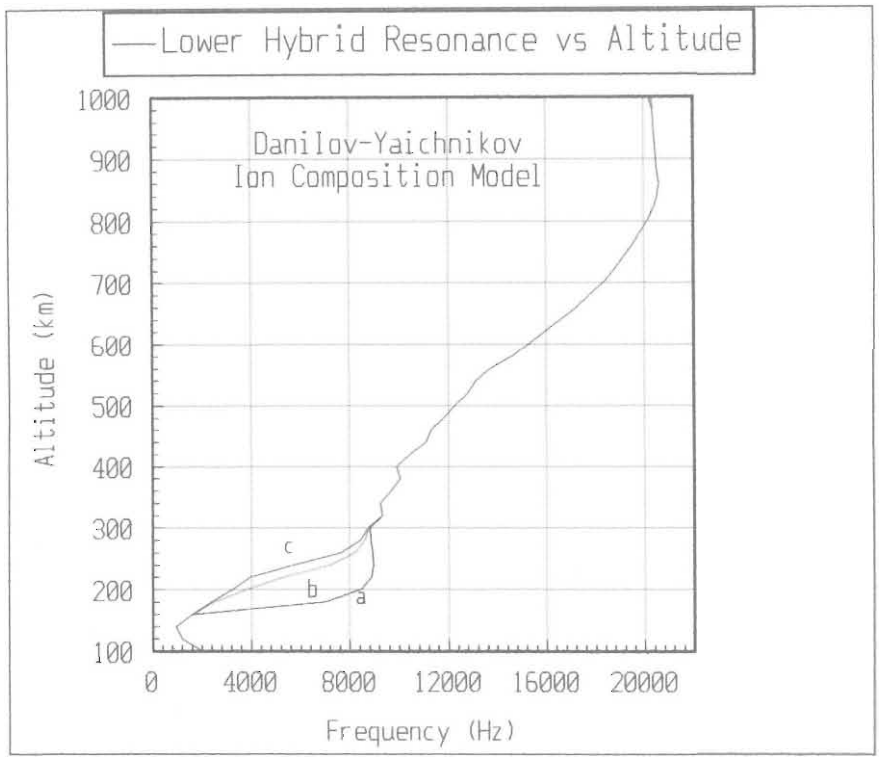

Figure 5.19: Lower Hybrid Resonance versus Altitude for the Danilov-Yaichnikov ion composition model and (a) Lay function electron density (b) Standard electron density (c) Gulyaeva electron density models.

the order of hundreds of kilometres are to be expected for a delay of this order of magnitude. The proposed reflecting mechanism requires that the wave travel upwards to the altitude where the LHR frequency equals the wave frequency, and then back down to the receiver on the ground, so that the altitude to which it travels is half the path length required for the 15 ms delay. Thus for the observed reflection of frequencies between 2.5 and 3.7 kHz, it is possible that a LHR reflection took place. Considering the LHR frequencies predicted by models (b) and (c) in Figures 5.18 and 5.19 the altitude from which the different frequencies would reflect increases with increasing frequency, hence increasing the time delay between traces at higher frequencies, while the opposite is seen to be true. Model (a) has a reasonably flat frequency - altitude response in the frequency range of interest, which would correspond to constant time delay with frequency. So far the effect of a change in group refractive index with frequency has been disregarded, which would make the group velocity of the waves frequency dependent, and could compensate for the above discrepancies in reflection altitude. How-

ever, due to the travel time differences decreasing with increasing frequency, it is thought that a LHR reflection is not a satisfactory mechanism to explain the trace splitting in this case.

5.3.2 Other possible mechanisms of whistler trace splitting

The possibility was investigated that the dual traces below 3.7 kHz were caused by subprotonospheric propagation. These subprotonospheric whistlers are whistlers originating from the same lightning stroke, and that have several components, which are associated with wave packets entering the ionosphere at different altitudes and travelling along different paths. Raghuram (1975) has observed travel time delays of the order of 150 ms at frequencies of about 800 - 1000 Hz on data from the OGO 4 satellite. The mechanism he proposes is that wave packets from the same lightning stroke enter the ionosphere at different places, and are reflected back and forth between 100 and 1000 km by electron density gradients to manifest themselves as a subprotonospheric whistler. Walker (PHd thesis) has observed delays of 70-80 ms at 3.5 kHz and of 110-140 ms at 2.5 kHz. The delays observed are an almost an order of magnitude larger than those experienced in the Sanae and Halley Bay whistlers, so it is unlikely that the trace splitting is the manifestation of a subprotonospheric whistler at lower frequencies.

Strangeways (1986) has proposed mechanisms whereby whistler waves can escape from narrow ducts when the width of the duct is equal to the wavelength of a particular frequency of the whistler energy, and referring to Figure 2.8 it is seen that the lowest frequencies escape from the duct first since they have the largest wavelength, as described in chapter 2. A wave travelling outside of the duct would have a greater group velocity due to the lower plasma density. Since the two traces below 3.7 kHz are of the same amplitude, as shown in Figures 5.7 to 5.12, it is proposed that about half of the wave energy escapes from the duct when the duct width is equal to the wavelength, as described by Strangeways, the rest of the energy at that frequency continues to propagate trapped by the duct. The lower frequencies would escape first, which would result in a larger time difference between traces, as is seen from Figures 5.15 and 5.16. It is difficult in this case to predict an order of magnitude for the time differences, but the observed average of about 7 ms seems reasonable. The higher frequencies (above 3.7 kHz) continue to propagate along the duct, since the duct width remains greater that their wavelength.

Lichtenberger et. al. (1991) have observed whistler doublets aboard the ACTIVE satellite seperated by about 80 ms, which they have interpreted as ducted whistlers escaping at high altitude from the duct and reaching the satellite directly from above or after reflection from the ionosphere below. An alternative interpretation is that the energy travelled in two different whistler modes with slightly different group velocities. This theory could hold true in the case of the

observed trace splitting at Sanae and Halley Bay, but in this case only a range of frequencies could propagate in these two modes, those below 3.7 kHz.

5.3.3 Frequency dependant effect of decreasing duct enhancement at the lower end of the path.

Consider a wave with wave normal angle θ_0 to the magnetic field direction, propagating along a duct of enhanced plasma density in the whistler mode, as shown in Figure 5.20. The wave being trapped by the duct means that the wave normal angle at the edge of the duct is zero, the wave is being reflected back into the duct.

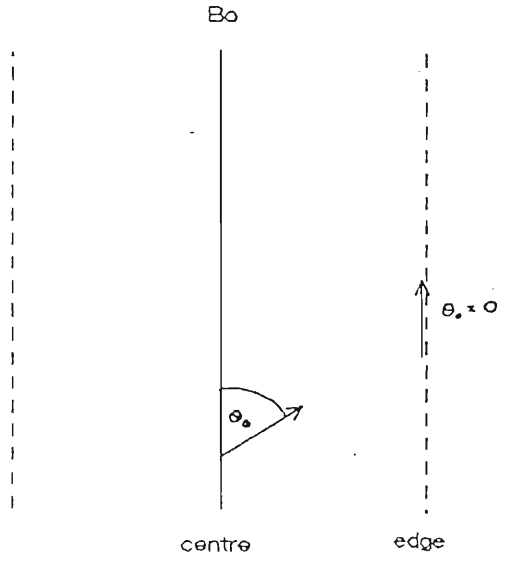

Figure 5.20: Wave normal angle direction of a wave at the centre and edge of a duct for a wave trapped by the duct.

If n_c and n_e are the refractive indicies at the centre and edge of the duct respectively, then by Snells law

$$n_c \cos\theta_0 = n_e \tag{5.2}$$

The phase refractive index is given by

$$n^2 = \frac{\omega_0^2}{\omega(\omega_H \cos\theta_0 - \omega)}$$

Substituting into equation 5.2 we get

$$\cos^2\theta_0 = \frac{n_e^2}{n_c^2} = \frac{\omega_{0e}^2}{\omega(\omega_H - \omega)} \frac{\omega(\omega_H \cos\theta_0 - \omega)}{\omega_{0c}^2}$$

$$\cos^2\theta_0 = \frac{\omega_{0e}^2}{\omega_{0c}^2}\frac{\omega_H\cos\theta_0\left(1-\frac{\omega}{\omega_H\cos\theta_0}\right)}{\left(1-\frac{\omega}{\omega_H}\right)}$$

$$\cos\theta_0 = \frac{N_e}{N_c}\frac{\left(1-\frac{\omega}{\omega_H\cos\theta_0}\right)}{1-\frac{\omega}{\omega_H}}$$

where N_c and N_e are the plasma densities at the centre and edge of the duct respectively. Using a binomial expansion of the denominator to first order, and disregarding second order terms,

$$\cos\theta_0 = \frac{N_e}{N_c}\left[1-\frac{\omega}{\omega_H}\left(\frac{1}{\cos\theta_0}-1\right)\right]$$

$$\frac{N_c}{N_e} = \frac{1}{\cos\theta_0}\left[1-\frac{\omega}{\omega_H}\left(\frac{1}{\cos\theta_0}-1\right)\right] \tag{5.3}$$

As can be seen from equation 5.3 the propagation of the wave in a duct of enhanced plasma density with gaussian distribution about a field line is frequency dependant, the higher frequencies requiring a smaller percentage density enhancement for propagation, and as a result the higher frequencies are confined to a narrower region of the duct (see Figure 5.21). The lower frequencies have a longer path length in the duct and thus a longer travel time. The whistler therefore exhibits increased dispersion, because of this effect, suggesting that it is travelling on a higher L-shell than it actually is. Substituting into the above equation values of θ_0, the frequency dependance of the enhancement is more clearly seen (see table 5.2 and 5.3).

For $\theta_0 = 30\,\text{deg}$:

$$\frac{N_c}{N_e} = 1.155\left[1-\frac{\omega}{\omega_H}\times 0.155\right]$$

frequency ω/ω_H	enhancement N_c/N_e
0.5	1.065
0.25	1.11
0.125	1.13
0.0625	1.14

Table 5.2 Plasma enhancement required for trapping at $\theta_0 = 30\,\text{deg}$ for various frequencies.

For a higher wave normal angle, $\theta_0 = 60\,\text{deg}$:

$$\frac{N_c}{N_e} = 2.0\left[1-\frac{\omega}{\omega_H}\right]$$

frequency ω/ω_H	enhancement N_c/N_e
0.5	1.0
0.25	1.5
0.125	1.75
0.0625	1.875

Table 5.3 Plasma enhancement required for trapping at $\theta_0 = 60\,\text{deg}$ for various frequencies.

The electron gyrofrequency is given by

$$f_H = f_{H0}\left(\frac{R_0}{R}\right)^3\left(1 + 3\sin^2\Lambda\right) \tag{5.4}$$

where Λ is the geomagnetic latitude, and f_{H0} the gyrofrequency at the earths surface, 880 kHz.

The minimum electron gyrofrequency along the propagation path of the whistlers (L = 4.25) is 11.46 kHz, so that the highest frequency that will propagate in an enhanced duct is $f_H/2 = 5.73$ kHz. Since the electron gyrofrequency increases with decreasing altitude, the ratio ω/ω_H decreases for a given frequency. As a wave of given frequency and given wave normal angle reaches lower altitudes in a duct it requires a greater enhancement to remain trapped. If this is not available the wave will escape from the duct. The lower frequencies which require the greater enhancements will escape first. It is suggested that the frequency of the branching point seen in the whistler fine structure corresponds to the minimum frequency that remains trapped down to the base of the duct.

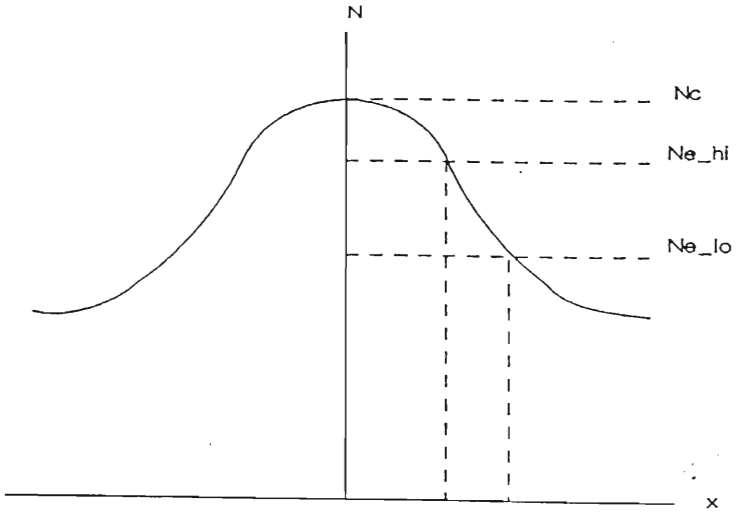

Figure 5.21: Gaussian plasma density distribution around a field line, showing duct width variation with frequency.

5.4 Conclusion

Several mechanisms have been considered to explain the splitting of the whistler trace below 3.7 kHz, as seen in the whistler fine structure of the Sanae and Halley whistlers. Since the time difference between traces increases with decreasing frequency, a lower hybrid resonance reflection of the low frequencies is thought to be unlikely, as in this case the traces would diverge with increasing frequency, while the opposite is seen. Similarly subprotonospheric propagation yields time differences between traces that are at least an order of magnitude too large, and is an unsuitable explanation.

Considering the derivation in the previous section of the frequency dependance of enhancement required for ducted propagation, it is seen that lower frequencies require a higher percentage enhancement to remain trapped in the duct. Strangeways' mechanism whereby energy can escape from the duct at altitudes where the duct width is comparable to the wavelength is not very well understood, since waveguide theory predicts that a wave will become *evanescent* when the duct width is equal to *half* the wavelength. It has been shown that lower frequencies can become untrapped more easily for a constant enhancement duct. There will exist a threshhold frequency above which the wave will be trapped for even a very small enhancement of plasma density, and this energy will exit at the base of the duct.

Referring to Figure 5.22(a) it is seen that the downgoing wave will begin to leak from the duct at an altitude where the enhancement is not sufficient to trap the lower frequencies, which can escape from the topside and bottomside of the duct.

If the receiving station is suitably positioned as shown in the diagram, it is seen that wave energy at lower frequencies (1) will arrive at the receiver first, followed by that trapped by the duct (2) which is of higher frequency and has not been able to escape, and due to the increased path length the low frequencies that escaped from the bottomside of the duct will arrive a little while later, as shown in Figure 5.22(b), a frequency-time spectrogram which has been normalised by subtracting the average travel time due to dispersion. The proposal by Lichtenberger et al. (1991) that waves can travel in more than one mode, with different travel times would not apply here, because the travel times they observed were an order of magnitude larger, and more importantly, this would not be a frequency dependant effect, dual traces would be present at all frequencies. Also, if higher order modes were present, the higher frequencies would be seen to split due to modes travelling at different velocities, since higher order modes at low frequencies would escape first, as described above.

Thus it is seen that the trace splitting common to 5 whistlers arriving at Sanae and Halley Bay can be explained by a succesive leakage of frequencies from the duct as the enhancement required for ducting increases. It should be noted that the splitting we have so far observed is for L=4.22 to L=4.27. A whistler propagating at L=4.01 and arriving just a few seconds later did not show this splitting effect.

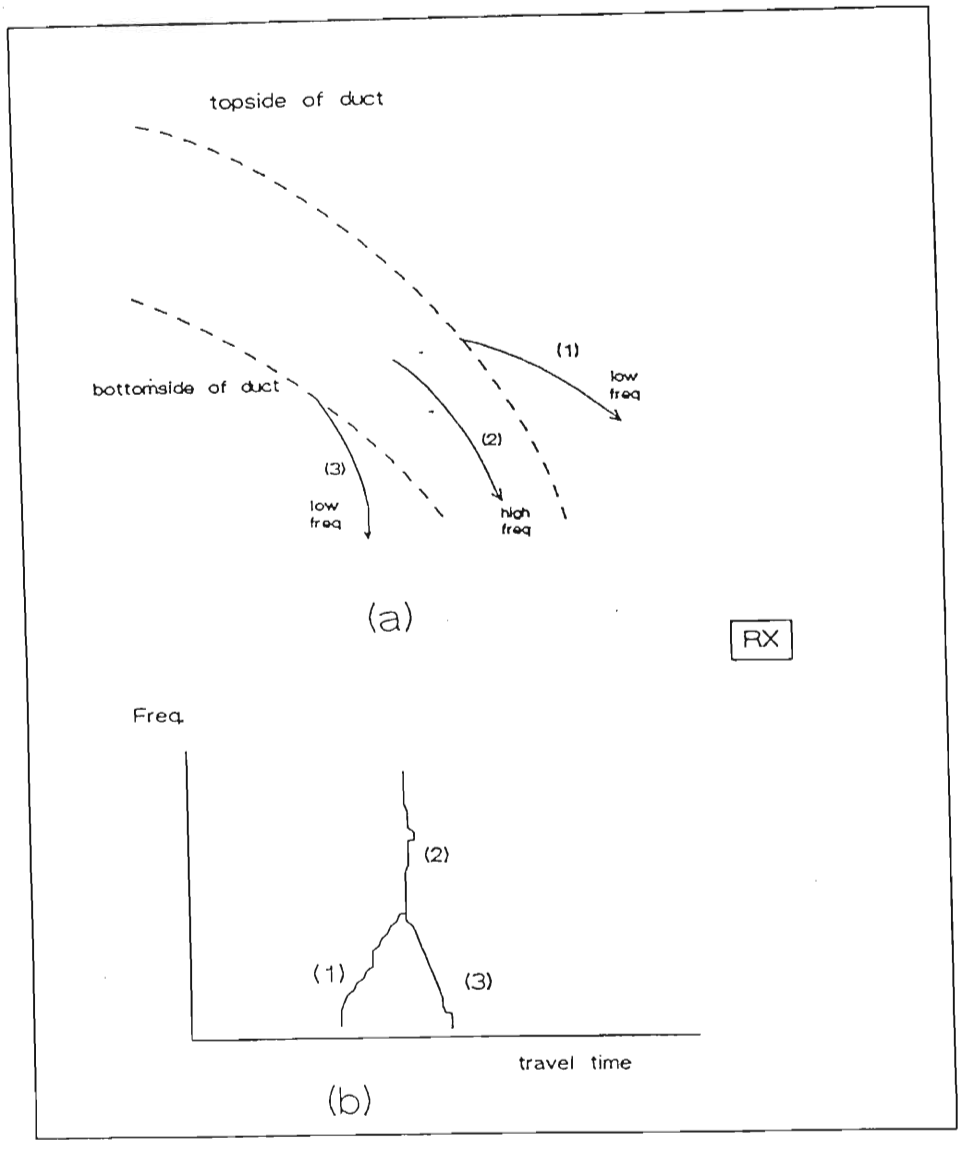

Figure 5.22: Leakage of low frequencies from the top and bottom of a duct, at a point where enhancement is not sufficient for trapping at low frequencies. Frequencies above a certain threshhold will be trapped to the base of the duct.

Furthermore, the whistler arriving at Halley Bay at 05:20:36 did not display the same fine structure as the other whistlers. This could be a function of the sub-ionospheric propagation path between the duct exit position and Halley Bay station at that time.

It has been shown that fine structure analysis by means of matched filtering is a powerful tool in the study of whistler propagation in magnetospheric ducts.

Appendix A

Circuit Diagrams and Source Code Listing

A.1 Masthead Preamplifier

The circuit for the masthead preamplifier is shown in Figure A.1.

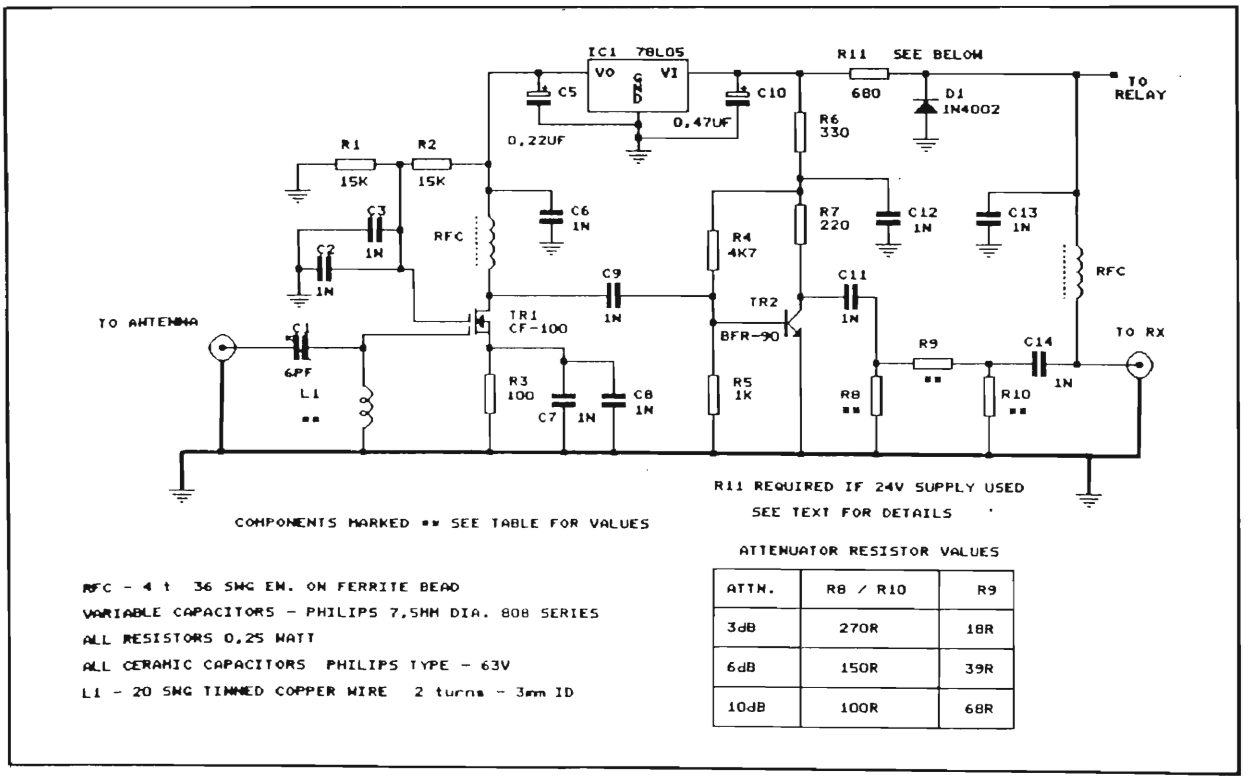

ATTENUATOR RESISTOR VALUES

ATTN.	R8 / R10	R9
3dB	270R	18R
6dB	150R	39R
10dB	100R	68R

Figure A.1: 460 MHz Preamplifier Circuit Diagram.

The input stage transistor, TR1, is a locally available GAAsFET, a CF-100 from Telefunken. The noise figure obtainable with this transistor is about 0,6 dB, and a gain of 12 to 15 dB is possible. Capacitor C1 and coil L1 form the input tuned circuit, which has a very high Q. The second stage uses a NPN RF transistor, the BRF-90, and interstage coupling is through capacitor C9. The second stage is untuned, since this could cause instability. Gain of 10 dB in this stage is possible if the impedance is optimally matched.

A.2 IF Amplifier and Comparator

The circuit for the IF amplifier and comparator is given in Figure A.2.

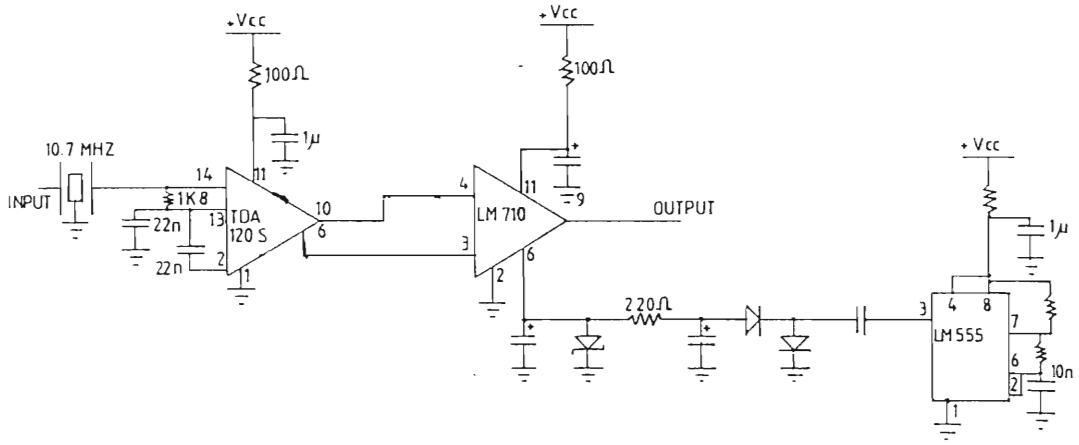

Figure A.2: IF amplifier between receiver and PSK demodulator.

The TDA 120 S is a video amplifier which amplifies the 10.7 MHz output of the receiver, and feeds this signal to the comparator, LM710. The comparator output amplitude is $-V_cc$ to $+V_cc$, which is TTl compatible, as required by the PSK demodulator. The LM555 circuit is used to generate a negative supply rail for LM710.

A.3 Antenna Tracker Interface

The 'Emotator' tracker, mounted on the antenna tower, is driven by a control box situated in the laboratory. This control box is in turn controlled from the personal computer, running 'Instantrack', via a hardware interface, the circuit diagram of which is shown in Figure A.3.

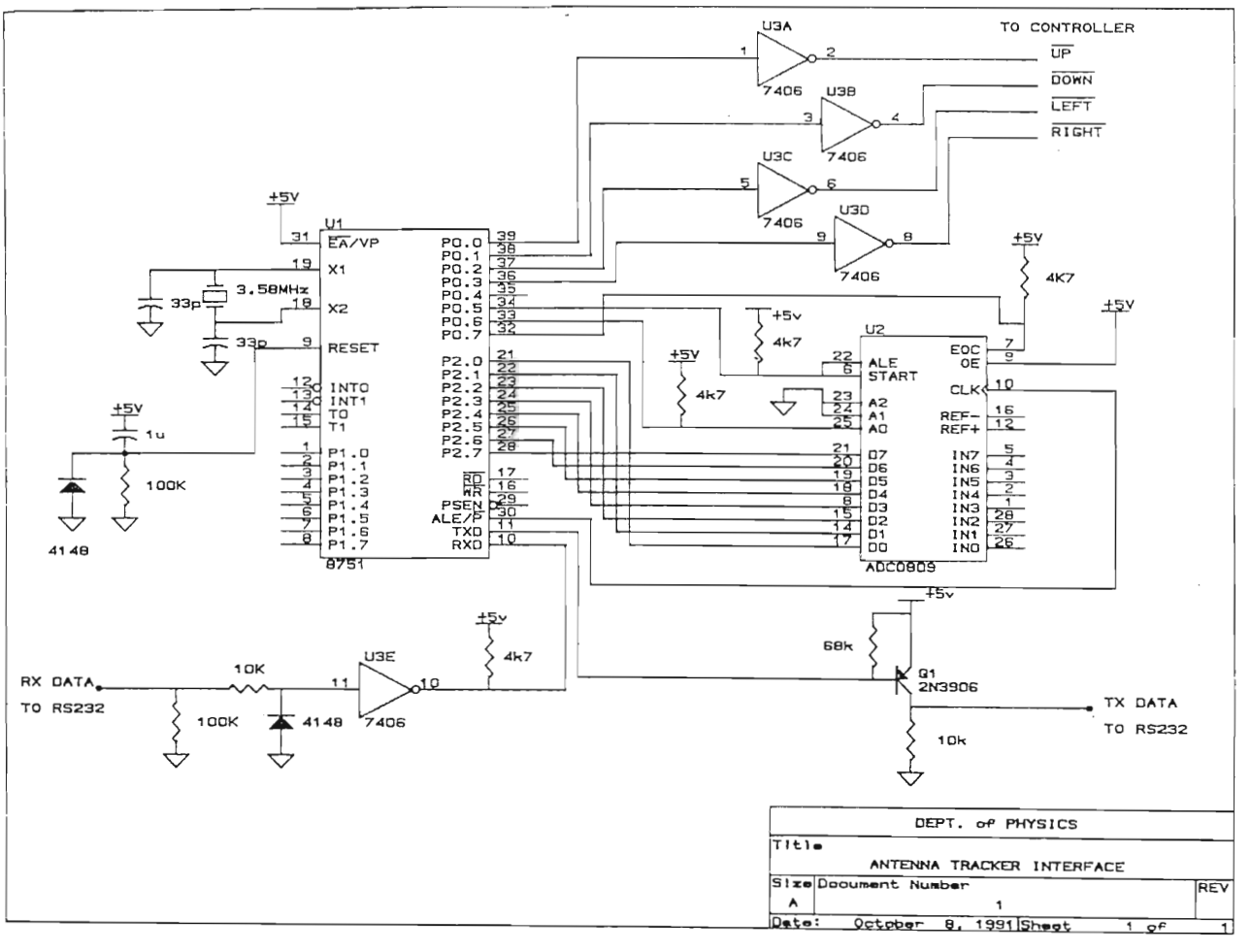

Figure A.3: Antenna Tracker Interface Circuit Diagram.

This interface is connected between the computer and the controller box, so automating the tracking of a satellite. Two potentiometers at the tracker motors send a signal back to the controller, the signal amplitude being related to the position of the motors of the tracker. This signal is connected to "IN0" and 'IN1' of the analog to digital converter ADC 0809, being the relative value of the azimuth and elevation. These inputs are converted to a digital form, and connected to the 8751 microprocessor, and so the microprocessor knows at any

time exactly what is the antenna elevation and azimuth. It compares the required azimuth and elevation bearings given by 'Instantrack' for tracking that particular satellite, and then outputs a high signal to the motor control signals p0.0 to p0.3 on the 8751. These signals are connected to the controller box, which then moves the motor positions. A memory resident program called 'ROTOR.exe' is run before entering 'Instantrack' which interfaces the computer to the interface hardware, and the tracking is enabled inside the 'Instantrack' environment by pressing the 'R' key.

A.4 Phase Shift Keying (PSK) Demodulator

The SAS signal is PSK modulated, and to extract the binary data bit stream PSK demodulation is neccesary. The circuit diagram of this demodulator, designed in Czechoslovakia and modified in Durban, is shown in Figure A.4.

The input 10.7 MHz signal is connected to an AND gate, which, together with the D-latches, is configured as a phase detector. The 10.7 MHz crystal provides a reference oscillator against which the input signal phase is referenced. The current mirror circuit VT6,7,8 and VT9 causes the input to NL2, which is the collector of VT9, to oscillate at 40 kHz or 80 kHz, depending on whether the input phase is +1 radian or -1 radian. NL2 is just an output buffer. VT12 is used to switch a relay when an input signal is detected, so that the demodulator can run automatically. PA2 is a tuning indicator, controlled by NL5 and NL6.

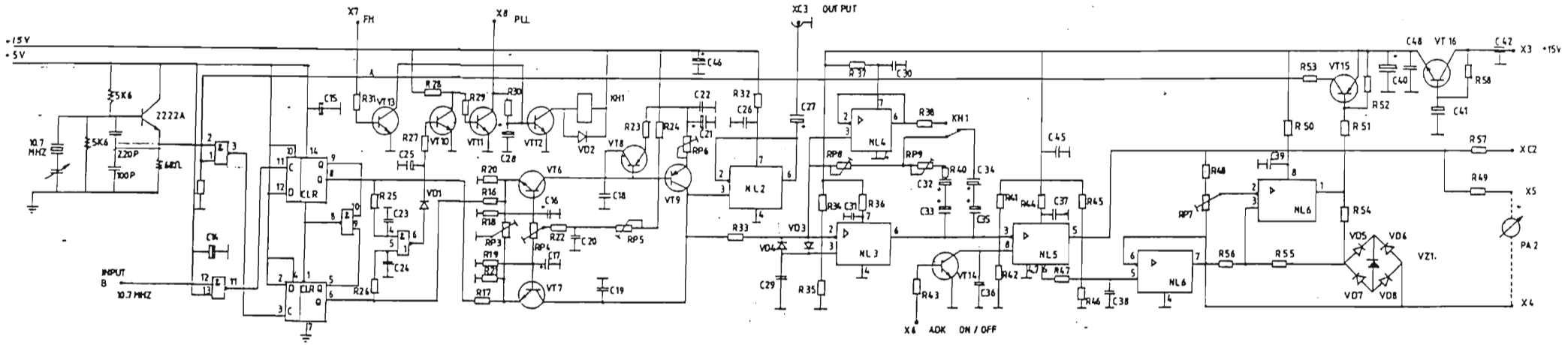

Figure A.4: Modified version of the original Czech designed PSK Demodulator.

A.5 Source Code Listing : Rotor.pas

The antenna tracker driver software is s memory resident program which is enabled by running "ROTOR.exe" before entering 'Instantrack'.

```
program Int63;
{                   Instant Track Interface for Emotator Tracker }
{                   ========================================== }

{                   R.J.Atkinson - Dept of Physics , UND         }
{                              21 March 1991                     }

{$M 1024,0,1000}
{$I- ,$R- ,$S- }

uses Dos,Crt;

var Rax,Rbx,Rcx,Rdx,Dval,
    Port,Params,P,SIVal,
    TempCX,TempDX,Q        : word;
    TrackerAzim,TrackerElev,
    ttazim,ttelev,
    SatAzim,SatElev,code,
    RelAzim,RelElev        : integer;
    Flag1, TX,TY, ComPort,
    IntCount,StFlag,AH     : byte;
    Ch,Schar,ChTemp,
    UDFlag, LRFlag         : char;
    F                      : string[12] ;
    TElev,TAzim            : string;
    Old1C                  : pointer;

procedure AuxInit(Port,Params: word);
         inline($58/$5A/$B4/$00/$CD/$14);

function AuxInChar(Port:word) : char;
         inline($5A/$b4/$02/$CD/$14);

procedure AuxOutChar(Port:word;Ch:char);
         inline($58/$5A/$B4/$01/$CD/$14);

function AuxInReady(Port:word) : boolean;
         inline($5A/$B4/$03/$CD/$14/$88/$E0/$24/$01);

procedure GoUp;
```

```
begin if UDFlag <> 'U' then
   begin AuxOutChar(ComPort-1,'F'); AuxOutChar(ComPort-1,^M);
         AuxOutChar(ComPort-1,'U'); AuxOutChar(ComPort-1,^M);
         UDFlag := 'U';
   end;
end;

procedure GoDown;
begin if UDFlag <> 'D' then
   begin AuxOutChar(ComPort-1,'E'); AuxOutChar(ComPort-1,^M);
         AuxOutChar(ComPort-1,'D'); AuxOutChar(ComPort-1,^M);
         UDFlag := 'D';
   end;
end;

procedure NotUpOrDown;
begin if UDFlag <> 'N' then
   begin AuxOutChar(ComPort-1,'E'); AuxOutChar(ComPort-1,^M);
         AuxOutChar(ComPort-1,'F'); AuxOutChar(ComPort-1,^M);
         UDFlag := 'N';
   end;
end;

procedure GoLeft;
begin if LRFlag <> 'L' then
   begin AuxOutChar(ComPort-1,'A'); AuxOutChar(ComPort-1,^M);
         AuxOutChar(ComPort-1,'L'); AuxOutChar(ComPort-1,^M);
         LRFlag := 'L';
   end;
end;

procedure GoRight;
begin if LRFlag <> 'R' then
   begin AuxOutChar(ComPort-1,'B'); AuxOutChar(ComPort-1,^M);
         AuxOutChar(ComPort-1,'R'); AuxOutChar(ComPort-1,^M);
         LRFlag := 'R';
   end;
end;

procedure NotLeftOrRight;
begin if LRFlag <> 'N' then
   begin AuxOutChar(ComPort-1,'B'); AuxOutChar(ComPort-1,^M);
         AuxOutChar(ComPort-1,'A'); AuxOutChar(ComPort-1,^M);
         LRFlag := 'N';
   end;
end;
```

```
{$F+}

procedure AuxInput;
begin
    P := 1; Q := 0; F[0] := #12; F[1] := #32;
     while (P < 13) and (Q < 6500) do
      begin
       if AuxInReady(ComPort-1)  then
         begin
            Q:=0; F[P] := AuxInChar(ComPort-1); Inc(P);
         end
         else Inc(Q)
     end;
     Delay(10);
end;

procedure CFunction;
begin
          if AuxInReady(ComPort-1) then Schar := AuxInChar(ComPort-1);
          AuxOutChar(ComPort-1,'C'); AuxOutChar(ComPort-1,^M);
          AuxInput;
end;

procedure TrackerPos;
begin
   CFunction;
     if F[1] = 'C' then
      begin
       TElev := Copy(F,4,4); TAzim := Copy(F,8,4);
       Val(TAzim,ttazim,code);     Val(TElev,ttelev,code);
       TrackerAzim := ttazim*9 div 25;  TrackerElev := ttelev*9 div 50;
      end
      else
        begin
          Delay(300);  AuxInput;  Delay(300);
        end;
end;

procedure SendTrackerPos;                    { AH := $03 }
begin
        Rax := TrackerElev; Rbx := TrackerAzim;
        Rbx := Rbx + 180;
        if Rbx > 359 then Rbx := Rbx - 360;
end;
```

```
procedure SetTrackerDrive;                          { AH := $04 }
begin
     SatAzim := Rdx; SatElev := Rcx;
end;

procedure TrackerDrive;
begin
   if Flag1 = 0 then begin NotUpOrDown; NotLeftOrRight; end else
    begin
    if SatAzim < 180 then SatAzim := SatAzim + 360;
       SatAzim := SatAzim - 180;
    if SatElev <   0 then SatElev :=  -2;
    if SatElev > 180 then SatElev := 180;
     TrackerPos;
     RelAzim := TrackerAzim-SatAzim ;  RelElev := TrackerElev-SatElev ;
     if Abs(RelElev) > 2 then
      if RelElev < 0 then GoUp else GoDown else NotUpOrDown;
     if Abs(RelAzim) > 4 then
      if RelAzim < 0 then GoRight else GoLeft else NotLeftOrRight;
  end;
end;

procedure IH1C;
interrupt;
begin
     inline($FB);                                   { sti }
     if IntCount <> 0 then
      begin
       Dec(IntCount);
       if IntCount < 5 then
        begin
         NotUpOrDown; NotLeftOrRight;
         IntCount := 0;
        end;
      end;
     SIVal := Ofs(Old1C);                           { Get Old1C Offset }
     inline($89/$C6);                               { mov si,ax }
     inline($9C/$FF/$1C);                           { pushf  call far [si] }
     inline($1F);                                   { pop ds }
end;

procedure IH63(Flag,CS,IP,AX,BX,CX,DX,SI,DI,DS,ES,BP:word);
interrupt;
begin
     AH := AX div $100;
     case AH  of
```

```
      $00 : AX := AX and $FF00;
      $03 : begin
              SendTrackerPos;
              AX := Rax; BX := Rbx;
            end;
      $04 : begin
              if Flag1 <> 0 then
               begin
                  SatAzim := DX; SatElev := CX;
                  TrackerDrive;
                  IntCount := 45;
               end;
            end;
      $09 : begin
               Flag1 := (AH and $FF);
            end;
    end;
end;

procedure Int63Inlet;
begin
         inline($50/$EB/$0F);
         inline($90/$00/$00/$00/$00/$00/$00);
         inline($52/$6F/$74/$6F/$72/$44/$52/$56);
         SIVal := Ofs(IH63);
         inline($89/$C6);
         inline($58);
         inline($FF/$E6);
end;

begin     { MAIN PROGRAM }
     if ParamCount > 0
      then Val(ParamStr(1),ComPort,code)
      else ComPort := 1;
       if  ( ComPort > 0 ) and (ComPort < 3 ) then
        begin
          AuxInit(ComPort-1,$C3);
          if AuxInReady(ComPort-1) then Schar := AuxInChar(ComPort-1);
          AuxOutChar(ComPort-1,'S'); AuxOutChar(ComPort-1,^M);
          AuxInput;
           if F[1] = 'S' then
            begin
             SetIntVec($63,Ptr(Seg(Int63Inlet),Ofs(Int63Inlet)+3));
             Writeln('Rotordrive loaded : COM port',ComPort,' initialized');
             LRFlag := 'N'; UDFlag := 'N';
             Flag1 := 0; StFlag := 0;
```

```
            IntCount := 100;
            GetIntVec($1C,Old1C);
            SetIntVec($1C,@IH1C);
            Keep(0);
           end
           else
            begin
             Writeln('Tracker not responding : loading aborted'); Halt(0);
            end;
       end
      else
       Writeln('Invalid Comms port parameter');
end.
```

Appendix B

Lower Hybrid Resonance Calculations

Using the International Reference Ionosphere software available in the Physics Department various models of electron density and ion distribution were used to derive lower hybrid resonance (LHR) frequency versus altitude profiles, shown in Figures 5.18 and 5.19.

The LHR frequency is given by

$$\frac{1}{f_{LH}^2} = \left(\frac{1}{f_0^2} + \frac{1}{f_H^2}\right)\frac{m_p}{m_e}M$$

where

$$1/M = \Sigma\alpha_i/m_i$$

and α_i and m_i are the fractional composition and mass of the i'th ion species respectively.

The electron plasma frequency and electron gyrofrequency altitude profiles are also required, and calculated as follows.

B.1 Electron Gyrofrequency vs Altitude

The magnetic field at a radius R from the earth's centre is given by

$$B = \frac{B_0 R_0^3}{R^3}(1 + 3\sin^2(\theta))^{\frac{1}{2}}$$

The electron gyrofrequency is

$$f_H = \frac{qB}{m}$$

therefore

$$f_H = \frac{f_{H0} R_0^3}{R^3}(1 + 3\sin^2(\theta))^{\frac{1}{2}}$$

At Sanae $R_0 = 6370$ km, $\theta = 63.5$ degrees, and $f_{H0} = 880$ kHz, yielding the electron gyrofrequency - altitude profile shown in Figure B.1.

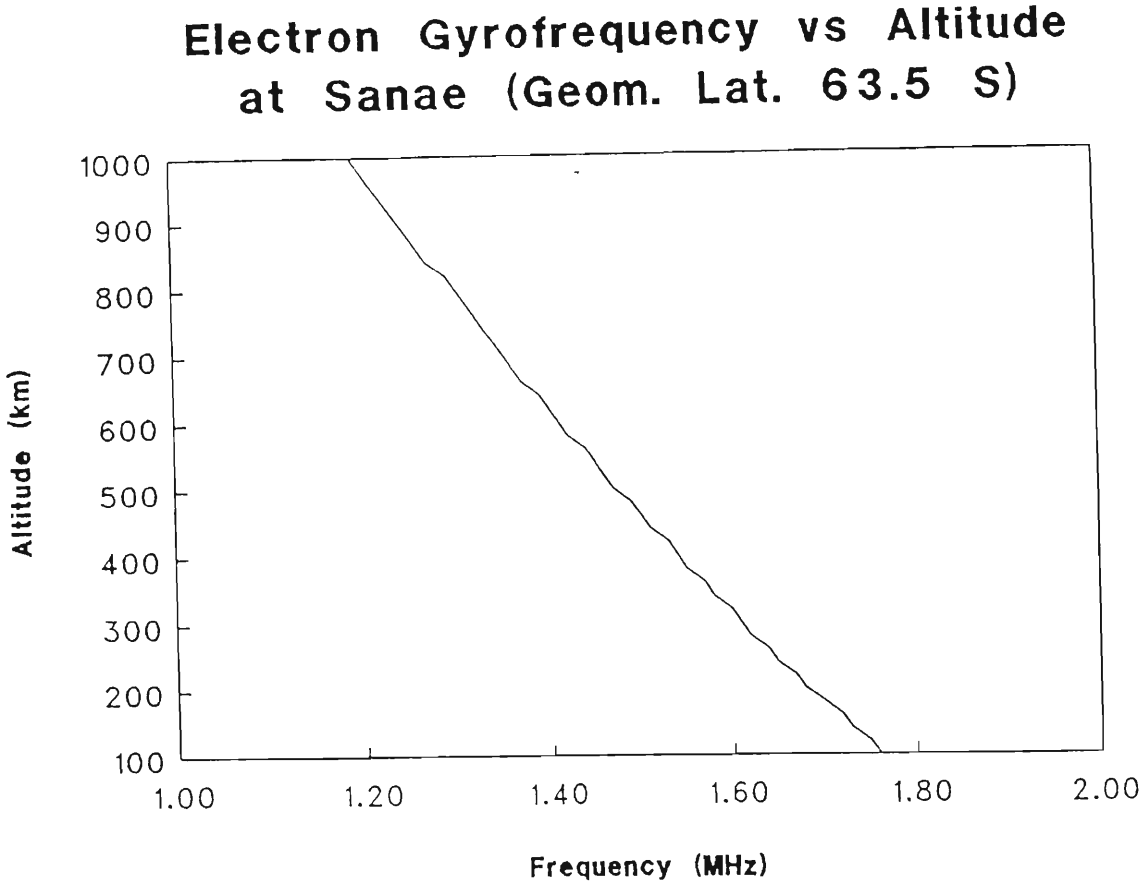

Figure B1: Electron Gyrofrequency vs Altitude at Sanae (Geomagnetic Latitude 63.5 degrees.)

B.2 Electron Plasma Frequency vs Altitude

The electron plasma frequency is given by

$$f_0 = \frac{1}{2\pi}\sqrt{(\frac{Ne^2}{\epsilon_0 m})}$$

where N is the electron density, ϵ_0 is Boltzmann's constant and e and m are the charge and mass of an electron, respectively. This approximates to

$$f_0 = 8870\sqrt{N}\ Hz.$$

Electron density and ion composition models proposed by the URSI/COSPAR working group, used as the International Reference Ionosphere 1990, are shown

in Tables A1 to A6. The values of electron density calculated by the models is used to calculate the electron plasma frequency at the corresponding altitudes (100 to 1000 km in 20 km steps). The plasma frequency versus altitude profiles are shown in Figure B2. Three profiles are shown for the standard, Gulyaeva and Lay function electron density models.

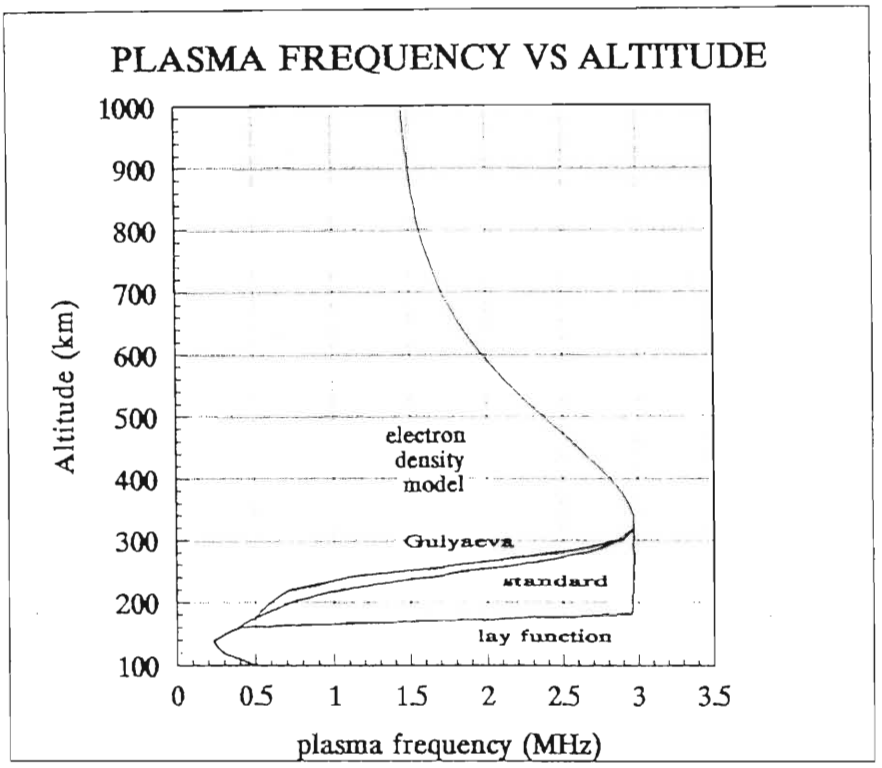

Figure B2: Plasma frequency variation with altitude for the (a) standard electron density, (b) Gulyaeva electron density and (c) Lay function electron density models.

REFERENCES

Alexander P.H. *Computation of ray paths for very low frequency radio waves propagating through the magnetospheric plasma.* PH.D. thesis, Univ. of Southhampton, England, 1971.

Angerami J.J., *A whistler study of the distribution of thermal electrons in the magnetosphere.* Stanford Univ. Tech. Report No. 3412-7, 1966.

Angerami J.J., *Whistler duct properties deduced from VLF observations made with the OGO 3 satellite near the magnetic equator.* JGR Vol. 75, No. 31, pp 6115-6135, 1970.

Antonio F., *Instanttrack software for satellite tracking.*

Barrington R.E. and J.S. Belrose, *Preliminary results from the VLF receiver aboard Canada's Alouette satellite.* Nature, 198, pp 651-656, 1963.

Bernhardt P.A and C.G. Park, JGR Vol. 82, pp 5222, 1977.

Bernhardt P.A., JGR Vol. 84, pp 5131, 1979.

Bernard L.C., *A new nose extension method for whistlers.* J. Atm. Terr. Phys. Vol. 35, pp 871-880, 1973.

Bhégin C. and C. Siredey, *Un procédé d'analyse fine des sifflements atmosphériques.* Ann. Geophys. 20 (3), pp 301-308, 1964.

Block L.P. and D.L. Carpenter, Geophys. Res. 79, p2783, 1974.

Brice N., J. Atm. Terr. Phys. Vol. 27, No. 1, 1965.

Brice N. and R.L. Smith, *Lower Hybrid Resonance emissions.* JGR Vol. 70, No. 1, pp 71-80, 1965.

Bullough K. and Sagredo J.L. *VLF goniometer observations at Halley Bay, Antarctica. 1. The equipment and measurement of signal bearing.* Planet Space Sci. 21, 1973.

Caldeira P.S., *Whistler analysis software using matched filtering and curve fitting techniques - Users Reference Manual.* 1992.

Carpenter D.L., J. Geophys. Res. 68, p1675, 1963.

Carpenter D.L. and N.T. Seely, *Cross-L drifts in the outer plasmasphere: Quiet time patterns and some substorm effects.* J.G.R. Vol. 81, No. 16, pp2728. 1976

Cerisier J.C., *Perpendicular propagation near the lower hybrid resonance frequency.* Intitute de Physique du Globe, Tech. Report No. GRI/NTP/55. 1968.

Chappel C.R. *Recent Satellite Measurements of the Morphology and Dynamics of the Plasmasphere.* Rev. Geo. Space Phys. Vol. 10, pp956, 1972.

DiFranco J.V. and W.L. Rubin, *Radar Detection.* Prentice Hall, Englewood Cliffs, 1968.

Dowden R.L. and G. Allcock, J. Atm. Terr. Phys. Vol. 33, pp 1125, 1971.

Fielding J., ZS5JF, *Mast Head Preamplifiers for VHF and UHF.* Radio ZS, April 1990. Published by the South African Radio League.

Friedel R.H.W., *Determination of duct exit positions using goniometer data.* Honours Project, Univ. Natal. 1987.

Hamar D. and G. Tarcsai, *High resolution frequency-time analysis of whistlers using digital matched filtering. Part 1: Theory and simulation studies.* Ann. Géophys. t.38, fasc.2, pp 119-128, 1982.

Hamar D., G. Tarcsai, J. Lichtenberger, A.J. Smith and K.H. Yearby, *Fine structure of whistlers recorded digitally at Halley, Antarctica.* J. Atm. Terr. Phys. Vol. 52, No. 9, pp 801-810, 1990.

Hansen H.J., M.W.J. Scourfield and J.P.S. Rash *Whistler Duct Lifetimes.* J. Atmos. Terr. Phys. 45, p789, 1983.

Helliwell R.A. *Whistlers and related ionospheric phenomena.* Stanford Univ. Press, Stanford, Calif. 1965

Ho D. and L.C. Bernard, *A fast method to determine the nose frequency and minimum group delay of a whistler when the causative spheric is known.* J. Atm. Terr. Phys. Vol.35, pp 881-887, 1973.

Hughes A.R.W., *Satellite measurements of whistler dispersion at low lattitudes.* Adv. Space Res. Vol. 1, pp377-380, 1981.

Hughes A.R.W. and A.J. Smith, *Further Evidence for the Ionospheric Contribution to Convection within the Plasmasphere.* Adv. Space Res. Vol. 6, No. 3, pp. 199-202. 1986.

Instantrack satellite tracking program, version 1.00
Written by Franklin Antonio for the American Radio Relay League.

Jiriceck F. and G. Tarcsai, *Analysis of whistlers observed simultaneously aboard the intercosmos satellite and on the ground.* Acta Geodaet. Geophys. et Montanist. Acad. Sci. Hung. Tomus 15 (1), pp 97-104, 1980.

Lalmani, J. Geophysics 56, p53 - 57, 1984.

Lichtenberger J., D. Hamar and L. Cserepes, *Computation of whistler wave normals using a combined matched filtering and parameter estimation technique.* J. Atm. Terr. Phys. Vol. 49, Nos. 11/12, pp 1075-1079, 1987.

Lichtenberger J., Gy. Tarcsai, Sz. Pástzor, Cs. Ferenz, D. Hamar, O.A. Molchanov and A.M. Golyavin. 1990. *Whistler doublets and Hyperfine structure recorded digitally by SAS on the ACTIVE satellite.* JGR Vol.96, No.A12, pp 21149 - 21158,

1991.

McChesney J. and A.R.W. Hughes, *Temperatures in the Plasmasphere Determined from VLF Observations.* J. Atm. Terr. Phys. Vol. 45, No. 1, pp. 33-39. 1983

Park C.G., *Methods of determining electron concentrations in the magnetosphere from nose whistlers.* Stanford Univ. Tech. Report No. 3453-1, 1972.

Power Divider/Combiner
Radio ZS, September 1989. Published by the South African Radio League.

Ratcliffe J.A., *The magneto-ionic theory and its applications to the ionosphere.* Cambridge Univ. Press.

Rycroft M.J., *VLF emissions in the magnetosphere.* Radio Science, Vol. 7, Nos. 8/9, pp 811-830, 1972.

Rycroft M.J., *Strange New Whistlers.* Nature Vol. 327, June 1987.

Sazhin S.S., A.J. Smith and E.M. Sazhina, *Can magnetospheric electron temperature be inferred from whistler dispersion measurements?* Annales Geoph. No. 8 (4) pp 273-286, 1990.

Smith R.L. and D.L. Carpenter, *Extension of nose whistler analysis.* JGR Vol. 66, No. 8, pp 2582-2586, 1961.

Smith A.J. and K.H. Yearby, *AVDAS - a microprocessor based VLF data acquisition, processing and spectral analysis facility for Antarctica.* Br. Antarct. Surv. Bull. No. 75, pp 1-15, 1987.

Storey L.R.O *An investigation of whistling atmospherics.* Phil. Trans. Roy. Soc. London, Ser. A, 246, 1953.

Storey L.R.O., *A method of interpreting the dispersion curves of whistlers.* Can. J. Phys. No. 35, 1107-22, 1957.

Storey L.R.O. and J.C. Cerisier, *Une interprétation de bandes de bruit au voisinage de la fréquence hybride basse observées au moyen de satellites artificiels.* Compt. Rend. 266, (8), pp 525-528, 1968.

Strangeways H.J. and M.J. Rycroft, *Trapping of whistler waves through the side of ducts.* J. Atm. Terr. Phys. Vol. 42, pp 983-994, 1980.

Strangeways H.J., *Investigation by ray tracing of the effect of a summer-winter assymetry on whistler ducting.* J. Atm. Terr. Phys. Vol. 44, No. 10, pp 889-899, 1982a.

Strangeways H.J., *The effect of multi-duct structure on whistler-mode propagation.* J. Atm. Terr. Phys. Vol. 44, No. 10, pp 901-912, 1982b.

Strangeways H.J., *Multi-station VLF direction finding in eastern Canada.* J.

Atm. Terr. Phys. Vol. 44, No. 6, pp 509-522, 1982c.

Strangeways H.J., *Whistler leakage from narrow ducts.* J. Atm. Terr. Phys. Vol. 48, No. 5, pp 455 - 462, 1986.

Tarcsai G., *Routine whistler analysis by means of accurate curve fitting.* J. Atm. Terr. Phys. Vol. 37, pp 1447-1457, 1975.

Tarcsai G., P. Szemerédy and L. Hegimegy, *Average electron density profiles in the plasmasphere between L=1.4 and 3.2 deduced from whistlers.* J. Atm. Terr. Phys. Vol. 50, No. 7, pp607-611, 1988.

Tarcsai G., H.J. Strangeways and M.J. Rycroft, *Error sources and travel time residuals in plasmaspheric whistler interpretation.* J. Atm. Terr. Phys. Vol. 51, No. 4, pp 249-258, 1989.

The ARRL UHF/Microwave experimenters manual, 1990.
Published by the American Amateur Relay League.

The Radio Communication Handbook, 4th edition.
Published by the Radio Soceity of Great Britain.

Tixier M. and G. Charcosset, *Partly ducted whistlers over Europe.* J. Atm. Terr. Phys. Vol. 40, pp 601-613, 1978.

Walker A.D.M. *The propagation of radio waves in the ionosphere and exosphere.* PHd. Thesis, Univ. of Cambridge.

Walker A.D.M. *The propagation of very low frequency waves in ducts in the magnetosphere.* Proc. Roy. Soc. London, Ser A, 329, 1972.

Walker A.D.M and K.F. Deane, *Methods of scaling whistlers in the absence of the initiating spheric and nose frequency.* S.A. Journal of Antarct. Res., No. 4, 1974.

Walker A.D.M. *The Theory of Whistler Propagation.* Reviews of Geophysics and Space Physics, Vol. 14, No. 4, November, 1976.

Whistler Analysis Software using Matched Filtering and Curve Fitting techniques

USERS REFERENCE MANUAL.

PAULO S. CALDEIRA

Submitted in partial fulfilment of the
requirements for the degree of
Master of Science
in the
Space Physics Research Institute
of the
Department of Physics,
University of Natal.

Durban
November 11, 1992

Introduction

This software manual describes the use of curve fitting and matched filtering routines used for whistler analysis. The software was written by János Lichtenberger, György Tarcsai and Daniel Hamar, of the Eötvos University Geophysical Institute, Budapest, Hungary. Only a brief description of the numerical methods used in the software is given here, a detailed derivation is given in Hamar et. al. (1990) and Tarcsai (1975,1977).
The hardware required to run the software is a 486 PC, or a 386 or 286 with numerical co-processor, and VGA graphics. This is neccesary because of the extensive number-crunching involved.

My thanks to Mr. János Lichtenberger, Dr. György Tarcsai and Dr. Daniel Hamar for giving us the software, and the patience shown while teaching me to use it. Also to my supervisor, Dr. Arthur Hughes, for the encouragement, and to the Space Physics Research Institute for financial assistance for my trip to Budapest during July 1990.

Index

About the manual

This manual describes the use of all of the different programs that make up the suite of whistler analysis routines. The command line format for invoking all of the programs is given, and the parameters used in the various parameter files called by the program are detailed.
The main procedures available are the whistler curve fitting and matched filtering programs, called FIT *[Tarcsai,1975]* and BURK *[Hamar, 1990]* respectively, but there are a host of others for selecting the data frame to be analyzed (QLS.EXE), performing fast fourier transforms on the binary data file (FFT.EXE), selecting frequency - time (f,t) pairs on which to run the curve fitting, viewing the output of the matched filtering routine (CELWPIX.EXE) and selecting points for a second, and hopefully more accurate curve fit.
The input data file format is described, in the event of the user wanting to digitize some of his own whistler data for analysis. The software was written to look mainly at digitized satellite data, off the ACTIVE polar orbiting satellite *[Lichtenberger et. al., 1991]*, a project with which the Hungarians are presently involved. This software was tested by the author on some of this data, currently available in this department.
The procedure for analysing a whistler is outlined, and some examples of results obtained as well as sample parameter files are given.

About the Software

The suite of programs presented here is a useful tool when analyzing VLF whistlers, especially when very high accuracy in plasma and whistler parameters and fine spectral resolution are required. The matched filtering technique *[D. Hamar et. al., 1990]* used by the **BURK1** program was implemented by the writers of the software to enhance the spectral resolution of the whistler traces, and show the fine structure of whistlers.

VLF data from the SAS experiment *[Lichtenberger et.al., 1991]* on board the ACTIVE(Intercosmos 24) satellite (NASA designated object number 20261), for the 17th of December, 1990, is available in the Space Physics Research Institute, Durban, for analysis. The flowchart of the analysis procedure is shown in Figs. 1.1 and 1.2, depending on whether the user is analyzing digital data files, such as SAS data, or analog VLF data, such as SANAE or ISIS satellite data, which needs to be digitized. The digitizing program written for the PC-30 A/D card has 12-bit resolution, so the sampled data is stored as two byte integers in binary form, whereas the SAS data is only one byte long integer data.

Refering to Fig. 1.1, the user runs program **QLS.exe** on the 280 second long SAS data file, called 0c171040.59!, for a quick look spectrogram of the entire data file. Once an interesting period has been recognised, normally a period during which a whistler is present, **SELECTS.exe** is used to "cut out" the desired window of data, and save it to a file. A full screen FFT, offering better resolution, is then performed with **FFT1.exe**, and using the computer mouse, frequency - time points along the whistler trace can be selected for curve fitting with **FIT0.exe**. **FIT0** uses Bernard's formula and Park's DE1 model, or alternatively R4 (collisionless) model *[Park, 1972]*, to fit a theoretical curve to the selected (f,t) pairs. An output file containing the whistler parameters, such as nose frequency, time of arrival of the nose relative to the initiating spheric and L-value along which the whistler has travelled, as well as plasma parameters, such as electron gyrofrequency and electron densities along the whistler path, among others, is produced by **FIT0**.

The next step is to perform matched filtering on the whistler using **BURK1.exe**, and view the fine structure with **CELWPIX.exe** or **CELWPIXB.exe**, the difference being that **CELWPIXB** allows the user to select (f,t) pairs as with the FFT routine, but with better accuracy. Alternatively, the user can run an autoscaling routine called **SAVA.exe** which automatically selects the peak amplitudes along the trace and saves these points to a file. A second curve fit, **FIT1.exe**, is then run on these points to give extremely accurate parameters.

Since sampled analog data (SANAE/ISIS) is two bytes long, the FFT routine used is **FFT2.exe**, and the matched filtering routine is **BURK2.exe**, otherwise all the other programs are common to both.

SAS DATA-ANALYSIS FLOWCHART

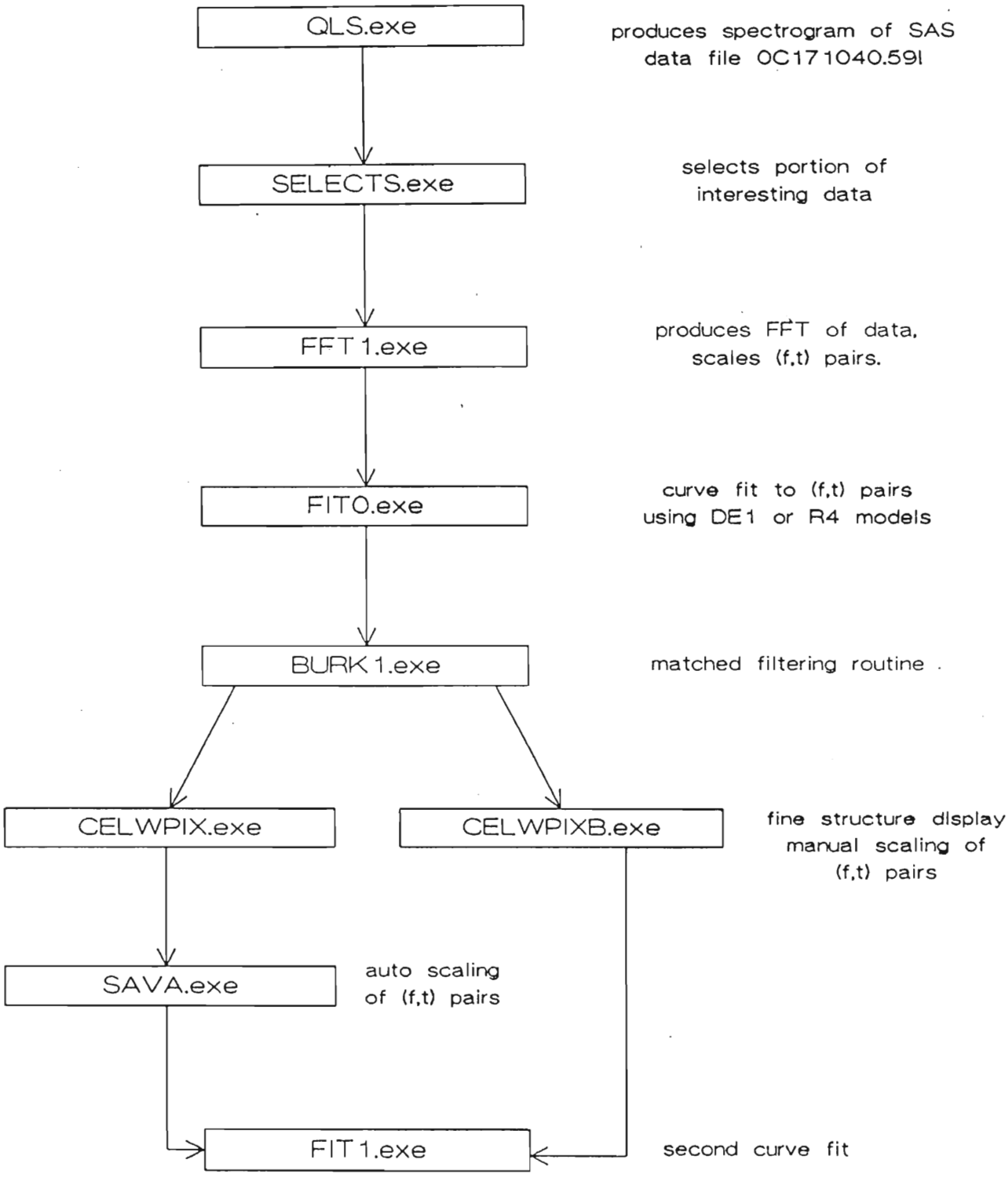

Figure 1.1

SANAE/ISIS DATA-ANALYSIS FLOWCHART

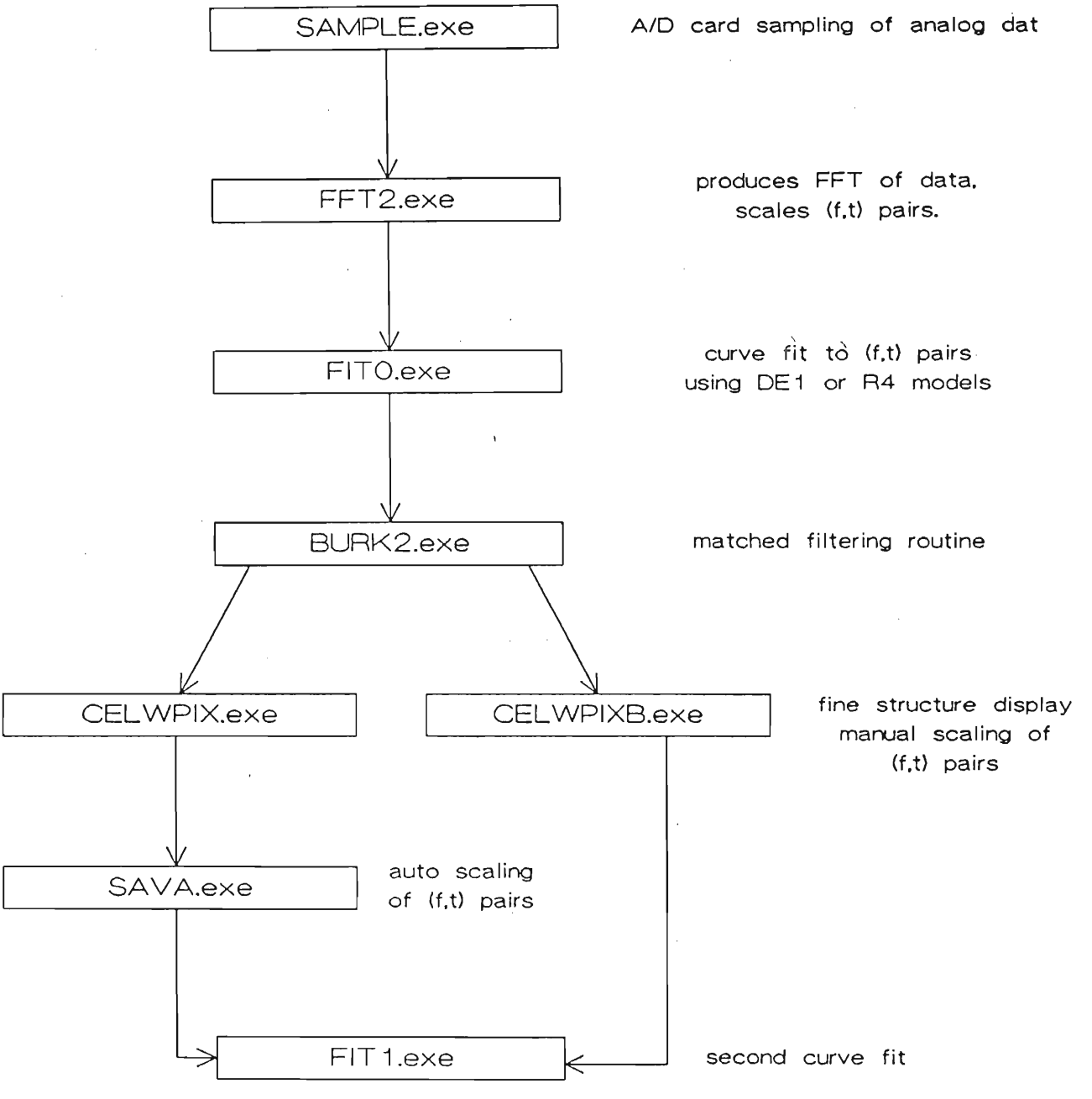

Figure 1.2

Sample.exe

PURPOSE : Samples analog signal (SANAE/ISIS data) connected to PC-30 analog to digital card and produces a binary file for use by FFT2.exe and BURK2.exe.

FORMAT : Sample

OUTPUTS : Binary file with sampled two - byte data.

DESCRIPTION : The analog signal (Revox cassette or VHS tape) of the data to be analysed is plugged into the A/D card in the computer, and the program SAMPLE.exe is run. The user is required to know the clock frequency of the PC in which the card is plugged very accurately, and this frequency can be measured on pin 20 of the output slots on the mainboard, and read with a frequency counter. The channel to be sampled is required, usually channel 1 is used, depending on the wiring of the A/D card connector. A sampling frequency is required, the maximum being 22 kHz. Nyquist's rule dictates that the selected sampling frequency should be at least twice the maximum frequency of interest, that is to say if the whistler frequency range is 0 to 5 kHz, the sampling frequency should be 10 kHz. It must be remembered that the sampling period, equivalent to the reciprocal of this sampling frequency, needs to be included as a parameter in the file FFT.dat, which is called when displaying the Fast Fourier Transform of the data. The maximum amount of data that can be sampled is 60 kbytes (maximum array size in turbo pascal is 64 kbytes), so the higher the sampling frequency the shorter the time period that can be sampled. If a sampling frequency of 10 kHz is selected, 20 kbytes of data are saved to an array by the program per second, so 3 seconds of data can be sampled and displayed.

AscToBin.exe

PURPOSE : To convert sampled ASCII data files to binary format for use with the curve fitting and matched filtering programs.

FORMAT : AscToBin infile outfile

OUTPUTS : Binary file with sampled two - byte data.

DESCRIPTION : AscToBin takes any ASCII data file of sampled data points, each points two bytes long, and converts it to a binary file required by the analysis software. The ASCII data must be two bytes per sampled point, each point seperated by a comma or a space. Being two byte long data, the values can range from -32767 to +32768. The standard PC-30 A/D card samples to 12 bit resolution, which gives values of -4095 to +4096. This is perfectly acceptable, since contrast stretching is easy to do when displaying the FFT of the data. It is important that the sampling frequency be known accurately, since this must be inserted in the parameter files used with the programs. Alternatively, the sampled data can be stored directly to a binary data file using the sampling routine **SAMPLE.exe**.

Active keys : none

Parameter files used : none

QLS.exe

PURPOSE : Quick look at SAS data spectrograms to choose suitable periods for analysis.

FORMAT : QLS infile

USES : QLS.dat, COLOR.dat

OUTPUTS : none

DESCRIPTION :

QLS.exe is used to perform a fast-fourier transform on the whole SAS binary data file and display the frequency - time spectrogram on the screen, in bars 2.5cm high, 4 bars per screen, approximately 7.5 seconds of data per bar. The data bandwidth is 5kHz wide, and the data has been sampled aboard the satellite at 10kHz, hence 10 Kbytes of data per second. We have 2.8Mbytes (280 seconds) of data in a file called 0C171040.59!, representing :

0	: year 1990 (1 = 1991)
C	: month december (C = 12 hexadecimal)
17	: day of month 17th
10:40	: hour : minutes
59!	: 59 seconds past the hour

Active keys : When the program is run it generates the first bar of 7.5 seconds of data, and pressing <**enter**> when this bar is complete generates the next bar, scrolling the bars when the screen is full. Pressing <**esc**> exits the program immediately.

Parameter files used : The parameter files the program calls while running are QLS.dat and COLOR.dat. An example of the QLS.dat file is shown below :

```
&QLDAT
NN    =128        /* Number of points between two consecutive FFT windows */
MM    =64         /* Number of points used for FFT */
OSZT  =15         /* Amplitude value of brightest colour for FFT display */
ISZN  = 15        /* Number of colours used in FFT display */
HATV  =.3         /* Power scale for colour function, 1 = linear scale */
```

```
DELTAT= .1e-3     /* Time between samples, 1/sample frequency */
TIME0 =150.       /* delay time of start from beginning of file in seconds */
ISORH =600        /* Screen width for display in pixels */
LIMIT =384        /* Amplitude limit of 3 consecutive data points */
/
```

COLOR.dat specifies the colours used in all of the graphics routines in this package, and should not be modified.

A photograph of the screen output is shown in Figure 1.3. From this frequency - time spectrogram, interesting periods may be selected for further analysis using the program SELECTS.exe.

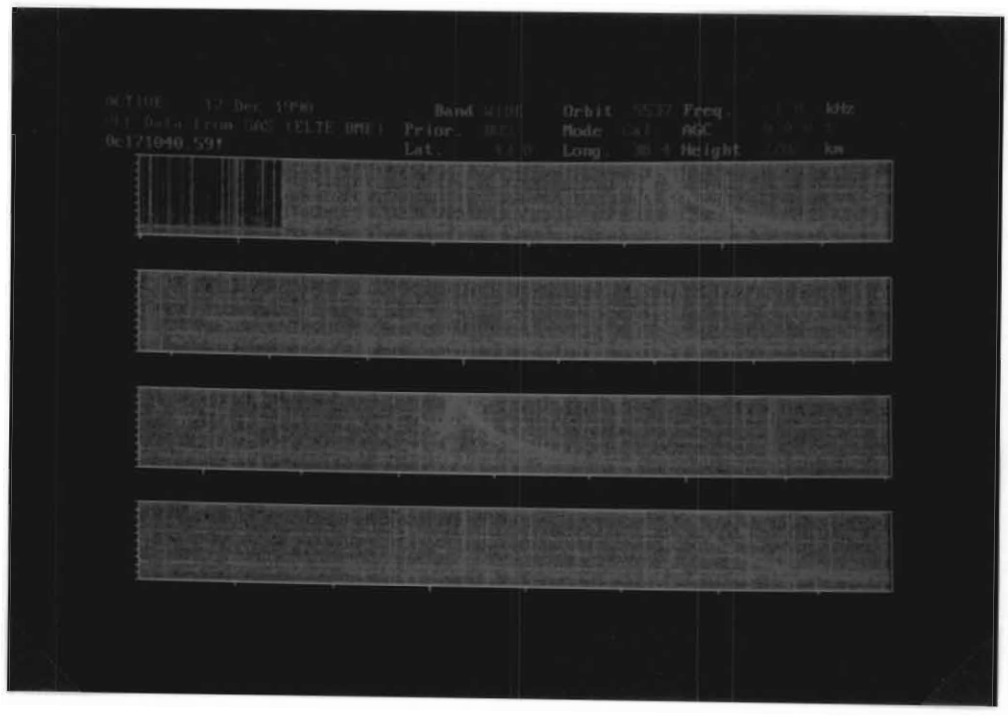

Figure 1.3: Photograph of VGA screen in program QLS.exe

Knowing the start time of the frame (TIME0 in QLS.dat), one can determine the start time of the whistler to be analyzed, and select this period to a file using SELECTS.exe.

SELECTS.exe

PURPOSE : Select portions of interesting data from the main ACTIVE satellite data file 0C171040.59! for further analysis.

FORMAT : SELECTS infile outfile

USES : SELECTS.dat

OUTPUTS : Outfile containing selected length of data.

DESCRIPTION :

Since the main data file 0C171040.59! contains 2.8 Mbytes of data, SELECTS.exe is used to select a period of data, defined in the parameter file SELECTS.dat, and create a smaller file (outfile) for further analysis. The prompt

Stop - Program terminated.

appears when this is complete. A high resolution Fast Fourier Transform can then be performed on this data using FFT1.exe.

Parameter files used : The parameter file used by the program is SELECTS.dat, an example of which is shown below :

```
&SELECTSDAT
TIME0 =184      /* Start time delay from beginning of file in seconds */
INUM  =70000    /* Number of points to save to file, 10 000 pts/sec */
/
```

Changing the TIME0 changes the start time of the window to be viewed, and INUM determines the length of the data file selected. Typically 7 - 8 seconds is as good as the horizontal resolution of the screen gets.

Outfile naming convention : For SAS (Active satellite) data it is conventional to name the file as follows : SASXXXa.s
where XXX is the time from beginning of file in seconds, "a" implies it is the first file looking at that window of data, and the .s extension implies that it is a selected portion of data from the main data file. Filename conventions are not critical at this stage.

If the output filename is not selected on the command line, the prompt

```
Filename missing or blank, please enter filename
UNIT 8?
```

appears, requesting a filename to which it will save the selected data.

FFT1.exe, FFT2.exe

PURPOSE : Perform a fast fourier transform on data files, and display the FFT. Also gives the user the option of selecting points along a whistler trace to be used for curve fitting. FFT1.exe is used for SAS data, and FFT2.exe for sampled SANAE or ISIS whistlers.

FORMAT : FFT1 infile [outfile]
FFT2 infile [outfile]

USES : FFT.dat, COLOR.dat

OUTPUTS : The user has the option of selecting frequency - time points along the whistler and saving these points to the outfile at termination of program. An example of an output file is given in APPENDIX A.

DESCRIPTION :

Since the sampled data can be either 1 byte long, in the case of SAS (ACTIVE) satellite data, or 2 bytes long, as in the case of sampled SANAE or ISIS data, the user runs FFT1 or FFT2 respectively to view the fast fourier transform of these data. If the mouse is active, freq. - time points can be selected along the whistler trace and saved to a file. The output file (outfile) can be selected either on the command line, and failing this the program prompts the user for a filename to save the (f,t) pairs on exiting the program. The (f,t) pairs are then used to determine the whistler parameters using the program FIT0.exe.

Attempting to run FFT1.exe on sampled two byte data or FFT2.exe on SAS data gives an error message on the display. Also, if the number of data points are not specified correctly in the file FFT.dat an error results.

Active keys : Provided the mouse is activated from DOS, the user has the option of selecting (f,t) pairs along the whistler trace. This is done by moving the cursor to the point to be selected, and pressing the right button on the mouse. Repeating this procedure, as many points as are desired can be saved to file, and to end this procedure press the left mouse button. Pressing <**enter**> at this juncture terminates the program, and exits to DOS. If an output filename was not selected on the command line, the prompt

(infile) exists! new filename:

appears, and entering a filename and pressing <**enter**> again terminates the

program. If no (f,t) pairs are to be selected, pressing the left mouse button and then <**enter**> terminates the program.

Parameter files used : The parameter files used are FFT.dat and COLOR.dat. An example of FFT.dat is shown below :

```
&fftdat
nnstep   =64        /* Number of points between two consecutive FFT windows */
mmfft    =256       /* Number of points used for FFT */
iwh      =70000     /* Length of input data file in points */
oszt     =4.00      /* Amplitude value of brightest colour for FFT display */
akuszob  =.05       /* Amplitude value of darkest colour for FFT display */
iszn     =15        /* Number of colours used for FFT display */
hatv     =.5        /* Power scale for colour function, 1 = linear scale */
deltat   =.1e-3     /* Sampling period, 1/sampling frequency */
time0    =0.        /* start time delay from beginning of file */
iprcol   =1         /* flag for hardcopy, 1 = 16 colours, 0 = 4 colours */
/
```

If the data is very noisy, and the whistler is not clearly defined, the user can adjust the values of OSZT and HATV to stretch the colour contrast. This may make the selection of points along the trace easier.

COLOR.dat specifies the colours used in all of the graphics routines, and should not be modified. An example is shown in APPENDIX A.

Photographs of the FFT1 screen output are shown in Figures 1.4 to 1.6.

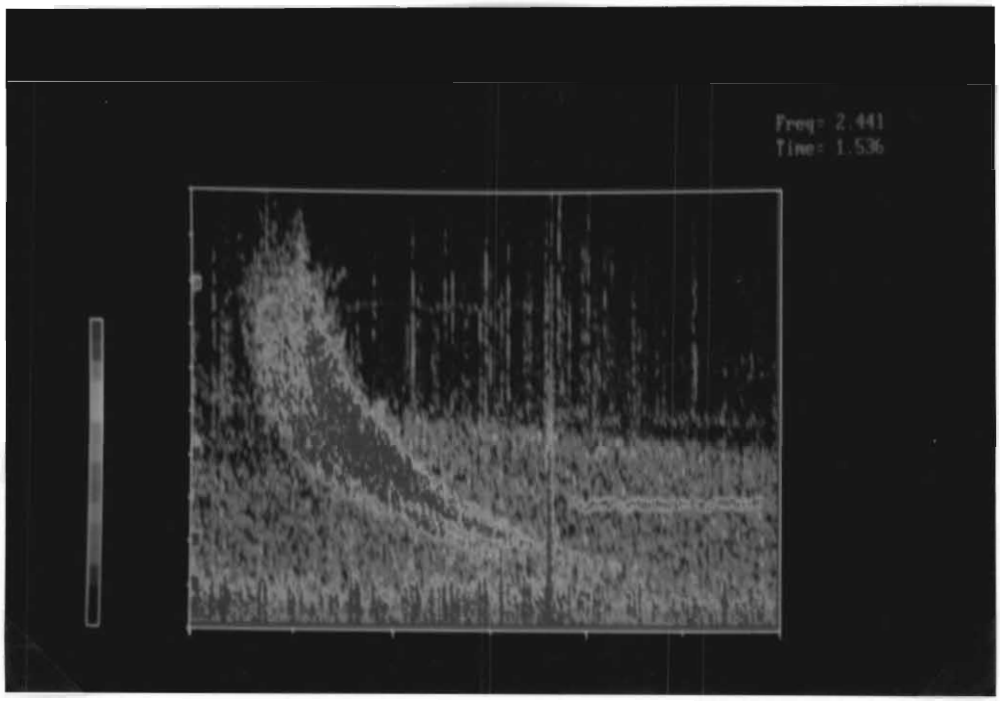

Figure 1.4: Photograph of VGA screen output of the FFT of a typical Sanae whistler

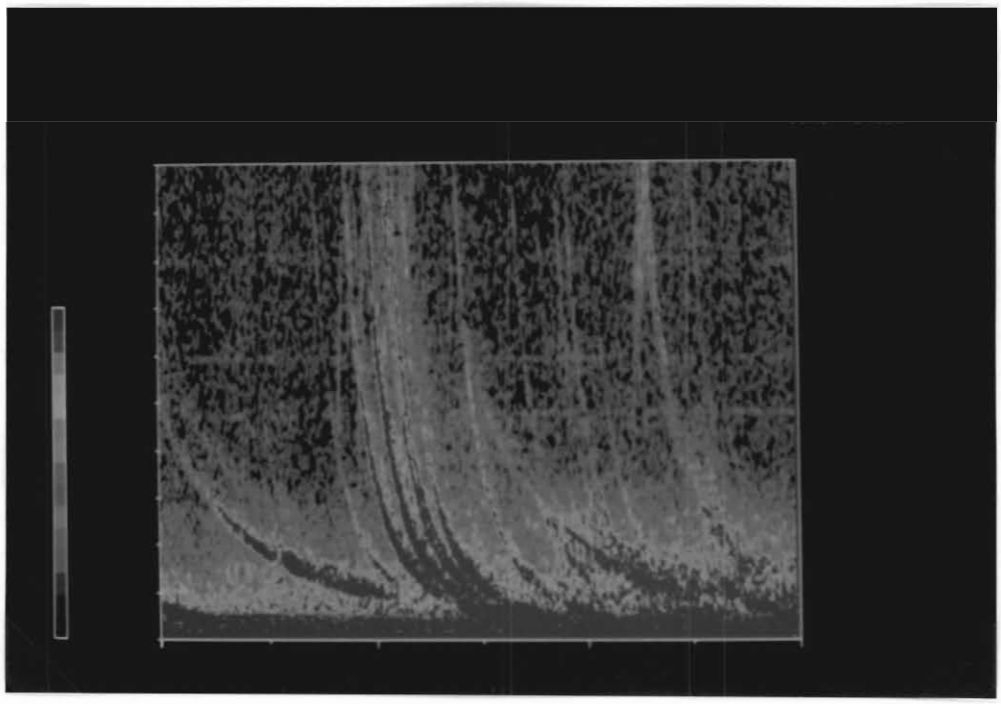

Figure 1.5: Photograph of VGA screen output of the FFT of a typical whistler recorded aboard the ISIS satellite. Note the low dispersion of these whistlers.

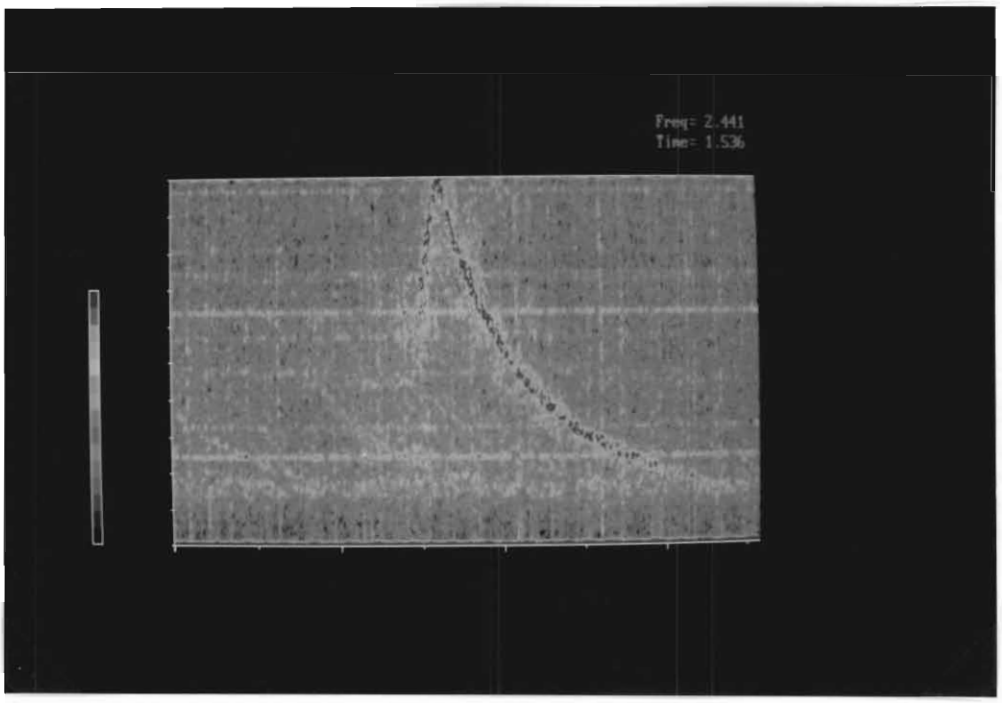

Figure 1.6: Photograph of VGA screen output of the FFT of a typical whistler recorded aboard the ACTIVE satellite.

FIT0.exe

PURPOSE : Calculates whistler and magnetospheric plasma parameters using Bernard's formula and the DE1 or R4 *[Park, 1972]* models of electron density from the scaled (frequency, time) pairs selected using FFT1.exe or FFT2.exe.

FORMAT : FIT0 infile

USES : WHEAD

OUTPUTS : Outfile containing whistler and plasma parameters and datafile BURK1XX.dat used for the matched filtering program BURK1.exe. An example of an output file and description of output parameters is given in APPENDIX A. Also modifies the parameters in the second half of the parameter file WHEAD, starting at &BURK1DAT, as shown overleaf.

DESCRIPTION :

FIT0.exe is run using the selected (f,t) pairs from FFT1 as the input file, and the program uses a least squares estimation procedure to arrive at the final solutions. This log file is saved using the input filename and modifying the last character of the infile to "i". The input filename needs to be longer than 5 characters, and it is suggested that some information about the whistler arrival time be included in the filename. The benefits become apparent when analysing a large number of whistlers.

ie. infile "infile1" produces outfile "infile1i"

infile "sas208a.s" produces outfile "sas208a.si" , etc.

The prompt

Stop - Program Terminated.

appears after the program has run. Quite often the iterative process diverges, instead of converging to a solution, which is due to the chosen starting values of the iterative procedure in the file "WHEAD", namely the estimated nose frequency FNIN, zero dispersion D0IN, and the time shift DTX. Marquardt's parameter FA is a convergence parameter, which speeds up convergence for low values of FA. Very low values can cause the procedure not to converge. It is also found that when analysing low latitude fractional hop whistlers with weak dispersion, such as ISIS satellite data, convergence is very rare, and even when the curve fitting procedure does converge, the error bars are very large. Bernard's formula does not hold very well for fractional hop whistlers, so calculated nose frequencies and

other parameters are usually erroneous. It is important to note that any duplicate points at the same frequency in the points selected for curve fitting should be deleted before running the FIT routines. In the instance of non-convergence, the output file does not contain parameters, only a log of the iterative procedure, and at the end of the file the message

End of iteration. (number) steps , error -1.

appears. The curve fitting program was unsuccessful with this particular set of starting values, and different starting values are needed for convergence. If the solution appears to converge to a solution, but does not change with succesive iterations and has the error message after the calculations, there are two similar frequency values in input data.

The file BURK1XX.dat is also created by the program containing the calculated parameters of the curve fitting procedure, which is used in the matched filtering program BURK1.exe. Caution must be taken before running FIT0 that the output filenames are not already in use, otherwise the program will not run. To solve this problem erase any files with the same filename as the FIT0 outputs, ie. infile+i and BURK1XX.dat.
The BURK data file is created and named using the word BURK1 .dat superimposed on the input filename, ie. infile "sas208a.s" produces BURK1**8a**.dat, infile "sas1.s" would produce BURK1.dat, since it is less than 5 characters long. It is inadvisable to use filenames with less than 5 characters since problems arise with filenames when using the BURK routines. Filenames consisting of 7 characters are preferable.

Active keys : none

Parameter files used : The program uses parameter file WHEAD, an example of which is shown below.

```
&FITDAT
MD    =0          /* model used, 0 = DE1, 1 = R4 (collisionless) model */
F2    =0.         /* foF2 in MHz, 0 if no ionospheric correction is used */
FNIN =5.0         /* Approximate nose freq. in kHz, starting point */
DOIN =60.        /* Approximate zero dispersion, starting point */
DTX   =1.         /* Approximate time shift (sec) between chosen time origin and
                     causative spheric */
FA    =100        /* Marquardt's parameter used in damped iteration (.01 - 100)*
/
&BURK1DAT
N        =70000    /* Length of input data file in points */
NF       =900      /* Number of frequencies to be filtered using BURK1.exe */
NSZ      =1000     /* Width of filter output in points */
DO       = 96.4    /* Whistler dispersion calculated by BURK1.exe */
FHEQ     =12413.   /* Equatorial electron gyrofrequency in Hz from BURK1.exe */
```

```
FN       =4609.     /* Nose frequency in Hz from BURK1.exe */
DT       =.1e-3     /* Sampling period, 1/sampling frequency */
DF       =200.      /* Matched filter bandwidth (100 - 600 Hz) */
T0       =1.750     /* Time of arrival of whistler relative to causative spheric*
AL       =0.        /* Phase constant of filter */
FRTOL    =0.        /* Centre frequency of received data , mixed down to
                       baseband. (= 0 in for our purposes) */
ELSOFR   =500.      /* Start centre frequency of filters */
FRLEPES  =5.        /* frequency step between centre frequency of filters */
/
```

These parameters can be modified to give more accurate results. The &BURK1DAT section of the file is modified by BURK1.exe, and is only used to do a second, and hopefully more accurate, curve fit using the program FIT1.exe. Suggested starting values for most whistlers are FNIN = 5.0 kHz and DOIN = 60 - 80.

BURK1.exe, BURK2.exe

PURPOSE : Uses the matched filtering procedure to enhance the time resolution of a window around the whistler trace, and thereby look at the fine structure of a whistler.

FORMAT : BURK1 infile outfile
BURK2 infile outfile

USES : BURK1XX.dat

OUTPUTS : Binary output file containing spectral output after matched filtering, which can be viewed using CELWPIXB.exe.

DESCRIPTION :

A full description of the matched filtering method is described in Hamar, et. al. 1990. Briefly, the input file, which is the original binary sampled data file produced by SAMPLE.exe or the selected SAS data file, is run through a series of filters, of specified bandwidth, and whose centre frequency is also a specified frequency apart, and this serves to enhance the time resolution of the spectrum. The output file's frequency - time spectrogram is then analysed using CELWPIX.exe, or CELWPIXB.exe, which resolves the spectral response more finely. Fine structure of the whistler trace becomes apparent, which is not so with just displaying the FFT.

The time axis is modified by subtracting the theoretical travel time, so that a perfect (theoretical) whistler would produce a straight line parallel to the Y-axis. In this way time differences between a theoretical whistler and the whistler being analysed are more easily resolved. Using the program CELWPIXB.exe to view the trace gives the user the option of selecting (f,t) pairs to a file, as before with FFT1.exe, for curve fitting using FIT1.exe.

Care must be taken when naming the output file of the BURK program, since the parameter file BURK1XX.dat called by BURK1.exe depends on this. As mentioned before, BURK1XX.dat is produced by the curve fitting routine FIT0, and is named using the input filename masked by the word "BURK1", ie. the parameter file will be called BURK1XX.dat where XX are 6th and 7th letters of the input filename. When running BURK1.exe and specifying the output filename on the command line, care must be taken that outfile also fits this mask, ie. that the 6th and 7th letters of outfile match the 6th and 7th letters of the BURK1

parameter file BURK1XX.dat. The filenaming convention used calls the output filename "infile.fb0", the fb0 extension indicating that it is a binary file, created after running BURK for the zeroth time. Also, the output filename cannot already exist in that directory, otherwise an error will occur. The command line format requires that an outfile be specified, otherwise the error message

File already connected to a different unit.

occurs.

example. FIT0 sas208a.ft0 ... produces BURK1**8a**.dat
BURK1 sas208a.s sas208a.fb0 ... uses BURK18a.dat

BURK2.exe is used in exactly the same manner as BURK1.exe, only BURK2 is for 2 byte per sample SANAE/ISIS data files, and BURK1 for 1 byte per sample SAS data files. BURK2 uses BURK1XX.dat as its parameter file.

If the filter bandwidth is too high for a particular data set, the error message

Runtime error F6204 : write(con) - unformatted i/o not consistent with open options

occurs. The filter bandwidth needs to be decreased (make DF lower) and BURK run again.

Active keys : none

Parameter files used : The parameter file BURK1XX.dat, created by FIT0.exe is used, an example of which is shown below.

```
&BURK1DAT
N =         70000                    /* Length of input data file in points */
NF =          100                    /* Number of frequencies to be filtered */
NSZ =          1000                  /* Width of filter output in points */
D0 =         93.624209573741310      /* Whistler dispersion calculated by FIT0 *
FHEQ =     15261.749465431840000     /* Equatorial electron gyrofrequency */
FN =      5663.347115666302000       /* Nose frequency */
DT =    1.000000000000000E-004       /* Sampling period, 1/sampling frequency */
DF =       200.000000000000000       /* Filter bandwidth to be used */
T0 =         1.514376156096725       /* Time of arrival of whistler relative to
                                        causative spheric */
AL =    0.000000000000000E+000       /* Phase constant of filter */
FRTOL =    0.000000000000000E+000    /* Frequency from which data has been mixed
                                        down to baseband (=0 fo our purposes */
ELSOFR =      500.000000000000000 /* Start centre freq. of filter */
FRLEPES =         5.00000000000000 /* Freq. step between center freq. of
                                        adjacent filters */
/
```

The parameters normally modified are the start centre freq. ELSOFR, and the frequency step between filters, FRLEPES. Values of FRLEPES of 2 Hz and 5 Hz give good results, but using a frequency step of 10 Hz and higher worsens the resolution when viewing the spectrogram using CELWPIX.exe. The length of the input data file, N, has to be set for different files, and the number of frequencies to be filtered, NF, is set depending on the desired frequency band to be covered. The filter width, NSZ, determines the bandwidth around the filter trace to be analysed, points outside this window will be disregarded. A filter bandwidth, DF, of 100, 200 or 400Hz should be used for best results. D0, FHEQ, FN, DT and T0 are modified by FIT0, and should not be changed. The frequency bandwidth covered is then

Frequency band = ELSOFR to (ELSOFR + NF $\times$ FRLEPES)

CELWPIX.exe, CELWPIXB.exe

PURPOSE : Display the frequency - time characteristics of the matched filter output.

FORMAT : CELWPIX infile
CELWPIXB infile [outfile]

USES : CELWPIX.dat, BURK1XX.dat, COLOR.dat

OUTPUTS : CELWPIX is merely a graphic display and has no output. CELWPIXB, however, allows the user the option of selecting points along the trace and save them to a file for a second curve fit to determine more accurately the plasma and whistler parameters using FIT1.exe. The outfile on the command line is optional with CELWPIXB.exe.

DESCRIPTION :

CELWPIX and CELWPIXB display the frequency - time spectrogram of the window around the whistler, the width of which was chosen by the parameter NSZ in the BURK1XX.dat file, with the time axis "bent" so that the theoretical whistler travel time is subtracted from the measured data. A perfect (theoretical) whistler should then appear as a straight, continuous line parallel to the frequency axis. In CELWPIXB, freq. - time points along the trace can be selected in the same manner as with FFT1, by moving the cursor to the point to be selected, and pressing the right mouse button. After having selected all the points required, pressing the left mouse button and <**enter**> exits the program. If a file to which the scaled points are to be saved was not specified on the command line, then the prompt

(infile) exists! new filename:

appears, and entering an output filename and pressing <**enter**> twice exits the program.

Active keys : In CELWPIX , the <**enter**> key terminates the program. In CELWPIXB the mouse is active if the user wishes to scale points for curve fitting as described above. To select points press the right mouse button on the points to be written to file, and the exit press the left mouse button and <**enter**> twice. If no points are required from CELWPIXB.exe, press the left mouse button and <**enter**> twice.

Parameter files used : The parameter files used are CELWPIX.dat, BURK1XX.dat and COLOR.dat. An example of CELWPIX.dat is shown below :

```
&WPIXDAT
IN      = 0      /* shift trace by N pixels in time to centre trace in display *
ISZN    = 15     /* Number of colours used for display */
LEPFR   = 6      /* Display freq. step (y axis resolution) in Hz */
AMPMAX  = .35    /* Amplitude value of brightest colour for contrast stretch */
ALSFR   = 2500.  /* Freq. at Y=0 on display */
LEPES   = 10     /* Time scale (x-axis resolution) */
HATV    = 1.     /* Amplitude vs Colour function, 1 = linear */
TTAV    = .05    /* Time grid intervals in seconds */
FTAV    = 250.   /* Frequency grid intervals in Hz */
IPRCOL  = 1      /* Hardcopy flag, 1 = 16 colours, 0 = 4 colours */
/
```

The input filename to the CELWPIX routines (outfile of BURK1) needs to follow a strict filenaming convention, since CELWPIX calls BURK1XX.dat, where XX must correspond to the 6th and 7th letters of the input filename. Usually the outfile of BURK1 is named after the infile, but with extension fb0. In this way the input filename of CELWPIX remains standardized, and the program will have no problem calling the corresponding BURK1XX.dat parameter file. The outfile name should be the same as the infile name, since FIT1.exe, run on the (f,t) pairs selected by CELWPIXB.exe, uses and modifies BURK1XX.dat.

COLOR.dat is standard, as before.

A photograph of the CELWPIX graphics display is shown in Figure 1.7. For a better interpretation see Hamar et. al. 1990.

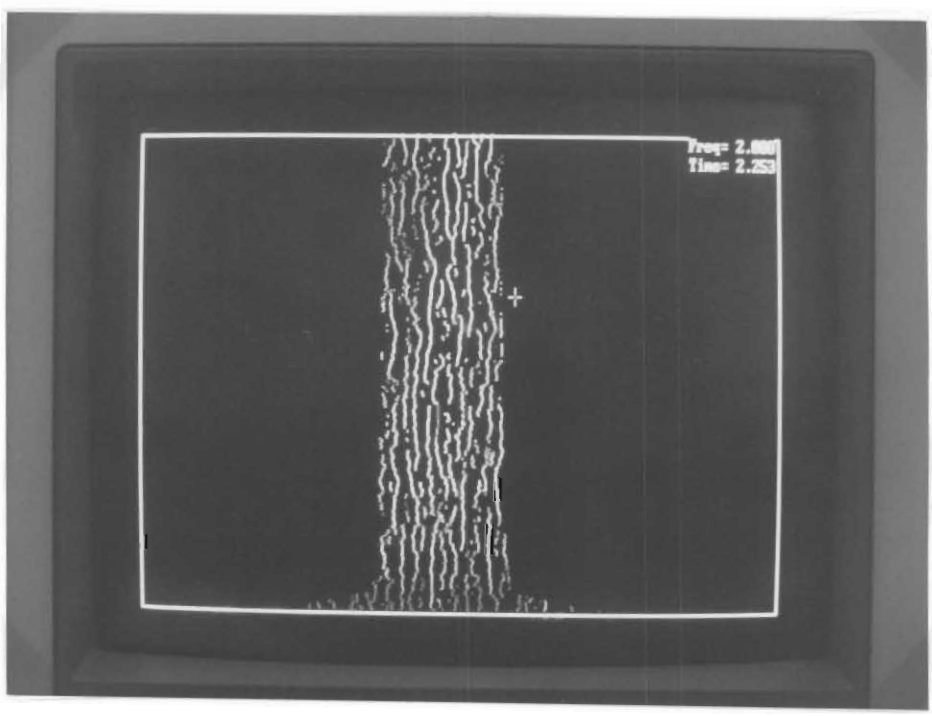

Figure 1.7: Photograph of the VGA screen display of the fine structure of a whistler observed at SANAE.

SAVA.exe, SAVB.exe

PURPOSE : Automatically select points from the output of the BURK1.exe or BURK2.exe programs, and save these (f,t) pairs to a file for curve fitting using FIT1.exe.

FORMAT : SAVA infile outfile ISAV
SAVB infile outfile ISAV

USES : none

OUTPUTS : SAVA produces an ascii file containing frequency - time pairs for use with FIT1.exe. SAVB produces a similar binary file.

DESCRIPTION :

SAVA is run using as input the output of the BURK1/2 programs, and it selects the highest amplitude points at a particular frequency. If two or more points at a particular frequency are of the same amplitude, both are written to the output file. The parameter ISAV on the command line stipulates the width of of the extracted filter output around the theoretical whistler, in points. By modifying ISAV the user can make wider or narrower the interval around the theoretical whistler from which the points will be chosen. The ascii output file is then used by FIT1.exe to give a (hopefully) more accurate curve fit. SAVB is similar, only a binary output file if produced.

Active keys : none

Parameter files used : none

FIT1.exe

PURPOSE : Calculates whistler and magnetospheric plasma parameters using Bernard's formula and the DE1 or R4 *[Park, 1972]* models of electron density from the scaled (frequency, time) pairs selected using CELWPIXB.exe or SAVA.exe.

FORMAT : FIT1 infile

USES : WHEAD

OUTPUTS : Outfile containing whistler and plasma parameters and modifies datafile "BURK1XX.dat" used for the matched filtering program "BURK1.exe". An example of an output file and description of output parameters is given in APPENDIX A.

DESCRIPTION :

FIT1.exe is run using the selected (f,t) pairs from CELWPIXB.exe or SAVA.exe as the input file, after the matched filtering procedure BURK1/2.exe has been run on the data. The procedure used is similar to that used for FIT0.exe. The log file produced as output is saved using the input filename and modifying the last character of the infile to "i". The input filename needs to be longer than 5 characters, and it is suggested that some time information about the whistler be included in the filename. The benefits become apparent when analysing a large number of whistlers.

ie. infile "infile1" produces outfile "infile1i"

infile "sas208a.s" produces outfile "sas208a.si" , etc.

The prompt

Stop - Program Terminated.

appears after the program has run. The starting values used in the iterative procedure are in the second half of the parameter file "WHEAD", which is modified by BURK. If no convergence is reached, the message

End of iteration. (number) steps , error -1.

appears at the end of the log file. The curve fitting program was unsuccessful with this particular set of starting values, and different starting values are needed for convergence.

Caution must be taken before running FIT1 that the output filenames are not

already in use, otherwise the program will not run. To solve this problem erase any files with the same filename as the FIT1 output, ie. infile+i.

Active keys : none

Parameter files used : The program uses the second half of the parameter file WHEAD, starting at &BURK1DAT, an example of which is shown below.

```
&FITDAT
MD    =0          /* model used, 0 = DE1, 1 = R4 (collisionless) model */
F2    =0.         /* foF2 in MHz, 0 if no ionospheric correction is used */
FNIN =5.0         /* Approximate nose freq. in kHz, starting point */
DOIN =110.        /* Approximate zero dispersion, starting point */
DTX   =1.         /* Approximate time shift (sec) between chosen time origin and
                     causative spheric */
FA    =100        /* Marquardt's parameter used in damped iteration (.01 - 100)*
/
&BURK1DAT
N        =70000    /* Length of input data file in points */
NF       =900      /* Number of frequencies to be filtered using BURK1.exe */
NSZ      =1000     /* Width of filter output in points */
DO       = 96.4    /* Whistler dispersion calculated by BURK1.exe */
FHEQ     =12413.   /* Equatorial electron gyrofrequency in Hz from BURK1.exe */
FN       =4609.    /* Nose frequency in Hz from BURK1.exe */
DT       =.1e-3    /* Sampling period, 1/sampling frequency */
DF       =200.     /* Matched filter bandwidth (100 - 600 Hz) */
TO       =1.750    /* Time of arrival of whistler relative to causative spheric*
AL       =0.       /* Phase constant of filter */
FRTOL    =0.       /* Centre frequency of received data , mixed down to
                      baseband. (= 0 in for our purposes) */
ELSOFR   =500.     /* Start centre frequency of filters */
FRLEPES =5.        /* frequency step between centre frequency of filters */
/
```

These parameters can be modified to give more accurate results. The &BURK1DAT section of the file is modified by BURK1.exe, and is only used to do a second, and hopefully more accurate, curve fit using the program FIT1.exe.

APPENDIX : FILE SUMMARY

Executable file	Input file	Output file	Files used
AscToBin	S89215a.asc	S89215a.bin	———
QLS	0C171040.59!		QLS.dat, COLOR.dat
SELECTS	0C171040.59!	SAS197a.s	SELECTS.dat
FFT1	SAS197a.bin	(SAS197a.ft0)	FFT.dat, COLOR.dat
FFT2	S89215a.bin	(S89215a.ft0)	FFT.dat,COLOR.dat
FIT0	S89215a.ft0 SAS197a.ft0	S89215a.fi0 BURK1xx.dat	WHEAD
BURK1	SAS197a.bin	SAS197a.fb0	BURK1xx.dat
BURK2	S89215a.bin	S89215a.fb0	BURK1xx.dat
CELWPIX	S89215a.fb0 SAS197a.fb0	———	CELWPIX.dat BURK1xx.dat COLOR.dat
CELWPIXB	S89215a.fb0 SAS197a.fb0	(S89215a.ft1) (SAS197a.ft1)	CELWPIX.dat BURK1xx.dat COLOR.dat
FIT1	S89215a.ft1 SAS197a.ft1	S89215a.fi1 SAS197a.fi1	WHEAD
SAVA	S89215a.fb0	S89215a.ft1	
SAVB	S89215a.fb0	S89215a.fb1	

Notes on filenaming conventions used by the author :

1. Filenames used are 7 characters long, with a 3 character extension.
2. The filename indicates the receiving station (SAS, SANAE, ISIS) and contains time information.
3. The extension describes the type of file :

(i) .bin - binary file
(ii) .asc - ascii file
(iii) .ft0 - output (f,t) pairs from FFT.exe, for use by FIT0.exe
(iv) .fti - output of FIT0 containing whistler parameters
(v) .fb0 - BURK output file for display by CELWPIX.exe

APPENDIX A

1. An example of the data file COLOR.dat.

```
0000000000150002A00003F00150000151500152A00153F002A00002A15002A2A002A3F003F
1500001500151500 2A15003F151500151515152A15153F152A00152A15152A2A152A3F153F
2A00002A00152A002A2A003F2A15002A15152A152A2A153F2A2A002A2A152A2A2A2A2A3F2A3F
3F00003F00153F002A3F003F3F15003F15153F152A3F153F3F2A003F2A153F2A2A3F2A3F3F3F
1 33 50 57 58 46 29 30 31 15 32 16 28 24 4  64
0 1 2 3 4 5 6 7 8 9 10 11 12 13 14
0 0 0 14 14 14 2 2 2 1 1 1 15 15 15 15 15 15 15 15
lityi intenzitasai: 0 14 2 1 15
eredeti kep
0 1 2 3 4 5 6 7 8 9 10 11 12 13 14
feketa alapu feher madar...
15 1 2 3 4 5 6 7 8 9 10 11 12 13 14
1 50 57 58 62 42 29 30 31 15 32 16 28 24 4  64
```

This is the standard data file used for the VGA colour function, and should not be modified.

APPENDIX A

2. Output file of FFT1.exe and FFT2.exe : frequency - time pairs selected along the whistler trace, for use by FIT0.exe.

2.8906	.6400
2.7734	.6656
2.6563	.6976
2.5000	.7360
2.3828	.7680
2.2461	.8128
2.1094	.8448
1.9727	.8960
1.8555	.9664
1.7383	1.0368
1.6406	1.1008
1.4844	1.1840

APPENDIX A

3. FIT0 or FIT1 output file containing a log of the iteration procedure, data points used for the iteration, and final results.

```
sas208a.s i

DENSITY DISTRIBUTION : 0  ( 0 : DE-1, OTHER : R-4 MODEL)
FOF2 =    .0 MHZ


 ORIGINAL F-T DATA
 3.7695E+03  3.9040E-01  3.2813E+03  4.7360E-01  2.9883E+03  5.3120E-01
 1.9336E+03  8.4480E-01  1.9336E+03  8.4480E-01  1.3867E+03  1.2032E+00
IT      FACTR          FN            D(0)           DT        FHEQ          TN

 0    100.00000   5000.00000    110.00000      1.00000  13469.56941    .00000
 1     10.00000   5667.09039    106.94178      1.07431  15266.65347   2.07221
 2      1.00000   7976.06430     98.52102      1.26931  21494.16508   1.60966
 3       .10000   8827.30223     92.78944      1.36437  23815.19686   1.44127
 4       .01000   5780.15205     90.09752      1.38474  15602.43763   1.72869
 5       .10000   7573.51996     91.40614      1.37405  20410.49430   1.53250
 6       .01000   6303.68866     90.06396      1.38777  17003.00523   1.65484
 7       .00100   6124.81642     91.02178      1.42690  16510.34395   1.69665
 8       .00010   5681.59593     93.19377      1.50041  15314.29816   1.80351
 9       .00100   5973.87872     91.79422      1.45301  16098.72229   1.73249
10       .00010   5689.04792     93.32010      1.50442  15333.29497   1.80478
11       .00001   5663.37636     93.62221      1.51432  15262.01962   1.81471
12       .00000   5663.34482     93.62422      1.51438  15261.74350   1.81476
13       .00000   5663.34712     93.62421      1.51438  15261.74947   1.81476


 N=  7

  F(HZ)       T(SEC)        RESID       F/FN       F/FHEQ

  3769.5       .39040      -.00899        .666        .247
  3281.3       .47360       .00554        .579        .215
  2988.3       .53120       .00871        .528        .196
  2675.8       .60160       .00690        .472        .175
  1933.6       .84480      -.01010        .341        .127
  1933.6       .84480      -.01010        .341        .127
  1386.7      1.20320       .00805        .245        .091
```

```
 RESULTS WITH ONE SIGMA ERROR LIMITS

    FHEQ= 15262. +-  2102.      FN= 5663. +-  780.
    D(0)=  93.6+- 4.9           TN= 1.815+-   .217
    DT=  1.514 +- .163          A= .2226
    RFD= -.95    RFT= -.98      RDT= 1.00

    L=3.854 +-.177              NeQ=  537. +-  72.
    NT= 4.28D+13 +- 2.7D+12     N1= 7.40D+03 +- 9.9D+02
1
```

Description of Parameters

FHEQ : Equatorial electron gyrofrequency.

FN : Whistler nose frequency.

D(0) : Zero dispersion of whistler.

TN : Time of arrival of nose frequency relative to initiating spheric.

DT : Arbitrary time shift between chosen origin for selection of (f,t) pairs and true initiating spheric.

A : Auxillary parameter, of no importance.

RFD : Error correlation coefficient in FHEQ.

RFT : Error correlation coefficient in D(0).

RDT : Error correlation coefficient in DT.

L : L-value of whistler propagation.

NeQ : Electron density at the geomagnetic equator.

NT : Tube electron content.

N1 : Electon density at 1000 km altitude.

REFERENCES

L.C. Bernard
A New Nose Extension Method for Whistlers
Journal of Atmos. and Terr. Physics, Vol. 35, pp 871 - 880, 1973.

D. Hamar, Gy. Tarcsai, J. Lichtenberger, A.J. Smith and K.H. Yearby
Fine structure of whistlers recorded digitally at Halley, Antarctica
J. Atmos. Terr. Phys., Vol.52, No.9, pp.801-810, 1990

J. Lichtenberger, Gy. Tarcsai, Sz. Pastzor, Cs. Ferenz, D. Hamar, O.A.Molchanov and A.M. Golyavin
Whistler Doublets and Hyperfine Structure Recorded Digitally by SAS on the ACTIVE Satellite.
Journal of Geophysical Research, vol. 96, No. A12, pp.21149-21158, 1991.

C.G. Park
Methods of Determining Electron Concentrations in the Magnetosphere from Nose Whistlers.
Stanford University Technical Report, 1972.

Gy. Tarcsai
J. Atmos. Terr. Phys., Vol.37, pp. 1447, 1975

Gy. Tarcsai
FORTRAN program for complete whistler analysis. Circulated to members of joint URSI/IAGA WG on passive electromagnetic probing of the magnetosphere, 1977.